Eco-efficient friction materials

Submitted by Michael Robert Sloan, to the University of Exeter as a thesis for the degree of Doctor of Philosophy in Engineering July 2008

I certify that all material in this thesis which is not my own work has been identified and that no material has previously been submitted and approved for the award of a degree by this or any other University.

…….

Abstract

Automotive friction materials are multi component composites in which fibrous materials play a fundamental role. Modern friction formulations have been developed around asbestos fibres, a heavily used material before legislation outlawed its use in the 1980's. The replacement adopted by the friction industry was aramid, a high performance, high cost synthetic fibre.

The work in this thesis investigates the role of aramid fibres in an economy friction material from the early mixing stages in manufacture using mechanical and optical analysis techniques through to the friction and wear performance of brake pads by employing instrumented friction and wear machines. Experimental procedures were designed and employed to quantify the performance of aramid pulp within the friction formulation as a function of volume fraction. Investigation showed a hierarchal fibre structure produced by an inherent molecular structure that encourages fibrillation producing complex fibre morphologies. This physical structure has been identified as fundamental to the success of aramid pulp in friction materials as the fibre network readily entraps small particles aiding the manufacturing process of friction materials. A structural model has been developed to describe both the particle retention performance of aramid fibres and the bulk structure of the pulp as a function of fibre geometry.

A dynamic mechanical test was used to measure the bulk elastic properties of fibre networks to assess their suitability as processing fibres in friction materials and providing a novel analytical technique for the friction industry.

Hemp, flax and jute are examples of high performance natural fibres that offer a significant cost saving over aramid, representing candidate replacements. Various natural fibres were trialled in friction formulations as direct replacements and also blended with aramid pulp. The results are compared to the baseline specification produced for aramid pulp allowing the suitability of natural fibres in friction materials to be discussed.

Acknowledgements

First and foremost I would like to thank my supervisors Ken and Bill for their guidance and inspiration through my research. Thank you both for your support, understanding, knowledge and sense of humour. I would like to thank everyone in Exeter Advanced Technologies, particularly the staff in the materials office. A special thank you is given to Oana for her determination to ensure I stayed on track during writing up. Neil Sewell has been invaluable for proof reading my work and always looking on the positive side of life and also Mark Beard for the advice and patience with Microsoft word. Thanks to Dave Baker for his help in designing the British racing green machine and most importantly to Pete Gerry for his skill and hard work to make it happen. Without you, it would still be in bits now! Thanks to Julian Wright for the data acquisition software and to Bob Hamilton for his electronic wizardry.

Thanks to Dr Gavin Edwards at EFI for his superb knowledge of brake pads, help on the dynos, bad jokes and bacon rolls at Ducati Bristol throughout the Ecopad project.

Thank you to Colin Lovell for all of the excellent SEM images taken throughout the work.

Thank you to Luke for writing the Ecopad project application and for the help at the SAE conference. Thanks to all of the industrial partners on the Ecopad project – EFI, PBW, Hemcore, Aptec and the Eden project – and also the DTI for the funding the Ecopad project as part of the sustainable technologies initiative.

Thank you to all my friends in Exeter who have supported me throughout my work and understood why I couldn't come out to play during the last 12 months!

A very special thank you goes to my Kate who has encouraged and supported me throughout this work without the slightest clue as to what I'm doing! Without you (and the regular tea supplies) I couldn't have done this.

My biggest acknowledgement goes to my family - Mum, Dad and brother Rich. This thesis is the highlight of my career so far and I have achieved this because of you.

List of Contents

List of figures

List of Tables

1 Introduction

Sustainable and environmentally friendly materials have seen a growth in applications and popularity over the last decade as a result of consumer awareness and government legislation pressurising industrial companies to reduce their impact on the environment through the cleaning of their products and process. Materials derived from sustainable sources can now be found in products ranging from home furniture to clothing to packaging and bio-fuels for internal combustion engines. The increasing demand for raw materials coupled with the pressure of a finite supply of fossil fuels has rekindled an interest in sustainable materials such as natural fibres. Prior to the invention of synthetic materials, natural fibres such as flax and hemp were the high performance fibres of choice and were heavily used for clothing, ropes, and ship sails to name but a few applications. The research work presented in the following chapters aims to extend the application of natural fibres in engineering systems by evaluating their performance in automotive brake pads. Modern automotive brake pads are composite materials composed of over a dozen diverse raw materials of which fibrous materials play a crucial part. The role of an existing synthetic fibrous material is explored and the performance contribution to the brake pad quantified in order for new formulations containing natural fibres to be proposed.

Natural fibres based on cellulose obtained from plants such as hemp, flax and jute are examples of nature's high performance fibres that will be used in this research

This thesis was funded by the DTI funded research project ECOPAD, the technical work was undertaken with the assistance of a number of industrial partners, each with a specific expertise in either the friction industry or natural fibre/fibre processing industry. The friction industry is a highly competitive, multi billion pound global businesses manufacturing safety critical automotive components for a wide range of vehicles. Asbestos fibres were heavily used in all types of brake pads until the 1980's when the health implication of the fibres became apparent. Currently aramid fibres represent a major share of the market but increased demand for the same fibres from the defence and military sector has inflated prices and capped supply for friction manufacturers. All factors favouring a high quality, cheap, readily available fibrous material and natural fibres represent unproven candidate materials, often overlooked for the low service temperatures in comparison to other mineral and high performance synthetic polymeric materials.

The performance of an automotive brake depends on the composition of the brake pad which is not only a function of raw material selection but also particle morphology, the combination of materials and the percentage inclusion in the composite as a whole. Recycled materials are widely used to reduce cost, sometimes exclusively or blended with virgin material to maintain performance. Frequently, raw materials are chosen by brake pad manufacturers based on empirical experience rather than a complete appreciation of performance and function within the friction material.

The core of this research aims to understand the function of aramid pulp in an economy friction formulation from initial stages of manufacture through to the friction and wear performance of composite brake pads. The results obtained from investigating the role of aramid fibres in friction materials will produce a baseline specification against which new friction materials can be judged. New friction materials containing natural fibres will be developed resulting in cost effective, environmentally friendly formulations.

The scope of possible research into friction materials is massive considering the number of vehicles, raw materials and potential formulations therefore this thesis remains focused around establishing the key functions of aramid fibres and matching the specification produced with a replacement natural vegetable fibre. Fibrous materials are fundamental in the manufacture of friction materials and aramid fibres are the world's most popular organic fibre for this. Clarifying the function of aramid fibres will provide a strong foundation on which new friction materials are developed.

1.1 Automotive brakes

The development of friction materials since early examples used on wagons and carts has been aimed at providing a safe, predictable and reliable means of slowing a travelling vehicle. Conventional braking systems function by converting the kinetic energy of a moving vehicle into heat energy which is dissipated into the surrounding brake components and atmosphere. Modern vehicle technology has seen a substantial increase in the power output and top speed of all vehicles. Consider the model T ford launched in 1908 whose braking system had to deal with a kinetic energy of 90 kJ against the 2008 Ford Mondeo 2.0 litre Duratec – a modern family car – with a maximum kinetic energy of 2.5 MJ, nearly a 30 fold increase. Modern super cars such as the Bugatti Veyron amplify this value considerably more when travelling at top speed, presenting the braking system with 12.16 MJ of energy to dissipate. Friction materials in particular have endured an equally large development program in the last century with the number of automotive manufacturers and vehicles more than ever.

The aim in this section is to provide a fundamental understanding of the components and operating requirements of an automotive brake. The history and development of friction materials is discussed in the next chapter.

1.1.1 Brake system requirements

A vehicle brake operates by pressing a stationary friction material against a rotating disc or drum which is fixed to the axles of the vehicle. The friction generated between the two rubbing components generates a retarding torque onto the wheel axles of the vehicle which transfers the force into the contact patch between tyres and road to slow the vehicle in a safe and controlled manner. Brake pads convert the kinetic energy of the vehicle into heat energy which is dissipated into the brake system components and surrounding atmosphere by conduction, convection and radiation.

Modern requirements of automotive brake systems born from consumer demand extend beyond safety, to include noise, vibration, pedal feel, and maintenance issues. The majority of brake induced problems are blamed on the friction material partly because it is far easier to change the brake pad than other brake system components. In the United States,

consumers demand silent operating brakes with a relatively soft pedal feel and so called high “comfort factor” where as in Europe, drivers demonstrate a different style of driving and require higher performance brakes with greater stopping power and more bite. The Japanese market requires brake pads to operate at lower speeds with no amount of noise or brake dust tolerated, leading to new classifications of friction materials based around consumer demands.

The performance requirements of a modern brake system have been taken from a variety of sources [1-6] and are listed below.

Requirements of friction material

- Satisfactory and stable coefficient of friction over a range of speeds, pressures and temperatures, regardless of age or conditioning history.
- Resistance to friction generated heat in the immediate contact areas i.e. thermal and oxidative stability
- Resistance to fade – i.e. loss in coefficient of friction due to high temperature.
- Good recovery from fade – i.e. quick return to stable operating coefficient of friction after fade.
- Fast pick up of steady state friction level.
- High resistance to thermal cracking and fatigue.
- High mechanical strength to withstand high compressive and shear forces over a range of temperatures.
- Minimal sensitivity to environmental conditions e.g. moisture, salt, corrosion, mud, water.
- High resistance to wear.
- Compatibility with metallic counter face, i.e. no excessive wearing or marking of disc or drum.
- Not contain Asbestos.
- It should not smell
- Consistent and cheap manufacture.

Brake system requirements

- Smooth predictable operation.
- Zero noise and vibrations.
- Good consistent pedal feel.

1.1.2 Brake system components

Disc brakes represent the most popular braking system, steadily replacing drum brakes on modern vehicles. Drum brakes are still popular on larger commercial vehicles whose operating speeds are low, for ease and low cost of brake system maintenance compared to discs. Disc brakes constitute the majority of brake systems in use today and as such will be the only type of rotor discussed in this section. A modern braking system is comprised of three distinct systems;

- Rotor
- Friction material
- Hydraulic system

Rotor

This research is concerned with developing a new composite friction material and not a rotor. However as one half of the friction couple it is essential to give a brief introduction to the operating characteristics of the rotor. Conventional brake discs are made from grey cast iron having a perlitic grain structure and can either be solid or ventilated in construction. Solid discs have much lower manufacturing costs compared to ventilated but their heat dissipation is very poor limiting their use to small private cars [7]. As a raw material, cast iron has dominated the market since the introduction of disc brakes due to a combination of low material and manufacturing costs and inherent mechanical and thermal properties. Desirable properties include high thermal conductivity and heat capacity, low thermal expansion, adequate hardness, low wear and high coefficient of friction. One crucial benefit that cast iron imparts to the discs is a resistance to thermal cycling and thermal shock, providing the temperatures do not regularly exceed 300 °C which can lead to the formation of hairline cracks [8]. It is also known that the thermal and mechanical properties of the

cast iron change according to the material phases in the grey iron which are influenced by the thermal history of the material [9]. As the second half of the friction couple, developments in disc materials have been relatively static compared to that of brake pads. Cast iron has a much higher thermal stability than organic materials in the friction material – which for this reason often bears the brunt of brake system complaints. It is known that unwanted brake phenomena such as judder, noise and even fade are as a result of the physical properties and shape of the disc [4,10,11]. If brake disc temperatures are allowed to rise to above 700 °C Coyle et al [12] discovered that the cementite phase in the cast iron changed from a lamellar to a spherical structure increasing pad wear by 15% and disc wear by 50%. Iron particles produced during disc wear are known to be the main constituent of brake dust [13,14] – a factor already noted as a cause for manufacture warranty claims – therefore any change in the friction material must consider compatibility with the cast iron disc.

Friction material / Brake pad

The friction material is the heart of the brake system, and together with the rotor, forms the tribological couple that slows the vehicle. The composite friction material is bonded to a steel back-plate during manufacture to become a brake pad. The back-plate provides mechanical rigidity to the composite, geometric fit with the calliper and a heat sink to prevent excessive heat flow into the hydraulic system. Composite friction materials can also be moulded into shaped linings, friction blocks and shoes depending on the brake system in use.

The complex specification of a brake system identified at the start of this section will illustrate why brake pads are no longer composed of monolithic materials. Historically, the major research and developments in friction materials have been accomplished by well established western companies using a combination of the latest technology with in house experience and close links with the major automotive manufacturers.

Hydraulic system

A hydraulic system is used on car braking systems to amplify and transfer the driver applied force on the brake pedal to the brake pad by means of a sealed hydraulic network.

Additional brake technology and safety systems such as the anti-lock braking system (ABS) are contained within the hydraulic system. The hydraulic system is designed independently of the friction materials and to a limited degree dictates the specification of the friction material as the hydraulic system determines how hard the brake pad is pressed against the disc and in what time frame.

1.1.3 Environmental, cost and market issues

The three key driving forces behind automotive brake development are performance, cost and environmental issues. Brake pad formulations are devised considering performance, material cost, and both ease and consistency of manufacture.

The high performance aramid fibres known as Twaron – sold by Teijin – and Kevlar – sold by DuPont are the current most popular replacement fibres for asbestos. The cost of virgin aramid pulp prohibits the use in friction materials above 10% with most European friction manufacturers typically using around 4% by volume. Recycled aramid fibres obtained from fire blankets are frequently used to suppress costs. Recent developments in world security have seen a sustained demand for monofilament aramid fibres from the military and security markets. Monofilament fibres return greater profits to Teijin and DuPont compared to the pulped fibres used in friction materials.

Environmental issues are a strong influence in the development of friction materials, dictating what materials and manufacturing processes can be used by industry. The prime example is the banning of asbestos fibres, a major upheaval in the friction industry that will be discussed in section 2.1.1, and also government studies attributing air pollution [15] water contamination and ultimately detrimental health effects to brake pad dust.

Health and safety regulations are tolerated by the industry and product formulations changed reactively as opposed to proactively. By including sustainable materials such as natural fibres in brake pads the industry would be leading the implementation of environmentally materials as opposed to the governments.

1.2 Aims and objectives of the thesis

The aim of the work in this thesis is to develop an eco-efficient automotive friction material by employing natural fibres in a composite friction material. Candidate natural fibres investigated for inclusion in brake pads were hemp, flax, jute, kenaf and sisal. The choice of fibres is justified in section 3.3. Researching the role of aramid – a popular synthetic fibre used in a large number of friction materials – forms the core of this thesis. The published benefits of using aramid fibres in friction materials will be investigated by varying the aramid content in an economy composite friction material and analysing the formulation to quantify the effect of the aramid inclusion. Scanning electron microscopy analysis (SEM) is used extensively to discuss the morphology of the aramid fibres and also the fibrillation mechanics of aramid that gives rise to a unique fibrous structure. This discussion is taken on to consider the results from bulk mechanical tests on the friction material in terms of mechanical strength, toughness, fibre dispersion and homogeneity of the composite brake pad. A novel mechanical test was employed to quantify the visco-elastic properties of aramid pulp and other organic and mineral fibres used in friction materials. Using a rotational rheometer – typically used for analysing polymer melts and other viscous materials – the mechanical response of a fibre network to an applied strain was evaluated. This allowed the suitability of various natural fibres and fibre blends to be discussed for the inclusion in friction materials.

This analysis formed the basis for a theoretical structural model of hierarchal fibre networks that allow the performance of fibre networks to be predicted. The fibre model based on the observed morphology and characteristics of aramid fibres predicts the particle retention properties of a fibrous network in addition to the structural rigidity of the same network.

A number of friction materials were manufactured containing controlled levels of natural fibres by substitution of aramid fibres and subjected to friction and wear testing using a specially commissioned testing machine. The sub-scale pad on disc testing apparatus characterised the friction and wear properties of the newly developed friction materials by monitoring the coefficient of friction, applied pressure and disc temperature.

New friction materials containing natural fibres were also subjected to full scale inertial dynamometer testing to a recognised industry standard to analyse the friction levels and stability over a wide range of simulated driving conditions.

Structure of chapters

1. Chapter one gives an introduction to the thesis and automotive braking systems in general. The aims and objective of the research work are discussed
2. The literature review covers the history of automotive friction materials, discussing the evolution of friction materials, classification of materials and modern material analytical techniques. An introduction is given to tribology, friction and wear. Natural fibres are discussed to introduce fibre types, processing methods and their role in engineering composites.
3. All the materials used in the research work are introduced in this section including the friction material formulation and the variations thereof.
4. The methods section covers the experimental methodology used to analyse the materials introduced in chapter 3. The methods associated with friction materials follow a sequential progression through the manufacture and testing of brake pads.
5. Experimental results are covered in chapter 5 and presented in the same order as chapter 4. Key results are highlighted in this section ready for discussion in a subsequent chapter.
6. The theoretical fibre model is developed and used in this chapter to model and predict the performance of aramid fibre in a friction material situation. Numerical results are used in conjunction with experimental data from chapter 5 to discuss the fibre pulp structure.
7. Results obtained in chapter five are discussed here to summarise the key results from the experimental work.
8. Conclusions finish the work in the thesis.

2 Literature review

2.1 Friction materials

2.1.1 History and development of friction materials

Herbert Frood is credited [16] with inventing the first brake lining material in 1897 for wagons and early automotives using woven cotton impregnated with bitumen, an invention that founded the modern day Ferrodo company. Other friction materials at the time used animal hair with bitumen [17] however this had the same thermal limit as the cotton of around 150 °C. Around 1908 organic fibres were superseded by asbestos as it possessed a much greater thermal resistance, higher strength, the net result being a more reliable coefficient of friction. In 1908 Dr Leo Bakeland filed a patent for the manufacturing process to react phenol and formaldehyde producing a highly cross-linked thermosetting resin made from two previously deemed waste materials. The new resin took the inventors name to become the famous Bakelite resin [18] and a crucial binder resin for friction materials over the next 80 years.

Friction material formulations increased in complexity with the arrival of drum brakes in the 1930's. In the 1950's a new breed of friction materials – semi metallics – were developed in response to asbestos supply problems as a result of World War II [19]

Described as a "god given' material for use in brake linings" [20] asbestos as a raw material was immensely popular due to a unique set of physical, mechanical and thermal properties making it an ideal medium to design a friction material around [2,21]. In fact the word asbestos describers the material's function perfectly as it is derived from the Greek language meaning indestructible [22]. The fibres posses both high strength and modulus and are held tightly together in bundles giving apparent flexibility making the material ideal for the diverse range of mixing techniques found in the friction industry. In fact most of the current day mixing techniques for dry friction materials are based around accommodating asbestos fibres [2].

The 1970's saw the arrival of the Federal Motor Vehicle Safety Standard FMVSS105 and the EEC directive71/320 both designed to improve braking systems on vehicles [20]. Smaller, lighter front wheel drive vehicles with smaller brake systems were introduced increasing the physical and thermal demands on friction materials.

Jacko et al [4] summarised the developments in both brake design and friction materials as shown in table 2.1

Period	Brake Design	Brake front to rear bias	Material	
			Front	Rear
Up to late 1960's	Drums on all four wheels. Front larger in surface area than rear	55:45	Primary and secondary Organic	Primary and secondary Organic
Late 1960's to early 1970's	Initial discs on heavy/performance cars	60:40	Class A disc	Primary – secondary organic combination
Mid 1970's	Improved discs on medium weight cars	60:40	Semi-metallics	Primary – secondary organic combination
Late 1970's early 1980's	Lighter front wheel drive vehicles	75:25	Semi metallics	Primary – secondary organic combination Or non-servo

Table 2.1 Friction material developments 1950's to 1980's [4]

Asbestos was such a multipurpose material that no one single material was found as a direct substitute [2,20] leading to over 1200 different candidate raw materials being tested over the next 15 years [1]. The loss of asbestos not only focused attention onto fibrous materials but also necessitated the development of the organic binder resins that were widely used at the time. Being forced to develop the resin matrix – the base starting point of a friction material – gave friction formulators somewhat of a clean sheet to design and develop

friction materials [20]. The new improved resins provided the foundation for non asbestos organic (NAO) friction materials and combined with reinforcing materials, friction modifiers and fillers form the basis of modern NAO brake pad formulations.

2.1.2 Classification of friction materials

Figure 2.1 shows the classifications of friction materials used by the friction industry

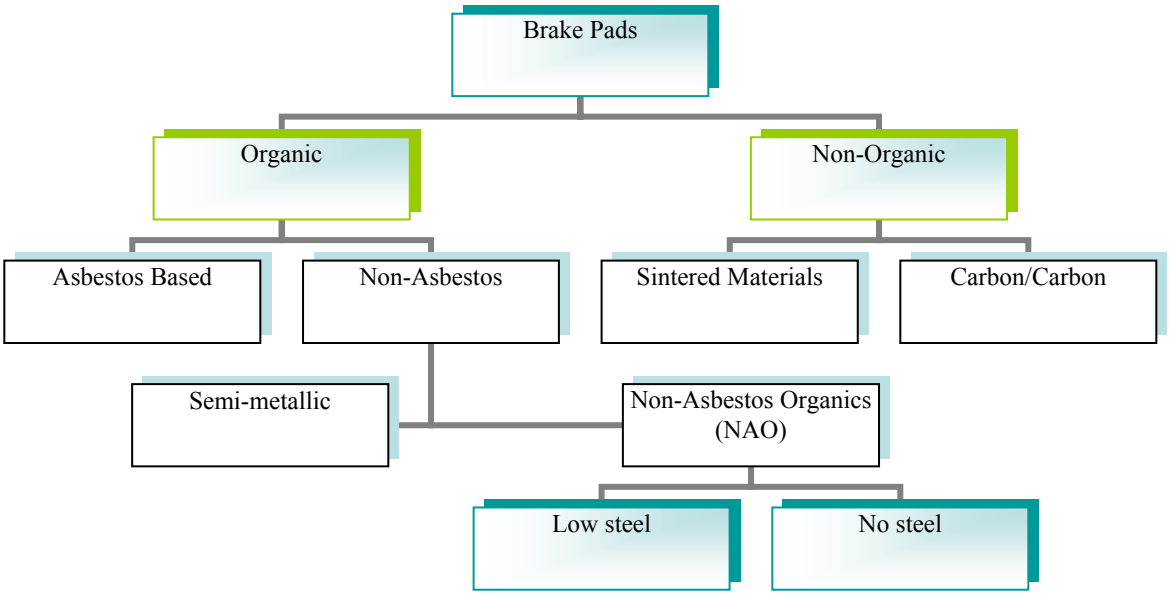

Figure 2.1 Classification of automotive friction materials

Organic

The basic friction material used throughout this research is based on a low steel Organic formulation. Organic friction materials derive their name from the organic resin matrix used to bind the other raw materials in the brake pad together – usually based on a phenolic resin – and represent the majority of friction materials found on modern vehicles. A wide range of chemically modified resins are easily mixed with other raw materials giving flexibility in formulations and manufacture. In non-asbestos organics the resin is combined with up to 20 separate raw materials each having a specific or combined purpose to the

performance of the friction material. Once cured, the resin provides the mechanical strength to the composite and also strongly influences friction levels and stability [11,23] and so denotes this classification of friction materials. NAO materials can be subdivided even further based on the steel fibre content of the formulation as a result of consumer pressure over brake performance. The Japanese market demands zero noise and brake dust, and steel in brake pads has been identified as the major source of disc wear which in turn makes up 90% of brake dust. Consequently, a new classification of brake pads was born containing no steel.

Non organic

This classification of materials was designed to cope with the performance of modern heavy high speed vehicles, including aircraft. Unsurprisingly, this classification of material does not contain an organic binder to form the matrix of the friction composite and uses both alternative and completely different manufacturing processes. The sintered and carbon/carbon composite materials within this classification are used in high performance applications where extreme braking conditions are experienced such as racing cars and motorbike and commercial and military aircraft. These high performance high cost friction materials do not contain aramid fibres and so lie outside the scope for natural fibre replacements.

2.1.3 Selection and performance of raw materials

Modern friction formulations contain up to 20 separate raw materials although it is more common to see 10-15 used, making brake pads one of the most complex composite materials in the engineering world. Controlling the friction characteristics of a brake pad by changing the raw ingredients is a very complicated task [24] as the relationship between formulation and frictional performance is not well known [25]. Complex blends of raw materials are historically selected and mixed on an empirical basis [26-32]. Successful formulations are closely guarded proprietary secrets and as such it is very difficult to establish exact compositions. The number of raw materials available is in excess of 2000 [17] giving a vast number of permutations but a “secret” recipe is only part of the picture as

raw materials have to be mixed and manufactured on a consistent basis. It has been reported by Nicholson [16] that brake pads manufactured from identical raw materials by different companies can have operating coefficients of friction that vary by over a factor of 2.

It is generally agreed [1,17,33,34] that raw materials can be grouped according to their role in the friction material, however some materials have multifunctional roles and cross between the boundaries listed below. For simplicity, raw materials will be listed here according to their primary function in the friction material.

Binders

These provide the matrix that holds all of the raw materials together in a three dimensional structure imparting compressive and shear strength to the composite. The binder is chosen so that it will not disintegrate under the thermal or mechanical stresses encountered during braking – doing so would result in complete structural failure of the composite. The choice of resin has profound significance to a friction material as it not only dominates the bulk mechanical properties [1] but also strongly influences the level and stability of the coefficient of friction [11,23]. The resin must demonstrate compatibility with all raw materials in the formulation and is required to flow and evenly distribute amongst the particulates during manufacture. The volumetric percentage of resin in a formulation varies between application and manufacturer but typically is around 20%. Phenolic resins are the most popular choice of binder for organic brake pads as they are inexpensive thermosetting materials with a good level of friction and thermal stability. They also readily accept chemical and physical modifications to tailor the thermal, mechanical and reactive properties for individual applications [34]. Epoxy and silicone are chemical modifications used to impart thermal stability and toughness, rubber is an example of a physical modification used to increase the compliance and damping of the resin [34].

Reinforcements/structural materials

Raw materials are grouped in this category if their primary function in a friction material is to support the resin matrix by providing mechanical reinforcement to the composite. Fibrous morphologies inherently bring these benefits to composite materials and so dominate this classification. The success of Asbestos in early friction materials was so great

that the choice of other structural fibres was very low, but nowadays there is an extensive array of organic, metallic and mineral fibre to choose from.

The performance, selection and combination of fibres in friction materials is fundamental to the research work in this thesis so section 2.1.4 has been devoted to discussing the subject in detail.

Fillers

Often referred to as the budget ingredients, fillers are inexpensive materials added in relatively large percentages to reduce the cost and also improve the manufacturability of brake pads. Early research by Spurr [6] classified all raw materials bar the binders as fillers, but as the complexity and understanding of raw material functions has increased, so has the classification terminology. The classification of filler materials play an integral part to the friction material and generally speaking will account for any material used in excess of 10% by volume. Intended to fill in the voids between other particulates, fillers are chosen based on their thermal stability and compatibility with other materials. Examples of popular fillers are barium sulphate (barytes) and calcium carbonate as these are regarded as inert materials over a wide temperature range and will not detrimentally affect the performance of the brake pad. In truth, it is difficult for any material to be truly inert at the tribological interface due to the extreme temperatures and mechanical forces experienced. Apparently stable materials tested under laboratory conditions can display a completely opposing performance when tested in a brake pad [21]. Vermiculite and Perlite are naturally occurring mineral fillers that are extensively used in modern friction materials imparting additional benefits such as suppressing brake noise [34] and controlling the density of the composite. Inorganic fillers are typically rubber crumb – obtained from recycled car tyres – and friction particles from cured Cashew Nut Shell Liquid (CNSL) resin are used to add compliance to the brake pad, increasing surface contact and damping vibrations [35,36].

Friction modifiers

A friction modifier can be a material that is used to lower (lubricants) or increase (abrasives) the operating coefficient of friction and modern brake pads contain a combination of both. Lubricants are used to stabilise and prevent the coefficient of friction

from reaching extreme values, thus keeping temperatures and wear rates low [37]. Solid lubricants with anisotropic bonding such as graphite and various metal sulphides lubricate the tribological couple by the lamellar layers sliding over one another when subjected to a low shear force. Graphite is an extensively used lubricant that provides a stable coefficient of friction at low speeds e.g. town driving but is used in low percentages due to poor compatibility with the organic binder. Metal sulphides based on antimony, copper and tin provide high temperature lubrication and so are used with graphite to lubricate over a wider temperature range. The lubricants have dissimilar thermal conductivities and are balanced to control the thermal properties of the brake pad.

Abrasive materials are hard particles added to the formulation in low amounts to increase the coefficient of friction and clean the surface of the disc. Examples include quartz, and refractory oxides and silicates as are metallic powders and chips. Abrasives help to reduce the wear of the friction material but increase the wear of the rotor so they are used in low amounts with a carefully selected particle size and morphology.

2.1.4 Fibres in friction materials

Published research in the last 25 years has discussed how fibres affect the processing characteristics, the mechanical strength, the coefficient of friction, the stability of friction, resistance to high temperature fade, resistance to wear, noise level and cost of brake pads [1-3,5,6,13,33,38-47]. Fibres in brake pads became the most important classification of raw friction materials in the 1980's after the removal of asbestos from formulations.

The desired properties of asbestos replacement fibres are listed below and ideal candidates would have matched asbestos in every criteria;

- Cheap
- Readily available
- Good mixing characteristics with other raw materials
- Good compatibility with organic resins
- Naturally high coefficient of friction against cast iron
- Thermally stable to 650 °C

- High strength and stiffness of individual fibres
- Reinforcing and toughness benefits to brake pads
- Not abrasive to cast iron – doesn't overly wear discs or drums
- Adds to the damping property of the friction material – reduces noise

Originally fibrous materials such as glass, metallic, mineral, ceramic, organic (Acrylic, Polyester) and synthetic (aramid) were trialled but soon other reinforcing materials and particulates were introduced to try and make up for the various shortfalls.
Modern friction materials can contain a vast array of natural and synthetic fibrous materials, the classification of such groups is shown below in figure 2.2

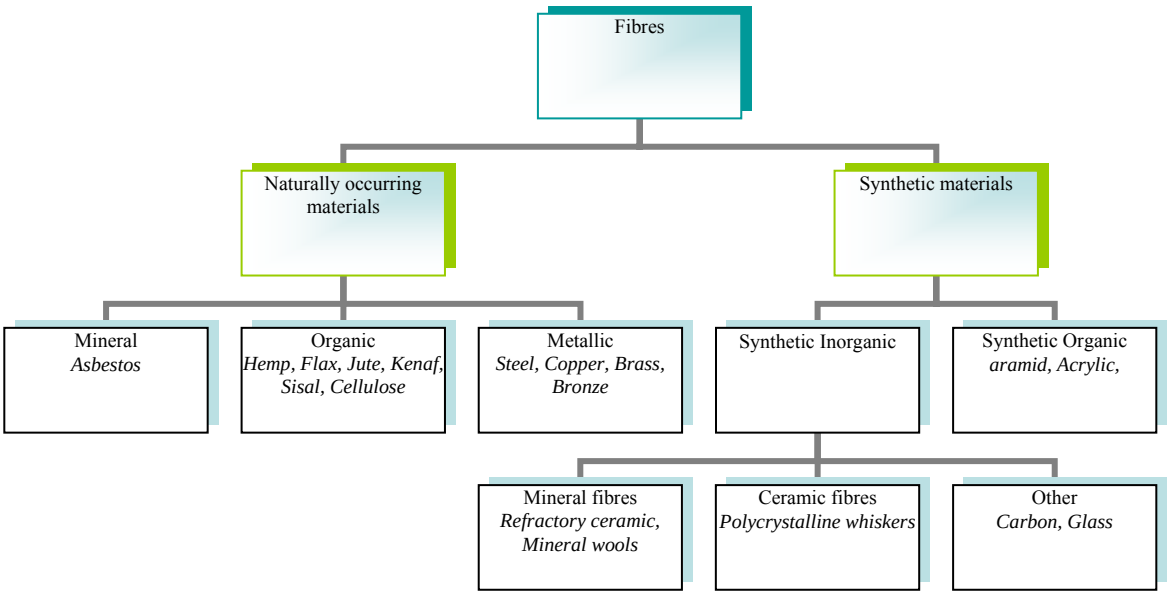

Figure 2.2 classification of fibres used in friction materials

Detailed studies of candidate fibres do not appear until the late 1980's when the performance of singular or multiple fibre combinations are discussed. A comprehensive study of a range of fibres was conducted by Crosa [48] who categorised fibres based on the processing or structural benefits brought to the brake pad (that would have all been previously accomplished by asbestos). Simple fibre reinforced phenolic composites were

manufactured into brake pads and tested on dynamometers for friction and wear properties. Mineral, ceramic, glass, steel, acrylic, aramid and carbon were all trialled with interesting results. All fibrous inclusions except for the carbon increased the coefficient of friction compared to the base resin, a result that is also reported by Longley [21]. Steel fibres (at 20% by volume inclusions) were reported to produce the highest wear rates of both pad and disc, followed by ceramic and glass. Some fibres performed well in one respect and very badly in others such as Acrylic that demonstrated excellent pad wear but very poor disc wear. Glass fibres were reported to pull out of the resin matrix at elevated temperatures and break down into smaller particles enhancing the wear of the brake pad. The results from the work by Crosa [55] suggested using a combination of fibres, taking optimum properties from different materials into the brake pad, an outcome that was probably not intentional at the start of the work. Subsequent research work tended to focus on individual materials and the effect that concentration or fibre orientation had on the friction and wear performance. This research is covered in detail in the following section.

Glass Fibres

Glass fibres were originally trialled in friction materials as they are extensively used as the reinforcement in thermoplastic and thermosetting composite materials as the fibres posses an excellent thermal stability, a good compatibility with organic matrices, a high strength and modulus and are cheap to buy. Longley et al [21] reported glass fibres as difficult to process due to the brittle fibres breaking down in industrial mixers to form a non-reinforcing glass powder that would impart no reinforcement to the composite. Friction materials containing glass fibres also tended to score the disc surface and were more prone to noise during use. Research by Subramaniam et al [49] focused on the volume percentage and aspect ratio of glass fibres in simple friction materials reporting that long thin fibres gave the best flexural reinforcement. Only tensile strength was affected by fibre length and the Young's modulus of the composites was independent of all fibre dimensions. The measured coefficient of friction was found to be lower than desired and did not correlate in any way to the observed mechanical properties. Three years later Gopal et al [40] compounded the research into glass fibres in friction materials by focusing on the friction and wear behaviour stating that the frictional performance was heavily dependent on the

tribological history of the material and decreased with high loads, speeds and temperatures. The results of the wear tests agreed with earlier reports [21] that glass fibres de-bonding from the resin matrix were responsible for high wear rates. Glass fibre of a predominantly borosilicate composition (E type) are used in brake pads but in low concentrations as high inclusions showed unstable friction levels, a fading tendency and high wear rates. They offer no processing benefits to the formulation, actually requiring special mixing procedures to accommodate their inclusion.

Metallic fibres

Steel fibres are extensively used in friction materials and the many different grades of steel offering varying degrees of mechanical and thermal properties require the correct grade to be chosen in addition to the fibre morphology [21]. Steel fibres are tough thermally resilient fibres with a high thermal conductivity that channels heat away from the friction interface. Friction and wear testing by Crosa et al [48] highlighted steel fibres as contributors to disc and pad wear although the fibres were included at very high percentages by modern standards. Typical percentages of steel fibres in modern automotive friction materials will be less than 5% by volume which reflects the trade off between the mechanical and thermal benefits and the high wear rate disadvantages of using steel fibres. The corrosion of steel is a well known problem in brake pads and additional materials such as zinc are sometimes added to provide a sacrificial anode for corrosion [34]. Other metallic fibres such as copper and bronze are used in friction materials but are over 2 ½ times more expensive than steel so are used in small amounts and in limited applications. The role of metallic fibres in friction materials gained significant interest after research by Eriksson et al [33] proposed a real contact situation between the pad and disc based around metallic fibres in the brake pad. A Light interferometer was used to map the surface of a used brake pad revealing a large number of plateau showing signs of sliding contact with the disc rising above the main surface. It was proposed that the steel fibres provided a mechanically stable nucleation site for the plateau around which wear particle debris collected and built up. Although transient in size and form, it was proposed that the plateaus formed the real contact area between pad and disc and at only 20% of the nominal surface area gave a completely new insight into the tribological contact conditions. The

friction materials tested by Eriksson contained steel, glass and aramid fibres but only the steel fibres were held accountable for the contact plateaus. The work of Eriksson et al has been well referenced and will be discussed further in the Tribology section of this chapter. Steel fibres in friction materials offer a processing enhancement when combined with softer organic fibres as the harder, sharp steel fibres impact the organic fibres during high speed mixing modifying the morphology and also the bulk fibre network structure to the advantage of the manufacturer. Steel fibres are used extensively in the friction industry except in the Japanese market where manufacturers have chosen to eliminate the fibres from all formulations for brake dust and noise issues. Elsewhere, friction manufacturers realise a number of benefits from using steel fibres such as increased toughness, thermal conductivity, low wear and processing benefits if steel fibres are used in correct percentages.

Carbon fibres

A seemingly ideal choice for asbestos replacement thanks to a low density, high strength and excellent thermal and oxidation stability, carbon fibres have produced mixed results when tested in organic friction materials [20,21,53]. Carbon fibres comprise long carbon molecular chains yielding very stiff fibres with a high thermal conductivity, manufactured from fibrous precursors such as polyacrylonitrile (PAN), Rayon or other sources of pitch. Whatever source material is used, a lengthy and expensive manufacturing process involving oxidation, carbonisation and graphitization are required dramatically increasing the cost of the fibres. Used extensively in non-organic friction materials carbon fibres are far less successful when used with organic resins due to a combination of factors such as the complexity of organic friction materials, the thermal limitations of organic resins and different operating conditions. Organic friction materials containing carbon fibres tested under light load and speed displayed a steadily increasing friction level that could peak at twice the original intended value [21]. High loads and speeds decomposed the fibres to a graphitic structure resulting in an unpredictable lubricating effect. The combined study by Crosa et al [48] reported carbon fibre inclusions to give low pad and disc wear but also a lower than required coefficient of friction. A new carbon fibre known as Carboflex produced from pitch manufactured by Ashland Oil USA was tested for friction stability and

fade [50] and compared to a similar material containing asbestos. The carbon fibres imparted a higher fade resistance, greater stopping power, lower wear rate, and presented no manufacturing problems.

Carbon fibres are a raw material used in present day organic friction materials but not to the extent that represents an asbestos replacement. Their high cost and restricted performance window see only a number of brake pad formulations including carbon in a fibrous form. The high performance stability of the fibres in conjunction with a lower thermally stable resin is a major reason for their lack of performance, so carbon fibres will generally be found in brake pads designed for high performance cars. As a very fashionable high technology material, carbon fibres are used for branding and as a marketing tool to increase sales in sports applications.

Mineral and ceramic fibres

Two classifications of fibres have been grouped together in this section as they exhibit very similar thermal and mechanical properties compared to other fibrous materials used in brake pads. The fibres are thermal stable to temperatures well in excess of 1000 °C, are hard, offer high reinforcing properties to friction materials and are man made so fibre morphology can be controlled. The downside of the fibres are the energy intensive process used to manufacture that is reflected in the price, the brittle nature of the fibres posing manufacturing problems [21], associated brake noise [51] and in for certain fibres health implications similar to asbestos [52]. The mineral family of fibres – to which asbestos belongs – has grown to encompass a number of new man made fibres manufactured from naturally occurring and recycled materials. In repetition of the asbestos demand 80 years, new companies have been born out of the success of mineral fibres. Lapinus fibres, the world largest supplier of mineral fibres, manufacture their product by melting volcanic rocks and recycled minerals in a furnace and spinning into fibres. In certain formulations mineral fibres offer high reinforcement and reduced disc wear [38], but no processing benefits are gained from using the fibres.

Potassium titanate is a ceramic fibre that attracted a lot of interest in the 1990's due to a high thermal stability and compatibility with binder resins [42]. The poly-crystalline ceramic produces very fine whiskers which Kim et al [42] reported to show an excellent

friction and wear synergy in conjunction with aramid fibres. The fine whiskers have been reported [52] as a potential cause of mesothelioma which has the potential of taking this development full circle back to asbestos. In response the friction company Akebono has developed a method of producing powdered potassium titanate at considerable expense.

The high cost of ceramic fibres was approached by the research of Ozturk et al [43] who blended ceramic fibres with much cheaper basalt fibres and obtained empirical data from a pin on disc type testing machine. The results demonstrated that inclusion of basalt fibres increased the coefficient of friction and also reduced the specific wear rate up to a critical fibre content of 30% by volume. The work by Ozturk is an example of how fibres can be combined to exploit cost savings, mechanical and physical properties and a synergistic effect otherwise missed using single fibres.

Mineral and ceramic fibres offer high thermal stability and can impart high reinforcements and friction stability however they offer no processing benefits, are expensive to buy and can induce brake noise.

Organic fibres

Organic fibres have been of particular interest to friction material formulators ever since the removal of asbestos as this category includes a large number of readily available inexpensive materials which research has shown carry out a number of essential roles in the friction material [1,41,42,44,45,53]. The friction industry classifies any natural or man-made fibre based on carbon, hydrogen and nitrogen as an organic fibre. Examples include aramid, cellulose, acrylic (PAN), cotton, hemp, flax and jute. They should not be confused with the organic resin matrix from which NAO friction materials derive their name. As a direct substitute for asbestos, organics fail predominantly by limited a poor thermal stability and so are only popular in friction materials with low operating temperatures such as train blocks and low performance automotives. aramid is the exception to the organic classification in terms of thermal stability and will be discussed in detail in the next section. In comparison to the other classifications of fibres, organics are soft flexible fibres offering excellent processing and reinforcing characteristics for friction materials. Organic fibres lend themselves very well to recycling and a large number of recycled fibres are used to reduce costs in brake pads. Recycled paper is a source of cellulose used in friction

materials to aid processing and reduce costs [16]. Cotton is an organic fibre that is used in either virgin or recycled form – shredded denim jeans have been used as a source of inexpensive cotton for some manufacturers. Natural fibres represent an untapped market for organic fibres in the friction industry and have yet to be extensively trialled in friction materials. Other than the published work in this thesis, one other research paper has discussed the use of natural fibres in an automotive friction material and then only looked at one type. The research of Xin et al [54] varied the amount of sisal fibres in a simple friction material and evaluated the friction and wear levels as a function of temperature. The results highlighted a critical ratio between resin and sisal fibres of 3:4 for optimum wear resistance and ultimately recommended sisal as an alternative organic fibre in NAO friction materials. The volume of fibre used was relatively high (between10-30%) and a operating threshold temperature of 250 °C was identified as changing the wear mechanism of sisal fibres from an abrasive mechanical cutting action to thermal degradation. Longley's paper in 1988 [21] makes short reference to trials using Jute fibres in brake pads but only describes the frictional performance as inadequate. The wear of Bamboo sliding against cast iron was investigated by Tong et al [55] who reported the orientation of the fibres bundles within the Bamboo to have great influence on the wear rate. All other natural fibre types are of a cellulose construction and will be discussed in a later section.

Satapathy and Bijwe [44,46] evaluated a series of friction materials by varying the content of organic fibres and although only low concentrations of fibres were used (3%) a difference in the friction and wear behaviour was recorded between fibre types. Brake pads containing cellulose fibres (paper pulp) were reported to produce a higher coefficient of friction the greatest wear rates and also the most tendency to fade. The wear of the pads was attributed to a combination of shear and thermal degradation of the cellulose fibres at the pad surface. The samples containing PAN fibres were reported to be the least sensitive to changes in load and speed showed low wear rates attributed to a self lubricating action of the fibres and did not influence the fade resistance of the brake pad. The worn surfaces of the brake pads showed dissimilar topographies indicating the fibre type was responsible for changing the contact conditions and wear mechanism of the brake pad.

The use of acrylic fibres in friction materials has been heavily promoted by Sterling fibres USA [53] who developed a new product by fibrillating short acrylic fibres to aid the

manufacturing process. The fibres were sold alone or combined with more rigid staple fibres such as glass, melamine and acrylic. Sterling fibres' products use fibre blends to alleviate the mixing problems associated with stiff short fibres but more importantly to offer an alternative processing fibre to aramid pulp. The fibrillated acrylic fibres were sold at half the price of aramid, primarily as a processing fibre to be blended with other more thermally stable materials [53]. This was a key development for organic fibres in two respects showing that materials have added value for the manufacturing process by having the correct morphology and that thermal limitations can be balanced with other raw materials. Fibrillated acrylic fibres are an attractive alternative to aramid at half the price yet natural fibres offer a significant cost saving again, costing only a fraction of acrylic.
Organic fibres are used in virgin or recycled form, and in the morphology to suit processing and performance requirements.

Aramid fibres

Aramid fibres are the most heavily used single fibre in post asbestos friction materials and although classified by friction manufacturers as an organic fibre, the combination of high thermal resistance, strength and stiffness of aramid far exceed those of other fibres in the same category. aramid is of great significance to the work in this thesis representing the target fibre to be replaced with a natural occurring alternative. This section will explore the published research in friction materials but also the material structure and manufacture of aramid fibres to produce an overall picture of the material.
Aramid is a term coined to describe the family of aromatic polyamide materials developed in research laboratories in the 1960's. An aromatic polyamide consists of an aromatic (phenyl) ring and an amide group that combine and form the repeat units of the polymer. The location at which the amide group attaches to the benzene ring is of great significance to the structure of the polymer chains and resultant thermal and physical properties of the polymer. If the amide groups attach to the phenyl ring so they lie directly opposite one another at carbons 1 and 4, a para-aramid is produced and if they are attached to carbons 1and 3 a meta-aramid is made. Figures 2.3 and 2.4 show para-aramid and meta-aramid structures respectively.

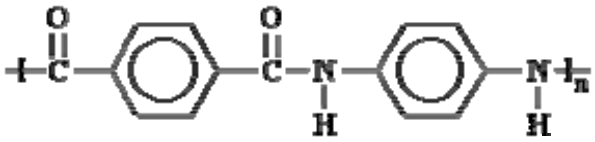

Figure 2.3 Para-aramid

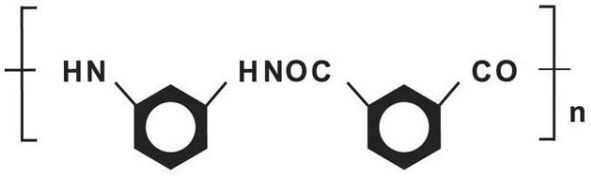

Figure 2.4 Meta-aramid

The aromatic ring structure gives both meta and para aramid a high thermal stability but the two types differ in mechanical properties due to the ordering of the molecular chains [57]. The Para configuration allows the same amide groups to form a trans conformation along the backbone of the structure to produce long straight polymer chains ideally suited to form fibres. A close packing of the polymer chains is possible which gain extra strength from hydrogen bonding between opposing oxygen and hydrogen atoms as shown in figure 2.5 giving para-aramid much higher strength and stiffness compared to meta-aramid.

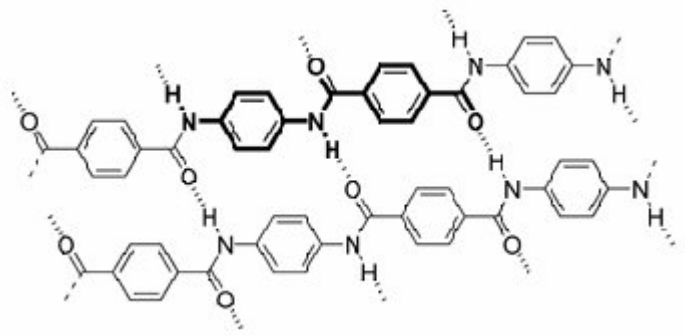

Figure 2.5 hydrogen bonding between para-aramid backbone chains

Para-aramid fibres are extensively used in the friction industry in the form of two heavily patented materials. Two companies manufacture the fibres under closely guarded processes

to produce Kevlar by DuPont and Twaron by Teijin. Teijin produces Para-aramid fibres by reacting para-phenylene diamine and terephthaloyl dichloride in N-methly pyrrolidone to produce poly para-phenyleneterephthalamide [56]. The reactant polymer crystallises into granules that are insoluble in most solvents except for concentrated sulphuric acid. Hot concentrated sulphuric acid is the solvent used to dissolve the granules into a 20% anisotropic liquid crystalline solution ready for spinning into fibres. The hot solution is extruded through a spinneret which orients the liquid crystal domains into a nematic state, parallel to the spinning direction. The solution passes through a small air gap into a coagulating water bath where the polymer crystallises before being wound onto bobbins and dried to remove excess water. Spinning the polymer into fibres aligns the molecular chains in the fibre axis direction to produce a highly aligned anisotropic fibre with a high strength and modulus in the axial direction but poor in the transverse direction. The modulus of aramid can be further increased if required by heat treating fibres under tension to produce a more ordered crystalline molecular structure within the polymer. Higher modulus fibres have applications such as ballistics protection and ultra stiff composites. The friction industry use aramid fibres in the lowest modulus form as high specific strength and modulus are not required in brake pads.

All aramid fibres are manufactured as mono filaments which can be subsequently woven into fabrics, chopped into short fibres or pulped to produce highly fibrillated short fibres for use in the friction industry. Aramid pulp was originally produced as a by-product from other fibre handling and processing activities but was discovered to perform very favourably in friction materials and included into most NAO brake pad formulations. Increased demand for aramid pulp from the friction industry saw intentional manufacturing of the material using a highly controlled and closely guarded fibrillation process. Chopped fibres are place in a water suspension and fed into a mechanical grinder that mechanically fibrillates individual fibres by generating small fibrils along the length of the main fibre surface. The degree of fibrillation is determined by energy input from the mechanical grinder but fundamentally takes advantage of a differential skin core structure on aramid fibres that is introduced during the manufacturing process. This structure was first observed by Morgan et al [57] who identified a skin along the fibre length having a lower crystalinity and more random crystallite arrangement compared to the core. The crystalline structure of

the skin promotes crack propagation along the fibre length and not in the transverse direction thus generating high aspect ratio fibrils. The presence of a skin ranging in thickness of up to 1 μm was confirmed by other researchers [58-61] using a range of analytical techniques such Scanning Electron Microscopy, Transmission Electron Microscopy and Interfacial Force Microscopy. The skin/core structure is formed when the polymer solution enters the coagulation bath and experiences a much higher rate of cooling rate at the surface of the fibre than in the core. Higher cooling rates and residual stresses imposed by the spinneret capillary contribute to the production of a skin structure possessing a lower crystalinity than the core but with more structural integrity in the fibre axis direction. The skin structure on aramid fibres was exploited by Padmanabhan et al [62] when fabricating aramid reinforcing epoxy composites. The authors exposed aramid fibre surfaces to acidic solutions to alter the surface morphology thus increasing the mechanical interaction between fibre and resin and the fracture toughness of the composite.

In friction materials, aramid has been shown to provide excellent processing properties in a similar manner to asbestos fibres [2,3,42,47,63] by providing a good filler retention and imparting excellent strength to pre-forms – these manufacturing terms will be discussed in detail in section 4.2.4. Kato and Magario [64] reported that short (≈ 2 mm) aramid fibres decreased both wear rate and the level of friction compared to virgin phenolic resins. The lowest wear was related to high inclusions of fibre (40 % by vol) and the friction level reached a steady state for fibre volumes ≥ 15%, highlighting that friction and wear properties could not be independently controlled by a single fibre. The authors attributed the friction and wear results to the effect of a strong, stable transfer film on the friction surface produced by the inclusion of aramid. Gopal et al [45] produced friction materials from aramid and blends of aramid, glass and steel, reporting on the friction and wear performance using a small scale testing machine. aramid pulp was reported to lower and stabilise the friction level, reduce the wear rate and eliminate noise, regardless of the other fibres in the composite. The authors also proposed a transfer film produced by the aramid pulp as responsible for these effects.

Briscoe et al [2] investigated the friction behaviour of aramid fibres in both phenolic and epoxy resin composites and concluded that aramid fibres were responsible for a transfer film that served to lubricate the friction couple. The authors proposed that the lubrication

effect of aramid made the fibres unsuitable for use in friction materials as the sole fibrous material.

Kim and Jang [3] investigated the effect of aramid pulp with modified phenolic resins and compounded previous research by demonstrating a stabilising effect from aramid on the friction level, this time showing no benefit of inclusions higher than 10% by volume. Kim's subsequent research paper [42] blended aramid pulp with potassium titanate in various ratios to investigate the friction and wear rate and repeated previous research to show aramid as a wear inhibiting material. The wear resistance of aramid fibres in polymers and composites has also been reported beyond materials used in the friction industry. Bijwe et al [64] investigated the friction and wear of polyethersulfone sliding against silicon carbide paper and reported that inclusion of aramid fibre increased the wear resistance of the composite by a factor of 9.5 as a result of fibrillation and elongation mechanics of the aramid fibres. The orientation of the fibres was reported to be of significance to the wear coefficient with fibres normal to the rubbing surface demonstrating the highest wear resistance. Yu and Yang [65] combined aramid fibres with polyphenylene sulphide to report over a five fold reduction in the wear rate compared to the virgin polymer when sliding against tool steel. Samples containing aramid established a transfer film between sample and counter face which the authors proposed was responsible for the greater wear resistance.

Aramid pulp is marketed by Teijin under the trade name Twaron as a range of products with varying fibre lengths and degrees of fibrillations for use in friction materials gaskets and paper.

Table 2.2 list the typical physical properties of Twaron as supplied by the Teijin [66].

PROPERTY	UNIT	VALUE
Density	gcm^{-3}	1.44
Tensile strength	MPa	2800
Young's modulus	GPa	80
Elongation at break	%	3.3
Thermal decomposition	°C	>500
Thermal expansion	$10^{-6}K^{-1}$	-3.5
Specific heat capacity	$Jkg^{-1}K^{-1}$	1420
Thermal conductivity	$Wm^{-1}K^{-1}$	0.05

Table 2.2 Typical properties of Twaron fibres

The fibre pulps sold to the friction industry are of most interest to this work and the product range is detailed in table 2.3 Pulp 1099 is the type used in this research and a more detailed specification will be given in a later section.

Twaron pulp type	Fibrillation	Fibre length
1095	medium	Medium
1099	high	Long
3091	high	short

Table 2.3 aramid pulps sold by Teijin

Teijin heavily market their products claiming numerous performance enhancing benefits to automotive friction materials in their promotional literature [66] and are listed below;

- Processing enhancement – filler retention, pre-form strength
- Stable coefficient of friction
- Reduced wear of brake pad
- Reduced wear of brake disc

- Reduced noise and vibration
- Provides reinforcement to friction composite
- High thermal stability

The performance of aramid fibres with respect to the above criteria has been discussed in the literature review demonstrating the multifunctional role of aramid fibres in friction materials. The demands on aramid fibres vary between friction materials depending on a number of factors such as manufacturing method, remaining raw materials and end use of the brake pad. Aramid pulp is selected in some formulations primarily for processing benefits and in others for friction and wear characteristics. Candidate replacement materials will have to match or exceed the performance of aramid in the key performance categories which incidentally are not always clear cut. The success of a material may only be limited to one specific formulation because of the complex thermal, physical and chemical interactions taking place in friction materials. Evaluating the performance of aramid in one automotive friction material to establish the benefits gained from the fibres will produce a baseline specification against which any replacement fibres can be judged. A scientific research methodology will certainly exceed that of empirical methods used by the friction industry as will be shown in the next section describing the analysis of friction materials.

2.1.5 Testing and analysis of friction materials

In the previous section, the function of various raw materials was discussed in terms of the thermal stability, friction levels and wear rates. The performance of brake pads is the result of a combined effect of numerous raw materials, the complexity of which is reflected in the analytical methods used to understand the tribological system.

At the start of the 20th century friction manufacturers used on-vehicle tests to evaluate new materials [20]. Testing between companies was very disjointed partly due to the lack of technology and also the absence of any industrial standards. Through the 1960's and the advent of strain gauges, high speed chart recorders and the microprocessor, friction material testing has developed in line with the friction materials themselves.

Regulation 90 [67] is a quality standard controlling the UK friction industry defining the minimum standards of friction, wear and mechanical performance for all friction materials. Time and financial pressures force brake pad manufacturers into doing only the minimum testing required to exceed to the standard whereas scientific researchers use a more refined methodology and a combination of techniques. The two approaches complement one another and manufacturers frequently sponsor academic research projects.

Friction and wear are the real acid test for brake pads and vehicle testing provides the service conditions experienced by a brake pad. As a sole development tool, on-vehicle testing is impractical due to the associated costs and difficulty in achieving repeatability over a sustained test. Instead inertial dynamometers are used to perform a series of controlled braking procedures while the coefficient of friction, brake pressure and disc temperature are computer monitored. Costing in excess of £100,000 an inertial dynamometer is the most sophisticated and flexible friction and wear evaluation tool available to the industry however it is not without errors. Slevin and Smales [68] reported a number of errors associated with dynamometer testing and modern machines are programmed to take into account rolling resistance and wind drag, variable vehicle loading, and gradient effects. Industry acknowledged test procedures such as the AK Master test will be discussed in the methodology section later in the thesis.

Smaller scale friction and wear testers are employed by industry and academic researchers [3,24,42,46,69-76] where cost and space do not permit an inertial dynamometer but predominantly as screening tools as the mechanical and thermal loadings experienced by brake pads do not scale down with machine and sample size [77].

Mechanical testing for the industry involves a compressive and a shear test to confirm compliance and structural integrity. The final stage of testing is usually an on-vehicle test driven by an experienced member of the R&D team who looks for any unwanted vibrations, noise and unexpected phenomena.

Scientific research papers focus on the mechanisms associated with the friction and wear and employ a wide range of analytical techniques to investigate the friction surface. High magnification microscopy is extensively used to explore the surface of worn friction materials and relate topography, surface features and elemental composition to friction performance. Light microscopy is used for both high magnification and to identify

dispersion and location of raw materials on the friction surface. Polarizing filters enable the identification of anisotropic materials such as coke [25] and fluorescence is used to distinguish organic materials such as aramid fibres and phenolic resin [25,66]. Interferometers have been used [33] to quantify three dimensional surface features and also atomic force microscopy for even higher 3D resolution [28].

Scanning electron microscopy (SEM) is the technique most widely used [25,29-31,33,78-81] to produce high magnification and resolution images of friction surfaces and the ability to use elemental analysis (EDAX) on sites of interest has proven to be a powerful research tool. A Transmission electron microscope (TEM) with x-ray diffraction capability was used by Osterle et al [26-31] to identify material phases in cross sections and wear particles of brake pads. X-ray diffraction was also used by Weiss et al [25] to identify different crystalline forms of carbon in a composite friction material.

Focused Ion Beam (FIB) instruments have been employed by Osterle et al [82] to image frictional surfaces and highlight regions that have experienced high mechanical stresses.

Auger Electron Spectroscopy allows sub surface identification of elements in a material and was used by Gudmand-Hoyer et al [29] to report on the migration of heavy metal lubricant from the brake pad into the brake disc.

Thermal analysis encompasses a family of techniques that are often used to predict raw material performance or investigate pad wear residues. Simultaneous thermal analysis (STA) was used to characterise the thermal events associated with various solid lubricants [83,84] by monitoring mass loss and heat flow under a controlled temperature profile. Ingo et al [78] used STA to comment on interface braking temperatures by referencing thermal transitions of the wear particles to those of virgin raw materials to predict the maximum interface temperatures experienced.

Characterisation of raw materials is carried out by material suppliers who simply provide manufacturers with a specification sheet according to the individual materials. Powders chips, flakes and other morphologies are analysed for average particle size and size distribution using methods such as laser diffraction and optical microscopy. The majority of fibrous materials are sold with only the average fibre length quoted, especially in the case of recycled materials. Virgin aramid is quality controlled by the manufacturers using specialised fibre analysis machines costing in excess of £100,000 to give fibre length

distribution and specific surface area in m^2g^{-1}. Composite brake pads are frequently tested for mechanical properties before friction and wear testing. In addition to the industry standard compression and shear testing, research papers often quote flexural strength, hardness and porosity when performing comparative studies between materials. Other physical measurements taken from composite brake pads are density, thermal conductivity, thermal expansion and specific heat capacity.

The number of analytical techniques used to investigate brake pads reflects both the complexity and diversity of friction materials. Testing methods are employed to further understanding in respect to all stages of brake pad manufacture, from raw materials through to inspection of worn surfaces. Most attention is focused to the performance of the bulk friction material and raw material effects are often discussed as a function of this. This is especially valid for fibrous materials that are analysed for thermal stability and basic morphology and subsequently discussed on performance as a function of the bulk friction material. While this is valid for the friction performance of fibrous materials, no in depth study has been published on the role of fibrous materials in the processing and manufacturing stages of brake pads. Manufacturers of aramid and acrylic fibres [53,66] have published data indicating processing benefits of using their fibres but only at a very basic level and no in depth study exists on the performance of fibres as processing aids as a function of morphology and fibre types. This leaves a gap in knowledge regarding the mechanical properties of fibrous materials and how this is exploited during the mixing and manufacture of friction materials. The fundamental mechanics behind the strength of fibre pulp and how this is derived from fibre structure, morphology and fibre interactions with one another are key to bridging this gap in knowledge. This work will research the physical structure and fibre pulp mechanics to identify the performance of fibres in the manufacture of friction materials. Friction and wear analysis will allow the in-situ performance of the fibres at the friction interface to be evaluated.

2.2 Tribology

Tribology is derived from the Greek word tribos (τριβοσ) meaning rubbing or attrition and is now a generally accepted term defined as [85] "the science and technology of interacting surfaces in relative motion" studying the mechanisms of friction, lubrication and wear. Friction is a phenomenon commonly taken for granted as simple everyday tasks such as walking and placing a cup of tea on the table rely on the coefficient of friction between two surfaces. Friction between surfaces is often undesirable and billions of Pounds are spent per annum reducing friction and wear in industrial equipment and machinery through design, lubrication and maintenance processes. Reduced friction in machinery prolongs component life, retains design tolerances and minimises frictional losses between rotating parts and the net energy consumed by a mechanical system Any mechanism involving friction will be subjected to wear – the progressive lost of material from a surface – and it will be shown that even extremely smooth surfaces are subject to friction as a result of asperity contact on a microscopic scale. Wear of friction materials is an inevitable process intentionally tailored by friction manufacturers to satisfy consumers while maintaining a high level of replacement pad sales. Predictable, progressive wear is also an important feature of friction materials.

2.2.1 Theories

Friction

When viewed on a short enough length scale it becomes apparent that all surfaces, even those polished to a mirror finish are not perfectly flat but composed of peaks (asperities) and troughs. When two surfaces come into contact it is the asperities that carry the load forming the real contact area which is far smaller than the nominal surface area of the surfaces. The real contact area can be increased by either reducing the hardness of the material or increasing the normal load between the surfaces, so for a given material, the contact area is proportional to the normal load.

Before two surfaces can slide relative to one another two frictional forces have to be overcome and exceeded if the surfaces are to remain in relative motion. The first is an adhesive force produced by attractive forces and plastic deformation of material between

the asperity contacts. The second is a deformation force needed to plough asperities of the harder material through the softer material so the coefficient of friction between two surface is the sum of an adhesive (μ_{adh}) and deformation coefficient of friction (μ_{def}) thus;

$$\mu = \mu_{adh} + \mu_{def} \tag{2.1}$$

Hutchings [85] modelled asperities as simple cones with very shallow internal point angles (>160°) to show that μ_{def} can be expected to be less than 0.1 implying the adhesive component to dominate as the expected frictional force if greater than 0.3 for most materials. The adhesive component of the frictional force is the product of the shear strength (all assumed to be identical) and the number of asperity junctions;

$$F_{adh} = \tau A \tag{2.2}$$

Where

τ = shear strength of asperity junctions

A = total area of asperity junctions (real contact area)

The load (L) supported by the asperities can be related to the yield stress of the material (σ) and the area A giving;

$$L = \sigma A \tag{2.3}$$

Combining equations (2.2) and (2.3) and simplifying confirms Amontons' first law of friction.

$$\frac{F_{adh}}{L} = \frac{\tau}{\sigma} = \mu_{adh} \Rightarrow F_{adh} = \mu L \tag{2.4}$$

Polymeric materials introduce additional complexity into the friction of surfaces as the asperities are able to undergo large elastic deformations and exhibit visco-elastic behaviour.

For elastic contact between asperities it is expected that [85];

$$\mu \propto \frac{A}{L} \propto \frac{L^{2/3}}{L} \propto L^{-1/3} \tag{2.5}$$

This shows that as the normal load increases the coefficient of friction falls because the real contact area is no longer proportional to the load – a fundamental relationship described by Hertzian contact mechanics.

.

The coefficient of friction between two surfaces is influenced by a number of parameters, most of which are interrelated. Mechanical properties of the materials have a governing effect but the friction level is dependent on temperature, sliding speed and lubrication, thus the friction levels are only constant for a given set of conditions. The complexity of designing and analysing brake pads is therefore illustrated by appreciating not only the great range of operating speeds, temperatures and lubrication levels experienced during service but also the diversity of materials used. Composite friction materials are especially difficult surfaces to predict as the hardness of the raw materials ranges from soft polymeric resins of around 0.2 GPa up to 10 GPa for abrasive mineral particles [72].

The tribology of brake pads and current research work is discussed in section 2.3

Wear

Wear is a phenomena resulting from the friction between two rubbing surfaces, therefore brake pads exhibiting high friction levels could be assumed prone to high wear. Fundamental wear mechanism will be covered briefly before more complex wear mechanisms of modern friction materials are discussed.

Two surfaces in contact and sliding relative to one another can produce a range of physical and chemical processes that result in wear – the progressive loss of material from a surface. Sliding wear is determined by the contact pressure between the surfaces, the sliding velocity and the time of contact between the surfaces. Any variation in these parameters can alter the wear rate by changing the wear mechanism which in turn can lead to more friction generated heat and a positive feedback on the wear rate. Ambient conditions such

as temperature strongly influence the wear rate by inducing thermal or chemical process and humidity has a strong affect by introducing lubrication between the surfaces by means of water vapour. The two major wear mechanisms associated with brake pads are adhesion and abrasion which will be discussed in this section.

Sliding wear

Archard [86] proposed that sliding wear takes place during the formation and destruction of asperity junctions, the area of which is proportional to the volume of material worn away. The Archard wear equation relates the wear volume per unit distance (*V*) to the yield stress of the material (σ_y) thus;

$$V = \frac{kL}{3\sigma_y} \tag{2.6}$$

The proportionality constant (*k*) is often combined with the numerical term (1/3) and referred to as the wear coefficient (*K*), a dimensionless coefficient between 0 and 1. The Archard equation (2.6) represents a way of comparing the magnitude of wear in materials based on the applied load and the reciprocal of the yield stress of the softer material. In practice materials tested experimentally show a good match to the Archard wear equation demonstrating a wear proportional to the sliding distance but this is not so for the relationship to the applied normal load [85]. Metals in particular show a critical load at which the wear increases dramatically due to the stability of naturally forming hard oxide layers between the two surfaces which if removed, change the wear mechanism and hence the wear rate. The wear mechanism of metals has also been shown [85] to vary with velocity and time with the main contributory factors being mechanical stresses, temperature and oxidation phenomena making it difficult to predict the wear rate if any number of operating parameters are changed.

Polymers demonstrate a similar adhesive wear mechanism to metals if the rubbing counter face is smooth and show a linear relationship over a greater normal load range than metals thanks to the higher bond strength between counter face and wear debris [85].

The effect of temperature on sliding wear is of greatest importance to materials whose mechanical properties are markedly temperature dependent e.g. polymers as the temperature will dictate the wear mechanism. Thermal softening of polymers dramatically increases the wear, therefore interfacial temperatures are intentionally kept low by either limiting the sliding speed or increasing the thermal conductivity of the counter face to remove heat from the interface [85]. Natural or synthetic polymers with an amorphous content will undergo a phase change at a characteristic temperature known as the glass transition temperature (T_g). Below the T_g polymers are glassy and stiff with asperity interfaces weaker than the polymer bulk and so undergo fatigue and abrasive wear mechanisms [85]. Above the T_g polymers are soft and easily transfer material to a counter face by adhesive mechanisms. The adhesive junction between the polymer and sliding counter face is stronger than that of the polymer therefore wear results from failure within the bulk of the polymer leaving a transferred particle on the counter face [85]. Particles from the bulk polymer build up forming a transferred layer that becomes the rubbing surface against the original polymer. Material transfer between similar polymers is very slow therefore the wear rate in polymers is strongly influenced by the existence of the transfer layer and the strength of adhesion between the layer and the counter face [85].

Abrasive wear

Abrasive wear differs from adhesive wear by employing hard particles to remove material from a softer surface by a ploughing or abrasive action. Abrasive wear is affected by the hardness ratio of the materials in contact and also by the location of the harder particles. Hard particles embedded within a surface or also protrusions of a hard counter face give rise to an abrasive wear known as two body wear an example of which is sand paper. Hard particles moving freely between two surfaces results in third body wear which again is undesirable and an example of which may be lubricated systems containing harder contaminant particles.

The ratio of hardness between materials is significant when it approaches the critical value when the hard particle starts to plastically yield under an applied pressure. The critical ratio of the hard particle to the softer surface is ≈ 1.2 and defines the hardness required for abrasive wear and also the basis of Mohs scale of hardness [85].

The contribution of the adhesive and deformation forces for a composite friction material are determined by a large number of parameters as shown in figure 2.6 [1] illustrating the complexity of the tribological interface. Simply removing one type of material from a formulation can upset a delicate design balance by altering material contact conditions and wear mechanisms. If friction materials are to be successfully developed by substituting materials, it is pertinent to firstly establish the effect of removing a material before replacement performances are established.

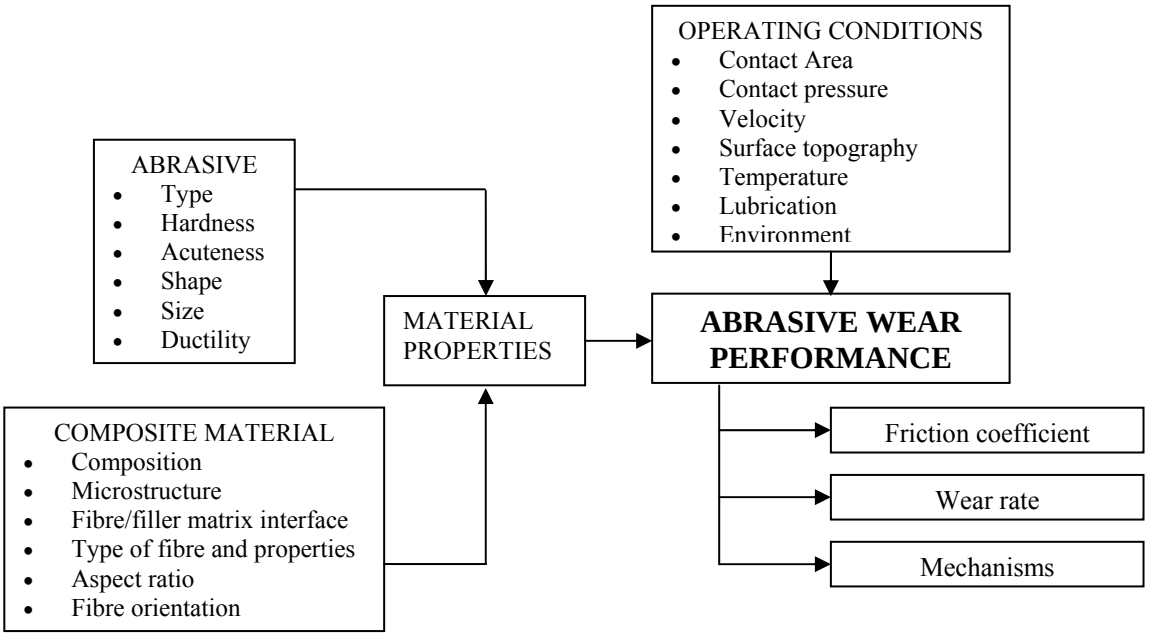

Figure 2.6 Parameters affecting friction and wear performance of sliding abrasive wear [1]

2.3 Tribology of friction materials

Friction and wear theory assumes homogenous materials so a composite brake pad containing 10 or more raw materials introduces a great deal more complexity to the tribological system. Raw materials differ in hardness, particle morphology, and thermal stability producing individual frictional and wear characteristics whilst operating simultaneously with one another. This makes the performance of one single material impossible to predict prior to testing [1,28]. The frictional heat generated during braking produces flash temperatures in excess of 1200 °C [87] that induce physical and chemical changes in the brake pad, the nature and extent of which affect the frictional performance.

Abrasive and adhesive wear dominate friction materials until a characteristic temperature for the friction material is reached [88] when the wear rate rises exponentially due to thermal degradation. Figure 2.7 clearly shows this relationship [4].

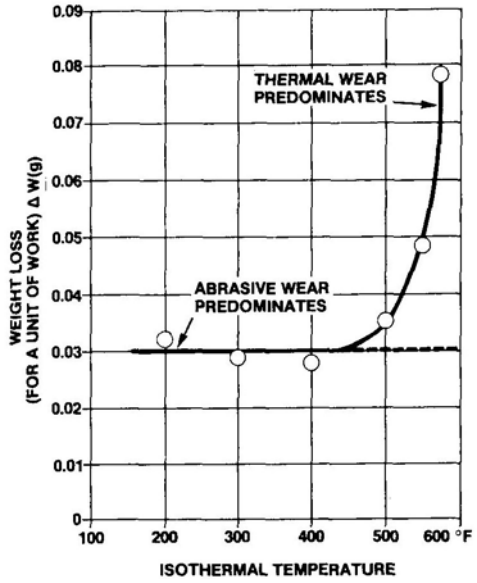

Figure 2.7 predominant wear mechanisms of friction materials [4]

Of significant importance to the friction performance is the thermal stability and degradation reactions of the organic resin matrix in the brake pad [89]. Certain phenolic resins were identified [90] as evolving volatile gases during degradation causing a back pressure on the brake pad resulting in brake fade. Other less thermally stable resins were identified as producing oily residues that again contributed to brake fade [91]. This highlights the necessity for thermally stable raw materials that will not evolve friction destabilising by-products during thermal degradation and represents one of the unanswered questions regarding natural fibres as a raw material in brake pads.

The thermal dependency and synergistic effect of composite brake pads makes the Archard wear equations insufficient to describe wear rates. Rhee [92] proposed a relationship between the mass loss (ΔM), Normal load (P), sliding speed (V), and time (t) to predict the wear under fixed conditions.

$$\Delta M = \alpha P^a V^b t^c \tag{2.7}$$

Where α is a dimensionless wear constant and a, b and c are experimentally determined parameters for a given friction pair. Any change in material composition will require the exponents to be determined again experimentally. The wear of the friction material in (2.7) is given as a mass loss as linear dimension changes are muddled by swelling and thermal expansion of composite materials. Since Rhee's wear equation was proposed in 1971 the friction and academic industry have adopted a common term for comparing the wear performance of friction materials by normalising the wear amount by the given friction energy. Equation (2.8) shows the typical formula used for evaluating the wear performance of friction materials when tested on sub scale machines such as Chase testers.

$$W = \frac{\Delta m}{dL\rho} \tag{2.8}$$

Where;

W= wear rate (m^3/Nm)

Δm= mass loss (kg)

d = sliding distance (m)

L = Normal load (N)

ρ = density of friction materials (kg/m^3)

As an organic friction material slides against a cast iron counter face, adhesive and abrasive wear mechanisms reduce the surface roughness of both disc and friction material until a steady state of wear is reached. The time taken for this to happen depends on the material structure, the initial surface roughness, the applied pressure, rubbing speed and interface temperatures. During the transitional period the friction level is variable as a transfer layer – also known as friction film – is formed between pad and disc as the product of compacted wear debris. As the softer of the tribological couple the brake pad mostly contributes to the composition of the friction layer although transfer of material from the cast iron disc does occur [4]. It is well accepted that the presence, composition and stability of the friction film is fundamental to stable friction, wear and noise suppression [29,31,33,80-84,93,94].

Ostermeyer [95] referred to a brake pad composition as “a warehouse for the friction process to build up structured layers in the contact zones” signifying the importance of the existence and stability of these structured layers/friction films. Wirth et al [93] examined the structure and morphology of friction films on automotive brake pads and concluded the composition of the film to have much greater influence on performance than physical parameters such as film thickness and topography. As a compacted alloy of wear debris from the brake pad, the composition of the friction layer depends on the raw materials used, their volumetric inclusion and stability under high temperatures and mechanical loads. Numerous raw materials including solid lubricants such as graphite and metal sulphides are selected in modern formulations for contribution to the friction film. As discussed in section 2.1.4 aramid fibres have been reported to add shear strength and thermal stability to friction films which may be lost if the fibres were removed in the composite. Any change in the friction film as a result of reduced aramid fibre volume or the introduction of natural fibres will manifest itself in friction and wear behaviour of the new composites.

A complete analysis of the formation, stability and influence of friction films on friction material performance is beyond the scope of this thesis so the intention of this section is an appreciation of the fundamental tribological mechanisms associated with brake pads and the role that fibrous materials play.

2.4 Natural Fibres

The classification of natural fibres describes a wide range of fibrous materials derived from Animal, Vegetable or Mineral sources. Mineral fibres, the most prominent being asbestos, are generally metamorphic or re-crystallised mineral rocks and no longer used in brake pads due to their carcinogenic effects as discussed in a previous section. Animal fibres such as hair, silk or wool are protein based structures combined with other waxes, fats and oils and for numerous economic and performance failings do not represent candidate fibres for trials in friction materials. Vegetable fibres are based on cellulose, a virtually inexhaustible substance produced naturally by plants. Only a relatively small proportion of the world’s cellulose is in a useful fibrous form, which even then, forms an integral part of plant crops such as hemp, flax, jute, kenaf and sisal. Of the 100-200 fibre producing plants world wide

only 15-25 are suitable for commercial fibre exploitation [96]. Cellulose fibres are high in tensile strength and stiffness due to the high degree of natural molecular orientation in the fibres but are also susceptible to water uptake and attack by micro-organisms. Compared to a commonly used synthetic fibre such as E-glass, natural fibres are a match in terms of mechanical properties and sometimes superior when compared on a density specific basis [97-99]. Table 2.4 [100] lists the mechanical properties of some natural fibres in relation to those of E-glass

PROPERTIES	GLASS	FLAX	HEMP	JUTE	SISAL
Density gcm^{-3}	2.55	1.4	1.48	1.46	1.33
Tensile Strength MNm^{-2}	2400	800-1500	550-900	400-800	600-700
E Modulus (GPa)	73	60-80	70	10-30	38
Specific (E/density)	29	26-46	47	7-21	29
Elongation at failure (%)	3	1.2-1.6	1.6	1.8	2-3

Table 2.4 Mechanical properties of natural fibres [100]

Analogous to the plants themselves, the natural fibres differ in chemical, physical and growing characteristics influencing the physical properties and cost of the fibres and also the number of practical applications. Natural fibres as an industrial material are faced with the challenge of a consistent and sustainable supply of high quality fibres from a naturally growing and environmentally variable plant.

2.4.1 Classification and life cycle of natural fibres

Man's use of natural fibres dates back thousands of years with examples of 8^{th} century BC flax twines and fishing nets [100] and higher profile examples found in Tutankhamun's tomb dating back to 1250 BC as well preserved linen curtains [101]. The Aztecs used sisal fibres to weave into a cloth for clothes and Scandinavians have used nettles for thousands of years to manufacture sails for ships [101]. Hemp is one of the most commonly known natural fibres and has been grown in Asia and China for over 6000 years making it one of

the oldest cultivated plants. Historically, hemp fibres have successfully been used to manufacture a variety of products such as twines, ropes, clothing, sacks, canvas and paper.

In contrast to the man made fibres used in brake pads which are born in laboratories and manufactured to well defined specifications, natural fibres are an integral part of a naturally growing composite plant structure with inherent natural flaws and influenced by numerous environmental and climatic growing conditions.

Figure 2.8 [100] shows the classification of natural fibres with specific emphasis on the vegetable fibres as these represent the candidate replacement fibres used in this research work. The first sub-division of plant fibres used by botanists is according to the number of embryonic leaves (cotyledons) in the plant. Vegetable fibres are subsequently classified according to the location of the fibres in the plant – bast, leaf and seed – these being the commonly used terms.

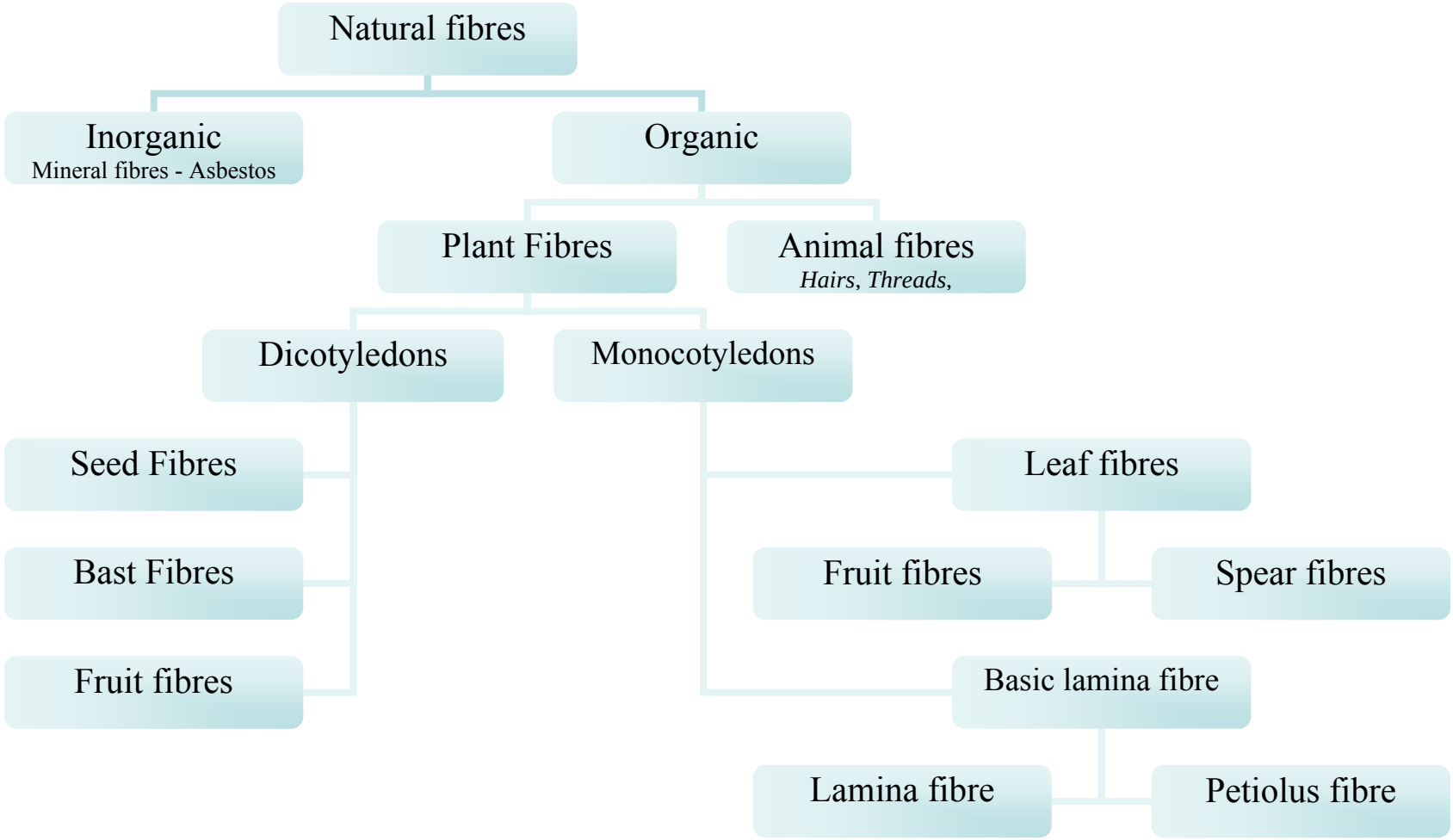

Figure 2.8 Classification of natural fibres [100]

For a natural vegetable fibre to be a viable industrial material the following economic and performance issues must be addressed.

- The pertinent properties of the fibres must equal to or exceed those of the existing material for the given product and process.
- The annual yield of the plant crop and fibres within the plant must be large enough to meet demand and repeatable every time.
- The method of extracting the fibres from the plant must be economical and not damage the fibres themselves.
- The overall cost of the fibres must be competitive with existing materials
- The preferred growing climatic conditions of the plants, eg is a plant limited to tropical climates.

2.4.2 Structure and processing of natural fibres

Variability in natural fibres is a significant difference to synthetic materials with changes in climate, soil type, fertilisation, cultivar and cultivation area all affecting the quality and homogeneity of the fibres [102]. In addition to the natural variability in structure, natural fibres require various processes to isolate the technical fibres from the plant and care must be taken as each fibre extraction stage can alter the fibres significantly [103].

Plant fibres are composed mainly of cellulose, hemi-cellulose, lignin and low amounts of waxes and other minerals, the relative proportion of which are characteristic to the species of plant. Cellulose is the largest naturally occurring polymer composed of repeating glucose units ordered in a highly crystalline manner in the form of micro fibrils up to 6 μm in length [102]. The high tensile strength of cellulose is the primary function of the fibres in the plants. Hemi-cellulose is a heterogeneous polymer that provides a linkage between the cellulose and lignin molecules in the plant. Hemi-cellulose polymer chains are branched increasing the accessibility of hydroxyl groups and as such the hydroscopic nature of the vegetable fibres. Lignin is a three dimensional amorphous polymer with a high molecular weight, that is insoluble in most solvents providing natural protection to plants from pathogens and herbivores [102]. Derived from the Latin for wood, lignin is a natural thermoplastic that cements the cellulose fibres in bundles giving plants rigidity and the

fibres characteristic colour. To make use of the cellulose fibres the lignin is removed from the plants by biological or chemical means before the fibres are mechanically processed. Table 2.5 shows the typical chemical structure of a range of natural fibres [100].

FIBRE	CELLULOSE	HEMI-CELLULOSE	LIGNIN	PECTIN	FAT/WAX
Bast fibres					
Hemp	67-75	16-18	2.9-3.3	0.8	0.7
Flax	62-71	16-18	2.0-2.5	1.8-2.0	1.5
Jute	59-71	12-13	11.8-12.9	0.2-4.4	0.5
Ramie	68-76	13-14	0.6-0.7	1.9-2.1	0.3
Leaf fibres					
Sisal	66-73	12-13	9.9	0.8	0.3
Abaca	63-68	19-20	5.1-5.5	0.5	0.2
Seed fibres					
Cotton	92-95	5.7	0	1.2	0.6
Coir	36-43	0.2	41-45	3-4	

Table 2.5 Chemical composition of various natural fibres [100]

Natural fibres benefit from a strong "green" image which encourages their use by consumer aware organisations such as the automotive industry. Natural fibres are easy to handle and do not present the respiratory and dermal irritations associated with glass fibres [104]. The fibres are carbon neutral materials that do not use hydrocarbon reserves to produce and actually reduce environmental CO_2 levels during plant growth. The entire plant is bio-degradable and bast crops such as hemp and flax use disregarded leaves and flowers to fertilise the soil for future crops [102]. According to a 1996 report from the German Institute for Energy and Environmental Research, each kilogram of hemp fibre replacing glass in automotive car panels saves 1.4 kg of CO_2 [100]. Wambua et al [98] used a range of bast and leaf fibres to reinforce Polypropylene and reported the mechanical properties of hemp reinforced samples to exceed those with glass fibres. Date palm fibres were

successfully combined with a phenolic resin and vacuum moulded into composite panels exhibiting a high dimensional stability and tensile strength [105].

The main drawbacks of natural fibres in such applications are poor wettability, incompatibility with certain polymeric matrices and high moisture absorption [103]. Moisture uptake by the fibres is due to an inherent polarity from the abundance of hydroxyl carboxylic groups on the fibre surface, which can be eliminated with various pre-treatments [97]. The addition of silanes, maleic anhydride and other coupling agents eliminate the undesirable functional groups significantly increasing the interfacial bond strength between fibre and matrix [106]. Continuous natural fibre reinforced composites were tested by Herrera et al [107] who reported an increased stiffness of the HDPE matrix of over 300% when using 46% w/w Henequen fibres and a silane coupling agent. Arbelaiz et al [104] compounded short flax fibres with polypropylene grafted with maleic anhydride to demonstrate how the chemical modification increased the fibre interfacial shear strength and reduced the water uptake of the fibres. A similar increase in interfacial bond strength was observed by Aziz et al [108] after alkali treating hemp and kenaf fibres with sodium hydroxide, however the authors noted a combination of desired mechanical properties could not be obtained simultaneously and that the composite must be tailored for the required mechanical properties.

Natural fibre composites using a cellulose fibre to reinforce a thermoplastic matrix have been produced for the automotive industry on an industrial scale since the mid 1980's [100]. A common misconception is that natural fibres were used to replace glass fibres in automotive interior panels when it was actually very short wood fibres that were being replaced [109]. In 2000 all major car manufacturers were employing natural fibres to reinforce compression moulded interior door and parcel shelf panels in at least one of their cars, with the market share projected to increase with the development of vegetable fibre injection moulded composites [100].

Natural fibres, especially bast fibres have been shown to produce high strength and stiffness composite materials that have been adopted by the automotive industry and are growing in size year on year. Cellulose fibres have been shown to be compatible with phenolic resins and other shortcomings associated with various polymer matrices have been overcome using chemical pre-treatments. The technical fibres from renewable vegetable plants offer

weight saving to existing materials without a loss of performance however the performance of friction material composites containing natural fibres has never been reported and is one of the objectives to be covered in this research.

3 Materials

3.1 Introduction

The base formulation used in this research is a popular economy non-asbestos organic friction material developed by European Friction Industries (EFI) and manufactured at their Bristol facility in the UK. This friction material is designed for use on small to medium sized private cars producing zero noise and vibration during use and also demonstrating a long service life with minimal disc wear. The formulation uses a combination of 13 different raw materials that vary in density, particle size and morphology, thermal stability and hardness. Material selection and percentage inclusion in the formulation is governed by the desired friction and wear performance of the brake pad in addition to raw material and manufacturing costs.

3.2 Friction material formulation

This section will introduce the composition of the commercial formulation and also describe the morphology of the individual raw materials and their intended purpose within the composite brake pad. Inclusion levels of raw materials are heavily driven by cost with expensive ingredients used at the lowest possible levels. aramid is the prime example as 3.75% is the lowest percentage by volume that can be used in this formulation – determined empirically by the R&D team at EFI. This percentage inclusion represents the minimum amount of aramid for the desired manufacturing and operating performance criteria yet questions regarding the performance attributes that these fibres provide and the mechanisms behind them remain unanswered.

The baseline formulation is shown in table 3.1 listing the raw materials, volumetric percentage in the formulation and cost.

Material	Volume (%)	Specific Gravity	Cost (£/Kg)
Phenolic resin	20	1.3	0.9
Barium Sulphate	14.75	4.25	0.12
Magnesium Oxide	13	3	0.26
Expanded perlite	12.5	2.2	1.07
Rubber crumb	8	1.1	0.26
Antimony Trisulphide	5	4.6	1.64
Coke	5	2.08	0.25
Exfoliated Vermiculite	5	2.6	0.42
Iron powder	5	7.59	0.46
Graphite	4	2.15	0.77
aramid pulp	3.75	1.44	20.4
Steel fibres	2	7.7	0.735
Uncured rubber	2	1.06	2.27

Table 3.1 baseline friction material formulation

Phenolic Resin

The phenolic resin is the matrix which binds all other raw materials and occupies the greatest percentage volume of the formulation, dominating the bulk mechanical, thermal and wear properties of the brake pad. Supplied by Bakelite AG, the powdered unmodified novalac resin – number 0229RP – was selected from numerous other phenolic resins for particular reactivity, rheological and mechanical properties. Phenol and formaldehyde are combine in controlled ratios to produce the novalac resin which is subsequently used in conjunction with the hardening agent hexamethylene tetramine (hexamine) to produce a highly cross linked thermo-set resin with a good thermal stability. Figure 3.1 [18] shows the reaction path during the curing of the resin.

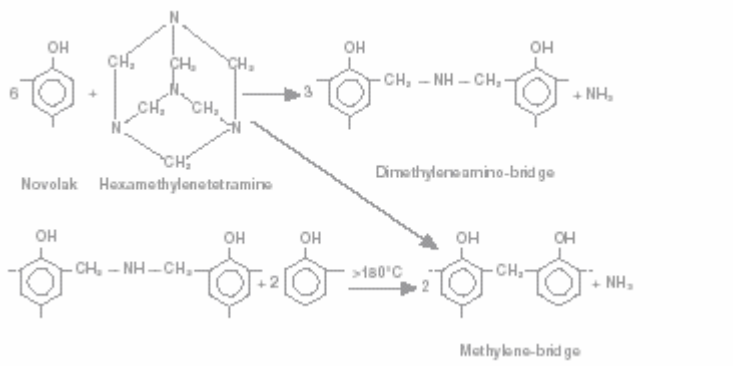

Figure 3.1 Reaction path of novalac phenolic resin [18]

The key features of this resin are a high reactivity, a long flow distance and a high hexamine content. A high reactivity allows short manufacturing cycles and high productivity but is highly sensitive to processing fluctuations such as temperature, pressure and time. The rheology of the resin is described by a long flow distance which produces a dense resin structure that bonds strongly with other raw materials. A high hexamine content give the resin a greater cross link density which increases the hardness and thermal stability at the expense of ammonia gas being evolved during the curing phase.

Barium sulphate

Also known as barytes, barium sulphate (Ba_2SO_4) is an inexpensive thermally stable compound mined in the UK and processed into a fine powder. High levels of barytes are used in this formulation as a space filler.

Magnesium oxide

This compound is used in similar levels in the formulation as barytes as a low cost filler material. Magnesium oxide is a refractory metal oxide that is mined in the UK and has mild abrasive properties and also acts a minor catalyst for the curing process of the phenolic resin.

Expanded perlite

Perlite is the generic name given to a naturally occurring siliceous rock that is mined in North America, China and Eastern Europe. A fine powdered form of expanded perlite is

used which is produced using heating to increase the surface area of the mineral by rapid expansion of bound water. A form of naturally occurring glass, perlite is an abrasive and is used in controlled volumes to generate the required friction levels for the brake pad.

Rubber crumb

Granulated rubber obtained from recycling vehicle tyres is used as a cheap source of increasing the compliance of the brake pad to reduce operating vibrations and noise. Low levels of rubber are included as lack of thermal stability induces brake fade during heavy use.

Antimony Trisulphide

Used as a friction modifier in the formulation, antimony trisulphide has the dual purpose of a lubricant and an abrasive. At temperatures below 570 °C the material lubricates the tribological couple, above this temperature the compound oxidises into an abrasive material that helps to counteract brake fade. Antimony trisulpide is also considered as a key material used in the formation of stable friction films.

Coke

Coke is the second form of carbon used in the formulation and is included for longevity of the brake pad. Coke is an inexpensive material that helps to prolong the service life of the friction material.

Exfoliated vermiculite

Vermiculite is hydrated laminar magnesium-aluminum-ironsilicate obtained from surface mines in South Africa and China. The mineral ore is heated in furnaces, exfoliating the structure of the material as the bound water is rapidly converted into steam, increasing the bulk volume around 8-10 times. The exfoliated variety of vermiculite is used in friction materials as the porous structure provides a degree of compliance and damping to the brake pad.

Iron powder

Inexpensive sponge iron in powdered form is included in the formulation to enhance the wet weather performance of the friction material as the abrasive particles cut through hydro films , removing the lubrication and restoring the required friction level. The high density particles provide secondary benefits during the manufacturing stages, providing a bulk mass that encourages mixing of the raw materials.

Graphite

The weak inter-planar bonds in graphitic carbon produce an excellent lubricant for which graphite is included in friction formulations. Adding powdered graphite is a low cost method of lowering the operating friction level which reduces the tendency of brake pad to grab against the disc. Adding graphite at the preliminary mixing stages promotes homogenous mixing by dissipating the electrostatic charge generated by the aramid fibres.

Aramid Pulp

Sourced from Teijin under the brand name Twaron, the aramid pulp is intentionally manufactured from a monofilament source to produce fibres with a controlled range of fibre lengths and degree of fibrillation. Of the 8 types of aramid pulp produced by the company, 3 are designed for the friction industry, and type 1099 is used in this formulation. Within the Teijin product range pulp 1099 is a highly fibrillated fibre with a long fibre length, marketed as a multi functional brake pad material. The fibres are primarily used in this formulation as a processing aid even though the fundamental mechanisms behind the performance are not understood. In addition to the processing benefits received from the fibres there are other uncertain benefits such as mechanical reinforcement and friction/wear stability. Teijin publish a fibre length range of 0.8 – 1.35 mm and a specific surface area of 8 – 15 m^2g^{-1} for pulp 1099.

Steel Fibres

Metallic fibres are included in the formulation to add toughness to the composite and increase the thermal conductivity to draw heat away from the friction interface. Low levels

of steel fibres are used as the operating coefficient of friction and the wear of brake discs is sensitive to the content of steel fibre in the formulation. The steel fibres benefit mixing when added at an early stage with the aramid fibres.

Uncured rubber

In addition to the rubber crumb an uncured form of rubber in granulated form allows an increased rubber content in the formulation without increasing the elastic recovery of the formulation after compression.

3.3 Natural fibres

The natural fibres used in this research were obtained from suppliers in the UK and abroad as virgin and recycled materials covering bast and leaf type fibres. The natural fibres sourced and used in the preliminary research are shown in table 3.2 and were received in various fibre lengths and aspect ratios. Only commercially available natural fibres were selected for the research. A ready supply of high quality hemp fibres was available from Hemocroe Ltd as an industrial collaborator in the Ecopad project.

For trials in friction formulations the fibres were chopped using a rotary milling machine with a blade separation of 6 mm, with the exception of the short hemp as the fibre. These fibres were obtained from the same crop as the Hemcore FC fibre but taken from the dust extraction system and so had a considerably shorter fibre length.

Fibre Type	Sample Notation	Length mm	Supplier	Place of Origin
Hemp	Hemp FC	6	Hemcore	UK
Hemp	Hemp Short	< 5	Hemcore	UK
Hemp	Hemp Unretted	6	Biofibres	UK
Flax	Flax	6	Goonvean	UK
Sisal	Sisal	6	University of Dar Es Salaam	Africa
Kenaf	Kenaf	6	SPDG	UK

Table 3.2 natural fibres sourced for formulation trials

A series of further fibre samples were produced with the aim of encouraging fibre fibrillation and increased surface area. Aptec Products are UK industrial fibre handling and processing experts and helped to process a series of fibrous materials for this research using the FC fibre from Hemcore. Aptec set up their carding machines to mechanically alter the morphology of the fibres by encouraging fibrillation along the fibre length. The machine settings of rotor speed, separation and needle density were fixed and samples were passed through successive times to produce samples FC+2, FC+3 etc, before the samples were finally cut to a length of 6 mm. The fibre handling technology at Aptec ensures the fibres are aligned perpendicular to the cutting blade ensuring an accurate fibre length and narrow length distribution. The notations used for the samples process by Aptec fibres are shown in table 3.3

Fibre type	Sample Notation	Fibre length mm	Supplier	Country of Origin
Hemp	FC+2	6	Aptec	UK
Hemp	FC+3	6	Aptec	UK
Hemp	FC+4	6	Aptec	UK
Hemp	FC+5	6	Aptec	UK

Table 3.3 fibrillated hemp fibre types

3.4 Organic and Mineral fibres

In addition to the organic fibres used in the baseline formulation four other fibres commonly used in friction materials were sourced for comparison with the Twaron 1099 pulp. Two recycled aramid fibres were obtained from different sources, both major suppliers to the friction industry. Two short fibres were also obtained, a cellulose based material obtained from recycled paper, the other, a mineral fibre produced from melt spun rocks. The organic and mineral fibres and their respective suppliers are listed in table 3. 4

Fibre type	Sample info	Supplier	Country of Origin	Cost £/kg
aramid	recycled	Goonvean	various	8.7
aramid	recycled	Sterling fibres	various	8.0
Cellulose	recycled	Goonvean	various	0.854
Rockwool	virgin	Lapinus	Holland	1.22

Table 3.4 Organic and mineral fibres

3.5 Brake Pad Geometry

The brake pad geometry for a Volkswagen Golf was selected for the dynamometer friction and wear trials throughout this research. The asymmetric inside and outside pads produce an imbalanced clamping pressure when the brakes are applied resulting in high mechanical loadings and stresses. As a result VW Golf pads are highly prone to noise, vibration and uneven wear, presenting new friction materials with harsh operating conditions compared to other pad geometries. The inside and outside pads from a VW Golf are shown in figures 3.2a and 3.2b respectively. Approximate length and width of the inside pad shown in figure 3.2a is 100 mm and 40 mm respectively.

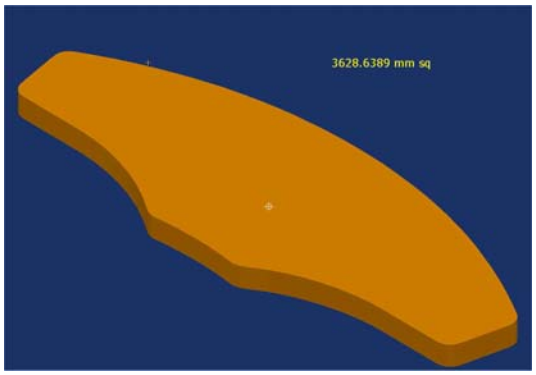

Figure 3.2a Inside pad from VW Golf

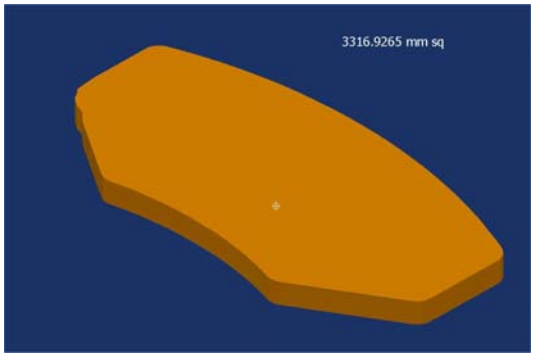

Figure 3.2b Outside pad from VW Golf

4 Methods

This chapter describes the analytical methods used to characterise the materials used in this study. The methods are ordered in sequence of the processing of materials starting with raw materials, moving on to the mixing of friction formulations, the pre-forming process and hot pressing to produce a cured composite material. The sequence follows the industrial method of brake pad manufacture – discussed in section 4.3 – to establish the performance of Aramid fibres throughout the manufacturing process. Once manufactured, cured composite friction materials are subjected to a friction and wear evaluation to establish the operating performance as a function of fibre type and volumetric loading in the formulation.

4.1 Thermo-gravimetric analysis of raw materials

Thermo-Gravimetric analysis was used to evaluate the thermal stability of the individual raw materials. A Netzsch TGA 209 was used to monitor the mass of a sample when subjected to a controlled heating profile. The atmosphere within the furnace was controlled by a gas supply at a flow rate of 70 cm^3/min of either nitrogen or dry compressed air. Both inert and oxygen rich atmospheres were used as a comparative study of thermal stability of raw materials. Samples were placed in an alumina crucible and their masses determined using the machine internal balance to an accuracy of 1 μg. Sample masses ranged between 10 – 20 mg depending on the material density. A constant rate heating temperature profile of 20 °C to 900 °C at 10 °C/min was used. Post data analysis to determine sample mass loss and onset temperatures was performed using the Netzsch TA software.

4.2 Dry formed fibre networks

The following section of work focuses on the structural properties of dry fibre networks formed by the interactions between adjacent fibres producing a bulk structure with specific mechanical properties. Light microscopy and SEM analysis was used to investigate the morphology of individual fibres and fibre networks and a mechanical test was employed to characterise the mechanical response of dry fibre networks to an applied stress. Particular

attention was focused towards aramid fibres with analysis extending to natural fibres and fibre blends.

4.2.1 Scanning electron microscopy

Scanning electron microscopy (SEM) was used to image fibre networks at high magnification to elucidate the complex physical structure and fibre interactions. Similar evaluation of aramid pulp by the manufacturers Twaron [66] displays low magnification images of highly fibrillated individual fibres giving minimal insight into the interactions between the fibres that generate the bulk properties of the fibre pulp. The aim of the evaluation was to examine the morphology of individual fibres, the mechanisms behind the morphology and the interactions between the fibres responsible for the bulk network mechanical properties. Fibrous samples were randomly taken from the material used in the bulk density method section 4.3.3 having experienced mixing for 10 minutes. Fibrous samples were gently secured on an SEM sample holder with carbon tape. A gold layer 5 nm thick was sputter coated onto the samples. Images at various magnifications were taken using a 25 keV accelerating voltage and the secondary electron detector.

4.2.2 Aramid Fibre length

The aramid pulp used in this research – Twaron 1099 – is marketed as a high surface area fibre with an average length range of 0.8 – 1.35 mm however longer fibres formed from the original monofilament tow were clearly evident. The morphology of individual fibres control the bulk mechanical properties of the fibre pulp, the importance of which for manufacturing friction materials was discussed in sections 2.1.4 and 3.2. Quantifying the size of these larger fibres assisted the understanding of the bulk structure. Large fibres within the pulp were randomly selected by eye and placed on a microscopy slide and secured beneath a slide cover. Optical images were obtained from the Carl Zeiss Axioplan light microscope in light field transmission mode at 12.5 times magnification. The high resolution images obtained from the microscope were used in conjunction with the length measurement facility in the Matlab software. The distance count was calibrated with a Carl Zeiss reference grid imaged at the same magnification. The length of the main trunk of the

fibres was measured to an estimated accuracy of 5 μm. The fibre length obtained from these tests was used as the target length for the natural fibres discussed on p64.

4.2.3 Dynamic mechanical testing

A mechanical test was employed to characterise the organic fibres used in this research and asses their suitability as processing fibres in friction materials via a critical strain onset. Effective processing fibres, such as aramid, can withstand the mechanical strains applied by mixers during the manufacturing process and retain an entangled bulk fibre structure without disentangling into a disconnected group of discrete fibres. Therefore, a key parameter to measure is the maximum applied strain before permanent structural damage occurs. The limits of elastic recovery of a material subject to an applied strain can be measured using commercially available machines such as a Dynamic Mechanical Analyser (DMA) or a tensiometer or in the case of fluids and gels, a rheometer.
A rotational rheometer was selected for the analysis of fibre pulps, the primary advantages identified are listed below;

- Machine and sample configuration allows accurate and repeatable loading of fragile materials such as fibre pulps
- A rotational shear deformation is applied, replicating shear deformations imposed during the manufacturing process.
- The accuracy of the machine – 90 nano radians – allows very small changes in the visco elastic properties of the material to be identified.

It should be noted that increasing the applied strain at a fixed frequency results in an equivalent increase in the strain rate. This was unavoidable as strain rate cannot remain constant using this particular apparatus. The results are discussed with the knowledge that strain rate is a variable during the test in addition to the magnitude of the applied strain. The fibre pulp samples are low density fibre networks with air occupying the voids. Therefore the starin rate dependence of air, the viscoelastic fibres themselves and the frictional nature of the fibre entanglements must be considered.

Due to the parallel plate geometry used, the applied strain is not uniform with respect to the radial displacement from the centre of the plate so the maximum strain is applied at the plate edge and the minimum at the centre. The true strain is therefore an average over the diameter of the plate over this is the same for all samples so results are comparative. Conventional cone and plate geometries used to maintain a uniform strain cannot be used for this test as the truncation that must be used can only accommodate a small number of fibre lengths and would not allow representative fibre pulp samples to be tested.

The experimental procedure was based on the work of Askling et al [110] using a Rheometer – a machine typically used to characterise visco-elastic liquids and gels – to evaluate the mechanical response of a sample to an applied stress/strain. Development of the tests provided a quick, quantitative measure of a fibre pulp's mechanical properties, allowing the procedure to be used as a quality control test and as a predictive tool for new materials. The AR2000 rotational rheometer supplied by TA Instruments was used for all tests. The rheometer uses an interchangeable parallel plate configuration to sandwich the samples between a fixed bottom plate and a top plate free to rotate around the vertical axis. The top plate is attached to the end of the drive spindle running on a very low friction air bearing and driven by a DC electric motor. An optical encoder accurate to 90 nano radians calculates the angular position of the drive spindle and a torque sensor measures the output of the drive motor. A 50 N load cell is located under the stationary bottom plate to measure the force exerted on the sample between the plates.
Test parameters were set using the TA instruments rheology software on the remote PC linked to the rheometer. The test is described in full in section 4.2.3.1.

4.2.3.1 Sample preparation and loading

Dry fibre pulps are fragile structures making samples handling and preparation a delicate operation. A repeatable accurate method of preparing and loading samples into the machine was devised. The 25 mm diameter parallel plate geometry was used throughout the tests and samples were produced to match. All compressive history of fibre pulp samples was removed by mixing the fibres in the Kenwood mixer for 10 minutes as described in 4.3.3. A

die and circular punch were produced by reaming a 25 mm hole in a block of mild steel with a clearance fit of 0.1 mm between die and punch. Samples were made by weighing 1g of fibre pulp on laboratory scales accurate to 0.001g and placing into the die. A Lloyds Instruments EZ20 mechanical testing machine applied a compressive load onto the die punch at a crosshead speed of 1 mm/s to a maximum load of 500 N, held for 10 seconds. The disc shaped fibre samples were carefully removed from the die and allowed to recover for a minimum of 24 hours before testing. Plate separation was zeroed before every test allowing the gap to be measured accurate to 1 μm. The pucks were secured into the Rheometer plates using double sided tape applied to the top and bottom plates. Using the machine control, the top plate was driven down towards the bottom plate thus compressing the sample and ensuring good adhesion with the tape. The compressive force exerted on the sample sandwiched between the two plates was monitored by the load cell under the bottom plate. An initial maximum load of 50 N was applied and held for 1 minute, before an automatic reducing force control was engaged to reduce the compressive loading by driving the top plate vertically. The machine control was used to reduce the loading force on the sample for 30 minutes or until a steady value of 0.1 N was recorded. A further manual separation of the plates ensured the compressive load reading on the sample was 0 N ± 0.005 N. Figure 4.1 shows a schematic cross section of the sample sandwiched between the two machine plates.

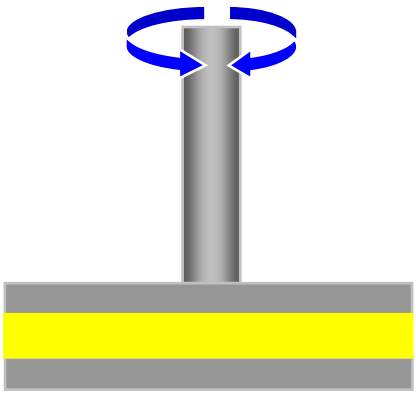

Figure 4.1 Side view of fibre puck between rheometer plates

4.2.3.2 Oscillation tests

A test was developed to look at the mechanical response of a fibre pulp sample as a function of the strain imposed on it. Fibre puck samples were prepared and loaded into the machine as described in 4.2.3.1. A strain sweep procedure was written to apply a ramped strain from 6.25 x 10^{-3} to 10 at a frequency of 1 Hz and a sampling rate of 20 points per decade. The elastic component of the shear modulus (G') was calculated by the internal software as a function of the strain recovered from the sample.

4.2.3.3 Fatigue tests

Fatigue tests were employed to evaluate mechanical response of a dry fibre network to repeated straining applications - as used in the oscillatory procedure in 4.2.3.2. The purpose of the fatigue test is to show the influence of repeated cycling at low strains on the elastic recovery of the fibre pulp. A fatigue test procedure was written to apply a low strain value of 6.25 x10^{-3} and frequency of 1Hz for the duration of 1 hour. Samples were prepared and loaded in the machine as described in 4.2.3.1. The elastic component of the shear modulus (G') was calculated by the internal software as a function of the strain recovered from the sample.

4.3 Friction material formulation

The manufacturing process is fundamental to obtaining the desired mechanical and friction and wear properties from a combination of raw materials. The methodology used in this research is based on industrial manufacture of friction materials at European Friction Industries in Bristol UK. Raw materials must be homogeneously mixed and manufactured to optimise the curing process of the resin binder producing a brake pad of the required geometric and structural integrity. The manufacturing route can be tailored to suit individual formulations but essentially follows a standard route of weighing, mixing, pre-forming, moulding and post baking. These five manufacturing stages were used to conduct the research in this thesis with experiments performed on the materials and formulations

throughout progressive stages of the manufacturing process. Figure 4.2 shows the industrial process which incorporates additional cosmetic and machining process for the brake pads. This research is concerned with the mixing, pre-forming and moulding of brake pads.

In comparison to industrial manufacture of friction materials, development of new materials on an R&D scale is of a magnitude 100 times smaller yet reflects the processing conditions used in commercial production.

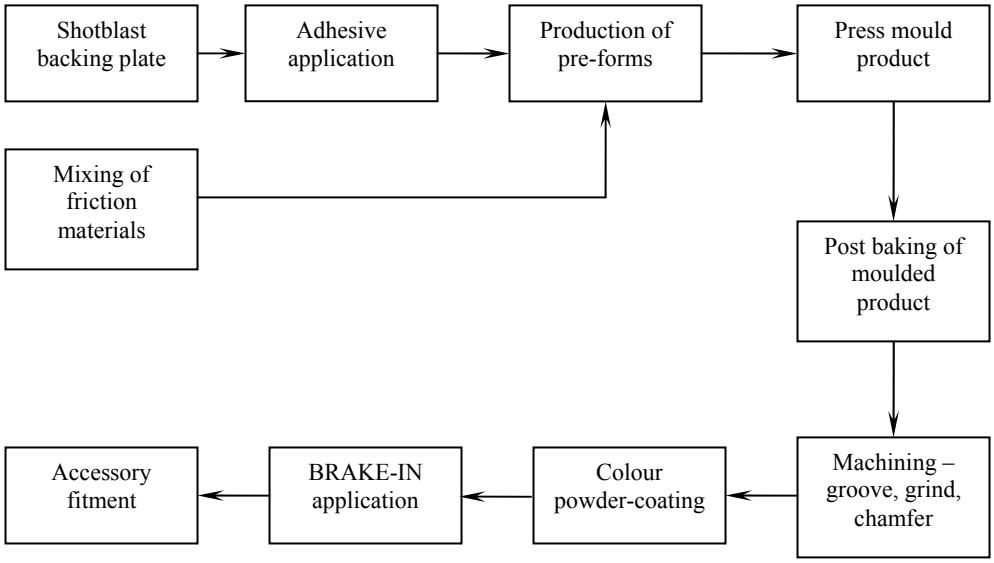

Figure 4.2 Industrial manufacture of brake pads

4.3.1 Mixing Friction Formulation

The baseline friction material used in this work is a successful economy formulation developed by European Friction Industries and has been used in commercial production for 7 years. Raw materials are formulated as a volumetric percentage of the total formulation and for ease of manufacture converted to a weight depending on batch size. A material development spreadsheet shown in table 4.1 was used to calculate weights and also allow adjustments of raw material inclusions.

Manufacture of the friction materials was identical to that used in the research and development laboratory in European Friction Industries (EFI). Mixing and moulding

equipment for the brake pads was obtained under guidance from the head of R&D at European Friction Industries to ensure consistent manufacture of materials.

A Kenwood mixer, as used by EFI, was used to mix all formulations using the standard mixing bowl and the stainless steel chopping blade attachment. Formulations were mixed in batch sizes of 500g which matched the volume of the 2.9 litre mixing bowl without over or under filling the mixing chamber. Raw materials were weighed on laboratory scales to an accuracy of 0.1g. For mixing purposes, the formulation was separated into two groups of materials. aramid pulp, iron powder, steel fibre and graphite in group one and all remaining materials in the second.

Material	**Volume (%)**	**S.G x Volume (%)**	**Weight (%)**	**Weight (g)**
GROUP 1				
aramid pulp	3.75	5.4	1.93	9.6
Iron powder	5	38.0	13.56	67.8
Steel fibres	2	15.4	5.50	27.5
Graphite	4	8.6	3.07	15.4
GROUP 2				
Phenolic resin	20	26.0	9.29	46.5
Barium Sulphate	14.75	62.7	22.40	112.0
Magnesium Oxide	13	39.0	13.94	69.7
Expanded perlite	12.5	27.5	9.83	49.1
Rubber crumb	8	8.8	3.14	15.7
Antimony Trisulphide	5	23.0	8.22	41.1
Coke	5	10.4	3.72	18.6
Vermiculite	5	13.0	4.65	23.2
Uncured rubber	2	2.1	0.76	3.8
Totals	**100**	**279.9**	**100**	**500**

Table 4.1 Master Batch Formulation

The first group of materials was mixed for 5 minutes on speed setting 1 – a measured 1500 rpm using a contact tachometer. During the initial mix the iron powder and steel fibres combine to produce a large mass of cutting particles that mechanically open up the fibre pulp, increasing the volume of the mixture and removing the compression history of the pulp during packaging. This is a crucial stage in optimising the bulk volume of the aramid fibre in preparation for the remaining raw materials. Graphite is included in the first group of materials as it dissipates the electrostatic charge generated by the fibres rubbing over one another at high speed, keeping the materials central within the mixing chamber. The remaining 9 materials were added and mixed for a further 5 minutes at the same speed setting, giving a total of 10 minutes mixing time for the formulation. This two part mixing process was used for all formulations produced and the homogenous blend of raw materials is referred to as the "mix".

To investigate the effect of aramid content a total of 7 formulations were made with aramid contents ranging from 0% to 7·5% by volume. To accommodate the change in aramid content, the volumetric inclusion of only barium sulphate was changed. The inexpensive, inert space filling powder is included at relatively high levels within the formulation allowing small percentage variations to be altered with negligible effect on the physical and tribological properties. For preliminary friction and wear analysis 5 formulations were produced using 5 different natural fibres completely replacing aramid in the formulation. A further 4 formulations were made containing a blend of aramid and hemp fibres in varying ratios to make up a 3.75% volumetric inclusion of fibres. Table 4.2 lists the samples made as a function of fibre content.

Sample Ref	aramid by volume	Natural fibre by volume	Natural fibre type	Total organic fibre by volume	Barytes by volume
	%	%	-	%	%
A0	0	0	-	0	18.5
A1	1	0	-	1	17.5
A2	2	0	-	2	16.5
A3	3	0	-	3	15.5
A3.75	**3.75**	**0**	**-**	**3.75**	**14.75**
A5	5	0	-	5	13.5
A7.5	7.5	0	-	7.5	11
Hemp FC	0	3.75	Hemp FC	3.75	14.75
Flax	0	3.75	Flax	3.75	14.75
Kenaf	0	3.75	Kenaf	3.75	14.75
Jute	0	3.75	Jute	3.75	14.75
Sisal	0	3.75	Sisal	3.75	14.75
Hemp Short	0	3.75	Hemp Short	3.75	14.75
Hemp Unretted	0	3.75	Hemp Unretted	3.75	14.75
HempFC+4	0	3.75	Hemp G+4	3.75	14.75
A1(FC+4)2.75	1	2.75	Hemp G+4	3.75	14.75
A2(FC+4)1.75	2	1.75	Hemp G+4	3.75	14.75
A3(FC+4)0.75	3	0.75	Hemp G+4	3.75	14.75

Table 4.2 friction formulations as a function of fibre inclusion

4.3.2 Dust suppression

The manufacturer's published benefits of using aramid in friction materials [66] asserts that the fibres suppress the dust generated by other powdered raw materials in the formulation giving both cost and health and safety benefits to industrial users. To quantify the dust suppressing effect of aramid pulp a simple sieve test was employed to agitate a formulation under controlled conditions and measure the mass of particulates able to fall through a sieve while capturing the aramid pulp. A sieve stack incorporating a mesh grade 40 sieve and bottom cup were placed on top of a laboratory magnetic stirring plate set at maximum agitation. For each formulation 10 g of material was placed on top of the agitated sieve for 1 minute and the mass of the fall through material was calculated afterwards and plotted against aramid content by volume. The dust suppressing performance of aramid pulp was assessed by analysing the average mass of particles collected over 3 runs for each of the following formulations – A0, A1, A2, A3 and A3.75. Material collected at the end of the test was measured on laboratory scales accurate to 0.1 mg.

4.3.3 Bulk density

The bulk density of a friction formulation is a useful measurement to establish the performance of the processing fibre in a friction formulation and also of the bulk structure of the fibre itself. Bulk density measurements of both aramid fibre pulp and friction mixes were measured using a rigid, open ended container of fixed volume manufactured from solid acrylic. A central void of square cross section was machined with large radii at the internal angles to minimise uneven filling and the opaque acrylic allowed inspection throughout the internal volume. The internal volume of the container was measured as 967.3×10^{-6} m^3 using a Renishaw cyclone reverse scanning machine with a 2 mm contact probe.

Bulk density measurements of friction formulations were performed immediately after the mixing process as described in section 4.3.1. The mix was carefully scooped out of the mixer and sprinkled into the acrylic container. Gently tapping the sides of the container ensured an even settling of material before a steel rule was drawn by hand along the top edge to level of the surface. The formulation was subsequently weighed on laboratory

scales to an accuracy of 0.1 mg and the bulk density calculated by dividing by the internal volume of the container.

The bulk density of aramid pulp was measured using exactly the same procedure as for the friction formulations. The bulk density of aramid pulp was measured before and after mixing to determine the effect of the friction material mixing process on the volume of the pulp. Firstly the Twaron 1099 pulp as received from the manufacturer was measured. The same pulp was then subjected to the 10 minute mixing cycle on its own in the Kenwood mixer before the bulk density measurement was repeated. The bulk density measurements allowed the volume fraction of fibres in the Twaron 1099 pulp to be determined according to equation (4.1)

$$V_{frac} = \frac{m_p}{V_v \rho} \tag{4.1}$$

Where;

V_{frac} = Volume fraction of fibres

m_p = mass pulp (kg)

V_v = Volume of acrylic vessel (m^3)

ρ = Density of fibre (kg/m^3)

4.3.4 Manufacture of Pre-forms

Pre-forming is the next stage in the manufacturing process after the raw materials have been combined and mixed to produce the formulation. Not all manufacturers choose to pre-form brake pads, however it is an essential part of the manufacturing process used by European Friction Industries. Pre-forms are produced by compressing a predetermined amount of mix at ambient temperature to set a geometric shape without curing the phenolic resin. A Letter Box shaped die of length 91.5 mm and width 25.5 mm was used to manufacture the pre-forms as shown below in figure 4.3. The die was also to be used for flexural tests on the cured

composites so the dimension of the die were taken from the relevant British Standard - BS EN ISO 14125 – Flexural test for fibre reinforced composites.

Figure 4.3 Letter box die

The pre-forms were manufactured by filling the die with material and carefully levelling the surface before inserting the die punch. Each pre-form was made using 40 g of mix, pre-weighed on laboratory scales accurate to 0.1 g The pre-forms had a length to thickness ratio of 7:1, an equivalent ratio for brake pad geometries. A Lloyds instruments LR300K mechanical testing machine was used to compress the formulation to a load of 53.3 kN to produce the pre-form, which equates to the pressure used in industrial manufacture. A crosshead speed of 1 mm/s was used to compress the mix to maximum load and hold for 10 s before the returning to zero load. Pre-forms were gently removed from the die by hand and left to recover on a flat surface for a minimum of 1 hour before testing due to the visco-elastic nature of some materials in the formulation. All pre-forms were manufactured to order and tested within 2 hours from being removed from the die.

4.3.4.1 Green strength

A mechanical test was devised to determine the resistance of a pre-form to indentation, replicating the manual handling of pre-forms by workers in the factory. This is a key test to determine wheter a friction formulation can be successfully manufactured using the pre-

forming process and will determine the success of a new fibrous material in the formulation. The indentation direction was chosen into the weakest face of the pre-form corresponding to the direction of handling by factory workers. Pre-forms were manufactured as described in section 4.3.4. The pre-forms were turned through 90 degrees so that the Y plane was facing uppermost and in line with the indentation direction. Figure 4.4a shows the orthogonal planes prescribed to the pre-form during manufacture and figure 4.4b shows the test configuration for pre-form indentation. The indenting head was chosen to replicate the pressure exerted by the fingertips of a production worker in the factory. A conventional 3-point-bend testing head when aligned with the major axis of the pre-form fulfilled such criteria. The head consisted of a 10 mm diameter bar, 55 mm in length.

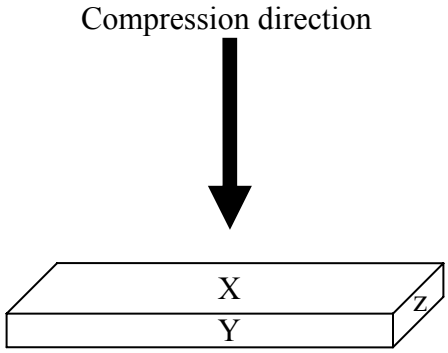

Figure 4.4a Orthogonal faces of pre-form

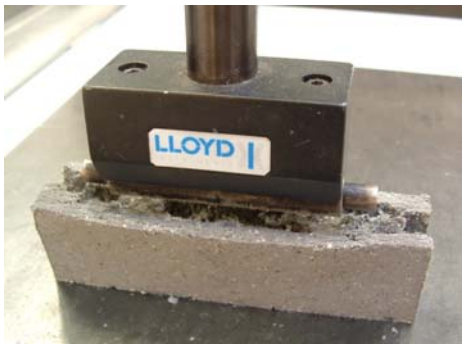

Figure 4.4b Indentation of pre-form

A Lloyd Instruments EZ20 mechanical testing machine with a 50 N capacity load cell was used to drive the indenter head in to the pre-forms at a speed of 2 mm/min while recording force versus displacement values. The load at failure for each pre-form was taken as the maximum load at the first peak on the load displacement graph. An average maximum load over 3 pre-forms was calculated to confirm the green strength of each formulation.

4.3.5 Manufacture of friction composites

Composite friction materials were manufactured for flexural strength analysis, material dispersion and for use in the lab scale friction and wear machine. Formulations were mixed as specified in 4.3.1 and manufactured into rectangular composite samples using the letter box die described in 4.3.5.1. The hot press manufacturing process used for brake pads in 4.3.6 was replicated to make one sample at a time.

4.3.5.1 Flexural strength

Aramid fibres have been reported to improve the physical strength of friction materials [3,66] epoxy and other themo-setting resins. A 3-point-bend test was employed to determine the reinforcing strength of aramid fibres in the DM1070 friction formulation by calculating the flexural strength of samples made with controlled inclusions of aramid pulp. Seven of the formulations listed in table 4.2 were used for the flexural test with five samples made for each formulation.

The sample dimensions and test conditions used were defined in BS EN ISO 14125 – Flexural test for random fibre reinforced composite materials. The letter box die described in 4.3.4 defined the lengths and width of the samples, thickness was controlled to 4 mm ± 0.2 mm as prescribed in the standard by using between 22 – 23 g of material depending on formulation.

Tests were performed using a Lloyds Instruments EZ 20 mechanical testing machine and 3-point-bend fixture using cylindrical sample supports with a 5 mm radius. A 500 N load cell recorded the applied force and deflection was taken from the internal machine extensometer. The machine cross head speed for each sample was calculated according to;

$$V = \frac{\varepsilon' L^2}{6h} \tag{4.2}$$

Where V = crosshead speed (mm/min)

ε' = Rate of applied strain (0.01/minute)

L = Outer support span (64 mm ± 1 mm)

h = Sample thickness (4 mm ± 0.2 mm)

The test set up used for flexural tests is shown in figure 4.5

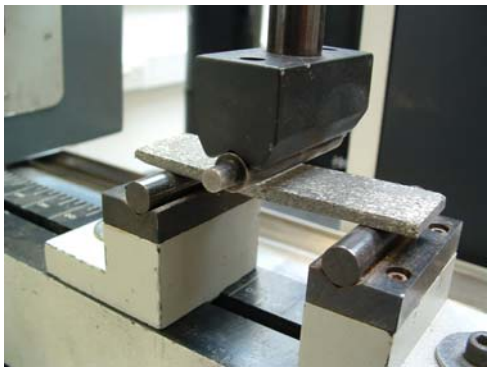

Figure 4.5 Flexural test set up for friction composites

4.3.5.2 Measurement of dispersion of materials

EDX

Energy Dispersive X-ray analysis (EDX) is an analytical technique used in conjunction with an SEM to identify the elemental composition of imaged samples. Samples manufactured for the flexural test procedure in 4.3.5.1 were used to investigate the distribution of raw materials in friction composites as a function of aramid inclusion within the formulation. Samples approximately 10 mm^2 were taken from the end section of the flexural samples away from the fractured surface and mounted on the SEM sample holder

using carbon tape. A 25 keV accelerating voltage was used in conjunction with the back scattered electron detector for high resolution imaging and EDX. Images were taken of areas selected at random as long as large particle such as vermiculite did not occupy a large proportion of the image. After generating images, the EDX mapping analysis was left to run for 30 minutes to produce a corresponding element distribution map.

UV Microscopy

Ultra Violet microscopy was used to image the surface of friction materials to locate the presence and distribution of aramid fibres on the surface of a sample. The location of virgin aramid fibres can be identified under ultra violet light due to the excitation of the aromatic ring structure in the polymer chains causing the fibres to fluoresce. This allows the dispersion and morphology across a surface to be identified. Samples were imaged at x12.5, x100 and x200 magnification using a DAPI filter which excites at 365 nm and emits at 400 nm (blue) wavelength clearly showing the aramid fibres.

4.3.5.3 Density

The density of the friction composites is required to calculate the work done per unit distance using equation (4.3) during the wear testing in 4.3.5.4. Samples were manufactured as described in 4.3.5 using 140 g of formulation to produce a bar 25 mm thick ± 1mm. The length, width and thickness of the samples were measured at three points along the respective dimension using calibrated vernier callipers. The volume of material was calculated in m^3. The bars were weighed on laboratory scales accurate to 0.001 g which converted to kg and divided by the volume produced the density for each material in kgm^{-3}.

4.3.5.4 Friction and wear testing – Chase tester

A lab-scale friction and wear tester – Chase machine – was designed and built to evaluate the friction and wear performance of new friction materials. This allowed greater control

over friction and wear testing compared to dynamometer work at EFI. The Chase machine is so called due to the original manufacturers of similar machines. The reduced scale friction and wear testing machines are acknowledged as not providing scaled down operating conditions compared to dynamometer tests [77] yet Chase machines are widely used by industry and academic institutions world wide for comparative testing and material development programs [3,24,42,46,69-76]. The design of the machine was based around a 7.5 kW three phase electric motor to drive a 150 mm diameter cast iron disc – equivalent to a full scale brake disc – at a constant 1450 rpm onto which a 20mm^2 sample of friction material is pressed at a constant pressure for a defined length of time. A pneumatic control valve was employed to press the friction material against the rotating cast iron disc at the desired pressure. A special "k" type rubbing thermocouple was used to monitor disc bulk temperature. A compressive load cell was located under the sample holder arm to measure the force as a result of the friction coefficient between sample and disc. An LVDT measured the linear wear of samples throughout the tests. All data channels were controlled via a data acquisition box linked in turn to a laptop computer sampling at a frequency of 10 Hz. A start/stop mechanism incorporating a mechanical timer was wired into the pneumatic system allowing accurate and repeatable time driven tests. The overall design and specification of the machine was combined with a review of similar machines used for academic research, [3,24,42,46,69-76]. The wear testing program was based on the international standard SAE J661a [111] which specifies a wear testing protocol for friction materials based on pressures, temperatures and testing duration. Figure 4.6 shows the machine in use including the data acquisition laptop for scale.

Figure 4.6 Chase machine

A burnish procedure was used for each sample at the start of wear testing to ensure an even contact between pad and disc. A high power air blower was used to ensure a large air flow over the friction couple to keep the temperature below 110 °C thus minimising thermal effects. The following settings were used;

Test speed	7.59 ms^{-1}
Sample size	20 mm^2
Normal pressure	689 kPa
Applications	20 x 20 s applications with cooling pause 5 sec ± 1 sec
	400s drag
	20 x 20s applications with 5 sec cooling ± 1 sec
	(total run time 20 mins)
Blower	On, top vent fully open

If sample not >95% contact area by visual inspection repeat 400s drag as necessary

Once a nominal contact of ≥95% between pad and disc was confirmed by visual observation the friction samples were blown with compressed air to remove any surface debris and weighed on a laboratory balance – sample holder included – to an accuracy of

0.1 mg. Samples were then used for the friction and wear analysis using the procedure below, again based on SAE J661a [111];

Wear Tests

Test speed	7.59 ms^{-1}
Sample size	20 mm^2
Normal pressure	1.032 MPa
Initial temperature	45 °C ± 2 °C
Applications	300s application (blower off) cool to 30 °C, repeat 10 times.

The cooling fan was not employed for the wear test procedure allowing the disc temperatures to rise independently. The wear test was repeated for each sample making a total of 20 constant load drag tests for each sample.

The wear of each sample was quantified using the specific wear rate equation by relating the mass loss of a sample to the applied load and the sliding distance. The equation used was;

$$K_0 = \frac{\Delta m}{\rho L d} \tag{4.3}$$

Where;

K_0 = Specific Wear rate (m^3/Nm)

Δm = Mass loss (kg)

ρ= density of material (kg/m^3)

L = average load on sample (N)

D = distance of sample run (m)

Over 60,000 data points were recorded for the wear tests on each sample. These were collated in an Excel spread sheet and formatted to calculate average load, coefficient of friction and distance travelled. A K_0 value was calculated for each of the wear tests giving two values for each sample from which an average value was calculated.

4.3.6 Manufacture of brake pads

Friction material formulations were produced as described in 4.3.1 and manufactured into brake pads for shear strength analysis and dynamometer testing. Two dies for the pad geometry described in 3.1 were supplied by European Friction Industries together with back plates in the appropriate geometry. Back plates were supplied coated with a temperature activated adhesive and pre drilled holes to accept the friction material and form a mechanical key between pad and back plate. Dies were pre-heated in ovens at 160 °C for 30 minutes before use and liberally coated with a water soluble release agent. Inside and outside VW brake pads were manufactured using 150 g and 135 g of formulation respectively. Filled dies were inserted into a preheated hot press at 160 °C set at a pressure of 30.4 MPa and programmed to run a time dependent pressure cycle as shown in figure 4.7. An initial dwell time of 1 minute was used to ensure even temperature distribution and resin flow thorough the thickness of the pad. A total of 7 venting cycles, each of 10 second duration is used to allow evolved ammonia gas to escape. A final dwell of 5 minutes is used to ensure a high degree of cure throughout the pad.

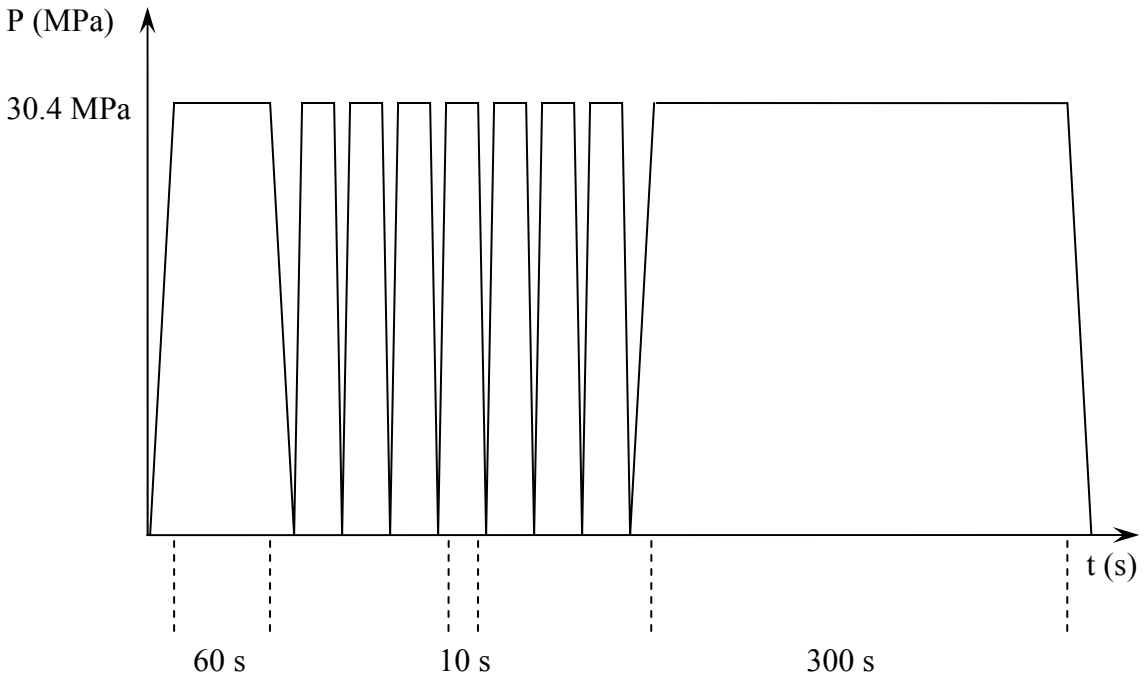

Figure 4.7 hot press cycle for friction materials

Pads were removed from the dies and placed in and oven at 160 °C to post bake for 6 hours to ensure a complete resin cure.

4.3.6.1 Back plate interfacial bond

The shear strength between the friction material and back plate is a critical safety parameter in brake pads as specified in Regulation 90 [67]. Brake pads were manufactured as described in section 4.3.6 and tested using the dedicated shear testing rig at EFI. A brake pad is located in a rigid fixture that prevents lateral movement by restraining the back-plate. A steel head is driven at a controlled rate into the brake pad to shear the friction material off the back plate. The cross section area of the friction material was entered into the machine software which calculated the shear strength using the maximum load before separation of friction material and back plate.

4.3.6.2 Friction and wear testing – Dynamometer

An industrial inertial Dynamometer located at EFI was used for friction evaluation of brake pads. Electric motors are used to spin high inertia flywheels at controlled speeds to replicate the kinetic energy of a travelling passenger car. A computer software program controls hydraulic actuators to slow the rotational speed of the flywheels at a predetermined deceleration or brake-line pressure. A braking geometry identical to that used on Volkswagen Golf's is used to dissipate the energy stored in the flywheels. The dynamometer flywheel and brake system is shown in figures 4.8a and 4.8b respectively.

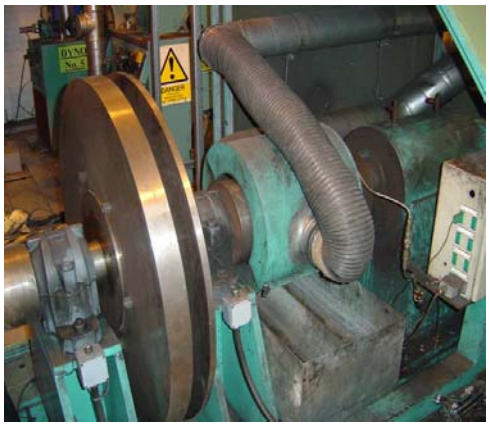

Figure 4.8a Inertia dynamometer

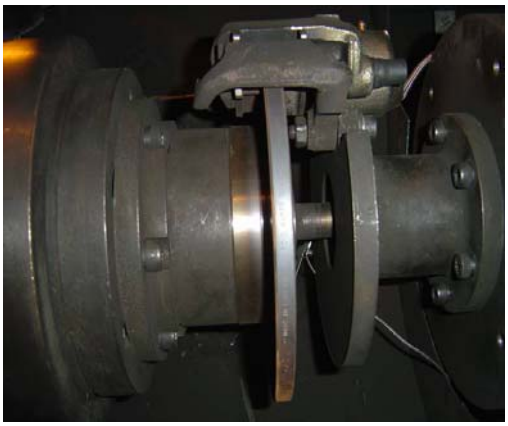

Figure 4.8b Braking components on dynamometer

Two pre-written software procedures were used to run the test brake pads on the dynamometer, an AKM master test and a constant torque procedure. A combination of tests was used due to dynamometer operating costs and demand for commercial testing. The pads used for all dynamometer runs were manufactured as described in 4.3.6.

AK MASTER TEST

Based on the German test standard, the AK master test is a comprehensive procedure designed to simulate real life driving conditions by subjecting brake pads to a variety of speeds, pressures, temperatures and deceleration rates. A complete test lasts well in excess of 12 hours, employing 20 individual tests over 15 test categories ranging from the Green performance of brand new pads to fade inducing high temperature stops and high load applications to replicate high speed driving on German autobahns. The AK master test is the most comprehensive dynamometer test used by EFI on automotive friction materials and is the closest automated test to on-vehicle testing available. A pair of brake pads manufactured were located and secured in the dynamometer brake callipers using the pad retaining pins and clips. The pre-written software procedure controlled the operation of the machine for the entire duration of the test. Results were collated by the control computer and graphically plotted to produce a two page report showing coefficient of friction, disc temperature and brake line pressure for each testing stage. A full description of the test procedures is given in appendix 1.

CONSTANT TORQUE

Using the same dynamometer and braking geometry as the AK master test, the constant torque analysis is based on Regulation 90 [67], a series of temperature limited brake applications against a brake disc powered by an electric motor supplying a constant torque output. Test parameters recorded by the dynamometer software were output torque (coefficient of friction) disc temperature and brake line pressure, reports are provided in graphical format detailing the operating (average) coefficient of friction throughout the test in addition to maximum and minimum values. A full description of the test procedure is given in Appendix 2

4.4 Statistical analysis of data

A Linear regression analysis was performed for data sets investigating the performance of materials as a function of aramid content using the Analyse-it software plug in for Microsoft Excel. A 95% confidence interval was specified and a linear regression line fitted to the data set. The probability of the slope and intercept of the regression line equalling zero was calculated allowing the influence of aramid content to be discussed on the measured performance criteria.

Statistical analysis was displayed in conjunction with the data plot allowing the raw data to be viewed in addition to the linear regression, 95% confidence interval and 95% prediction interval lines.

For data sets including more than one variable parameter such as those shown in figure 5.32 and table 5.3, a non-parametric data analysis was employed. The Kruskal-Wallis rank test was used to test the equality of data set medians using equation 4.4;

$$H = \left[\frac{12}{n(n+1)} \sum_{j=1}^{c} \frac{T_j^2}{n_j} \right] - 3(n+1) \tag{4.4}$$

Where;

n = total number of values over combine samples

c = number of groups

T_j = sum of ranks in the j^{th} sample

N_j = size of the j^{th} sample

The result obtained from the Kruskal-Wallis hypothesis is used to determine which of the two possible hypotheses are true;

H_O = All median values from data sets are equal

H_A = Median values re independent from one another

The H value obtained from the test is used to calculate the chi distribution probability using the CHIDIST() function in Microsoft Excel. This value known as the right-tail probability defines the probability of the data sets occurring by chance and as such is used to accept or decline the hypothesis base on a 5% standard. The right tail probability function is entered into Excel as shown in equation (4.5);

$$\text{CHIDIST}(H, \text{d.o.f}) \tag{4.5}$$

Where;

H = Kruskal-Wallis H test statistic

d.o.f = degrees of freedom = total data groups – 1

5 Results

In this section the results of the research work are presented together with a minor discussion of the findings. Significant results from the work are identified in this section although a more detailed discussion of the findings are presented in chapter 6 and discussed in context with published literature.

5.1 Thermo-gravimetric analysis of raw materials

A typical result for a thermo-gravimetric analysis of the composite friction material DM1070 in an oxygen rich atmosphere is shown in Figure 5.1. The change in mass of the sample as a function of temperature is the combined effect of the 13 raw materials within the formulation. The main thermal event is preceded by a slow and steady thermal degradation accounting for a 1.76 % mass loss before the onset temperature of 379 °C. After the onset, the formulation undergoes a well defined thermal degradation accounting for a 14% mass loss within a 220 °C window. Between 600 °C and 690 °C the oxidation of metallic compounds within the formulation such as iron, steel and antimony produces a gain in mass once the main thermal degradation event subsides.

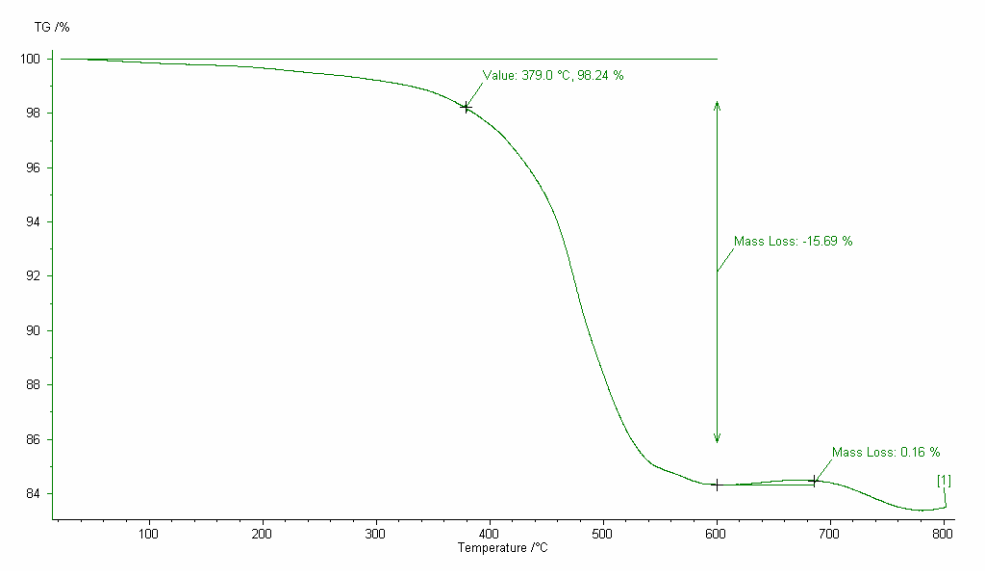

Figure 5.1 TGA of Cured Pad in air

Conformation of the thermal stability of the raw materials in the formulation was produced by subjecting each raw material to an identical TGA run and calculating the onset temperature of the corresponding change in mass. The temperature onset from the individual TGA runs are shown in table 5.1 The positive and negative notation indicates the direction of mass change.

Material	Onset °C
Phenolic resin	585.8 (-ve)
Barium Sulphate	638.1 (-ve)
Magnesium Oxide	285.1 (-ve)
Expanded perlite	N/A
Rubber crumb	254.1 (-ve)
Antimony Trisulphide	372.9 (-ve, +ve)
Coke	631.4 (-ve)
Exfoliated Vermiculite	N/A
Iron powder	409.7 (+ve)
Graphite	683.2 (-ve)
aramid pulp	465 (-ve)
Steel fibres	427.6 (+ve)
Uncured rubber	404.3 (-ve)

Table 5.1 onset temperatures of raw materials in formulation

The thermal stability of the raw materials varied widely in onset temperature, percentage mass change and the rate of mass change. The rubber crumb particles had the lowest

thermal stability demonstrating a mass loss onset of 254.1 °C and a 100% mass loss by 600 °C. All organic raw materials – the phenolic resin, rubber particles, carbons and aramid – demonstrated a clear single stage thermal decomposition. Metallic compounds of magnesium, barium and antimony demonstrated a much higher thermal stability but also more complexity in the nature of the thermal degradation. Barium sulphate demonstrated an onset of mass loss at 638.1 °C yet by 800 °C had only lost 1.21 % of the total sample mass. An onset of mass loss of 285.1 °C for magnesium oxide appears low for a refractory oxide yet only 1.1 % mass is lost during this initial degradation step. Antimony tri-sulphide underwent a combined mass change as the primary of mass loss onset at 372.9 °C was followed by a gain in mass of 0.77 % at 570 °C due to the oxidation of the metal. The ferrous based iron and steel materials both gained mass as a function of temperature after a well defined onset temperature.

The minerals perlite and vermiculite showed the highest thermal stability with no onset temperature and a total mass loss of 1.55 % and 1.07 % respectively at 800 °C.

The thermal stability of fibrous material is of specific interest in this work, in particular aramid and natural fibres. The TGA result of aramid in nitrogen and oxygen rich atmospheres are shown in figures 5.2a and 5.2b respectively.

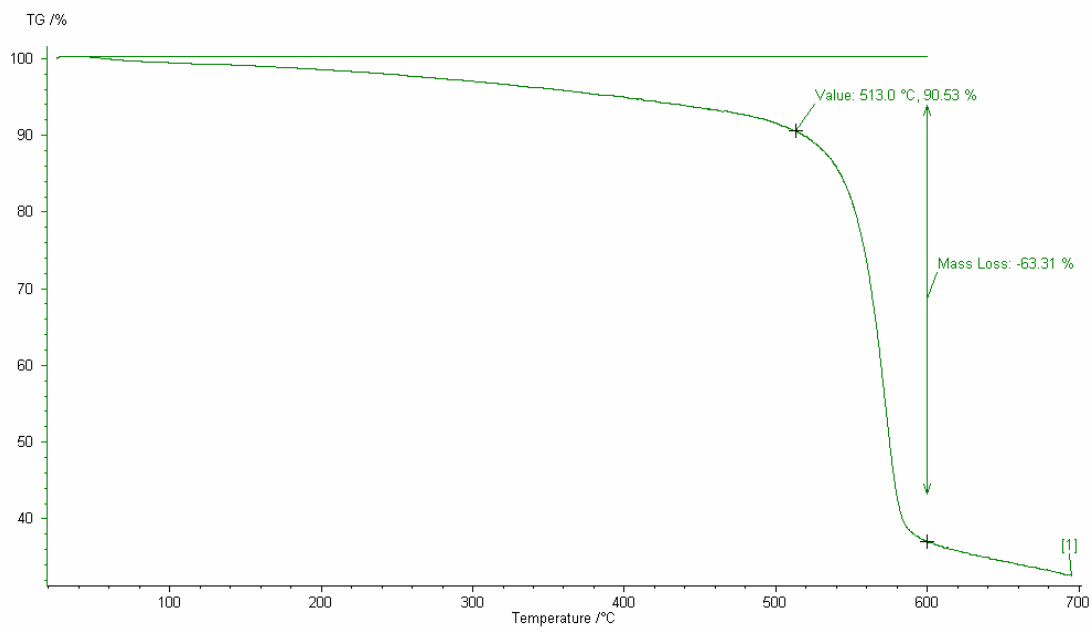

Figure 5.2a TGA of Twaron in N_2 atmosphere

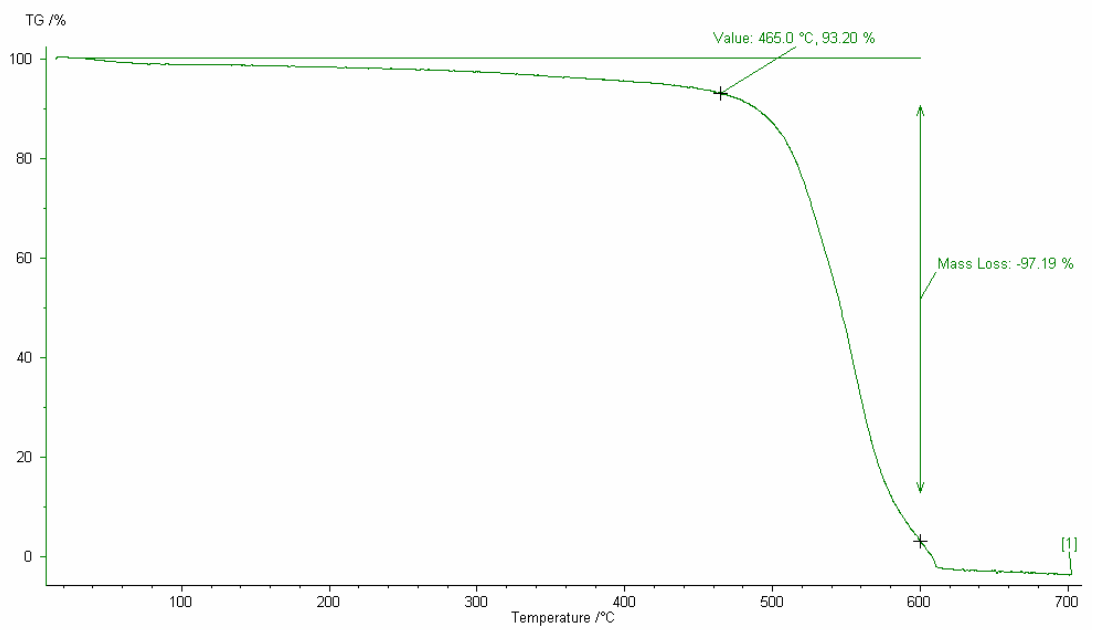

Figure 5.2b TGA of Twaron in air

The thermal degradation in both figures 5.2a and 5.2b is dominated by a single large mass loss defined by an onset temperature and the mass of sample lost during the thermal decomposition. The onset temperatures of thermal degradation of Twaron in the presence of nitrogen and oxygen are 513 °C and 465 °C respectively. In addition to the 48 °C offset in onset temperatures, the residual mass of Twaron was 33.9 % in nitrogen compared to a 97.2 % mass loss in the presence of oxygen. In a nitrogen atmosphere the aramid fibres will undergo a charring leaving a greater residual mass compared to a complete oxidative thermal degradation leaving only an ash residue.

The TGA plots for hemp, sisal, jute and flax in air are shown below in figure 5.3 all demonstrating a similar three stage thermal degradation comprised of initial, main and charring stages. The initial mass loss due to moisture takes place between 60 °C and the respective onset temperatures and is an expected feature given the hydroscopic nature of the fibres. At the onset temperature – given for each fibre type – a rapid mass loss takes place before briefly slowing during a charring stage, finished with a final complete mass loss of all fibres. All onset temperatures are within an 8.5 °C range due to the high cellulose

content in each fibre dominating the thermal degradation. The average onset temperature of the four natural fibres is 252 °C and a notable reference point for friction materials containing natural fibres.

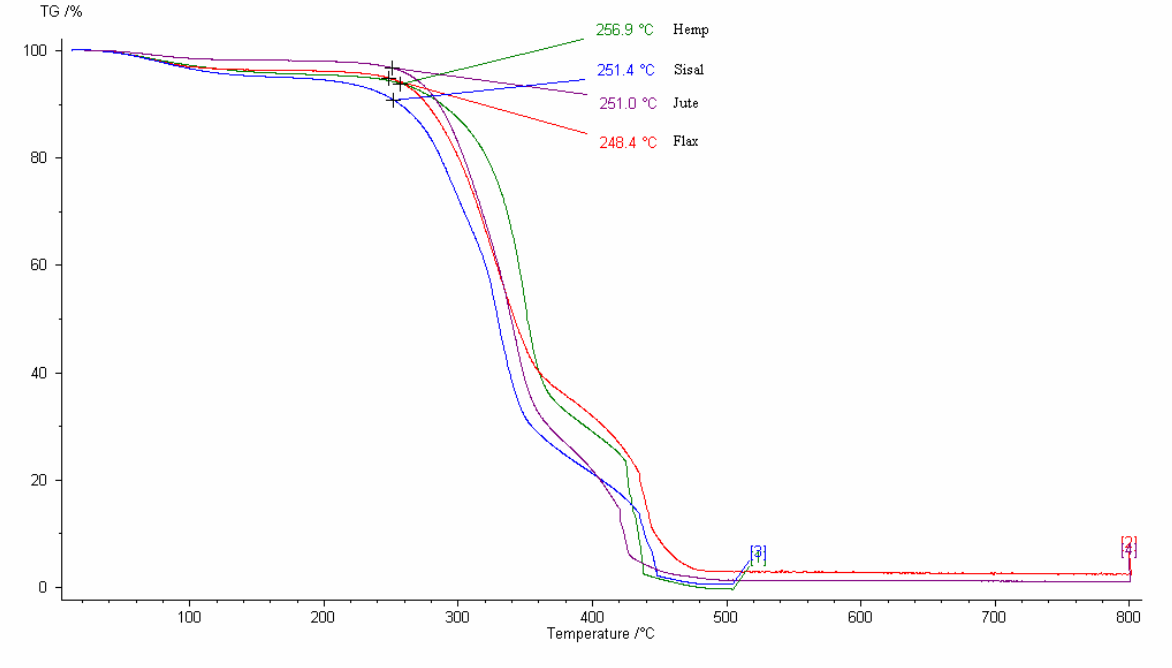

Figure 5.3 TGA of Natural fibres in air

5.2 Dry formed fibre networks

5.2.1 Scanning electron microscopy

Dry formed fibre networks are used in friction materials and a number of key results in this research have highlighted the reliance on the processing fibre within the formulation for the required level of performance. Fundamentally the performance and attributes of a fibre bulk is derived from the morphology and structure of the individual fibres within that network. This section of work shows SEM images of aramid pulp and discusses the morphology of individual fibres and the inherent material properties that tend towards the generation of such structures.

The image shown in figure 5.4 shows the scale of large fibres found in Twaron pulp 1099. Numerous fibres of this diameter were located in Twaron pulp and as discussed previously, all forms of aramid are manufactured as monofilament fibres in the region of 30 μm in diameter therefore these fibres represent the largest found in pulp 1099. Figure 5.4 shows a fibre of approximately 30 μm and smaller ribbon like fibrils in the background. On the surface of the large fibre appears a node like feature giving an increased fibre diameter in

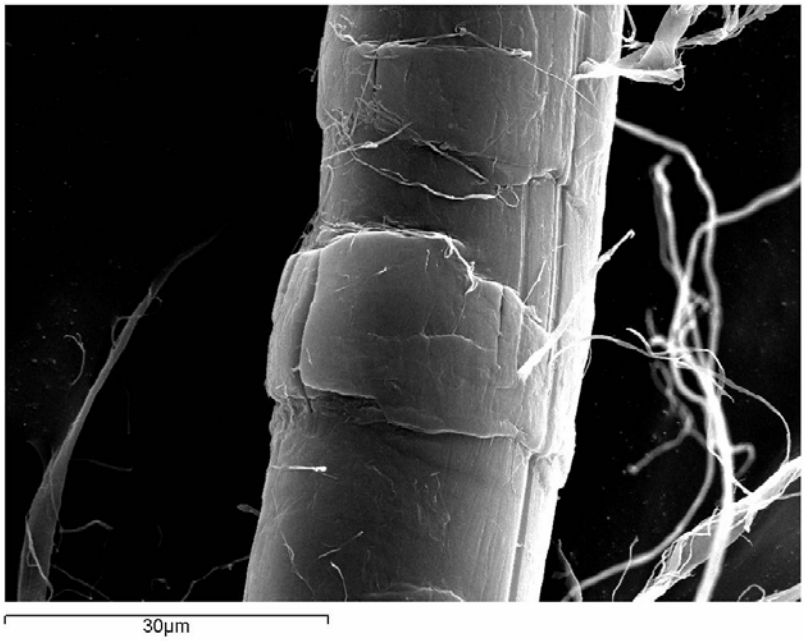

Figure 5.4 Large structural fibre in Twaron pulp

that localised area. Subsequent images and discussion will show this feature has been produced as a result of a skin core structure of aramid fibres as a result of differential molecular orientation across the fibre diameter.

The bulk of aramid pulp is occupied by ribbon like fibres much smaller than shown in figure 5.4. Figure 5.5 shows a typical mass of entwined high aspect ratio fibres that individually have a high aspect ratios and degree of curl and combine to produce a net like structure.

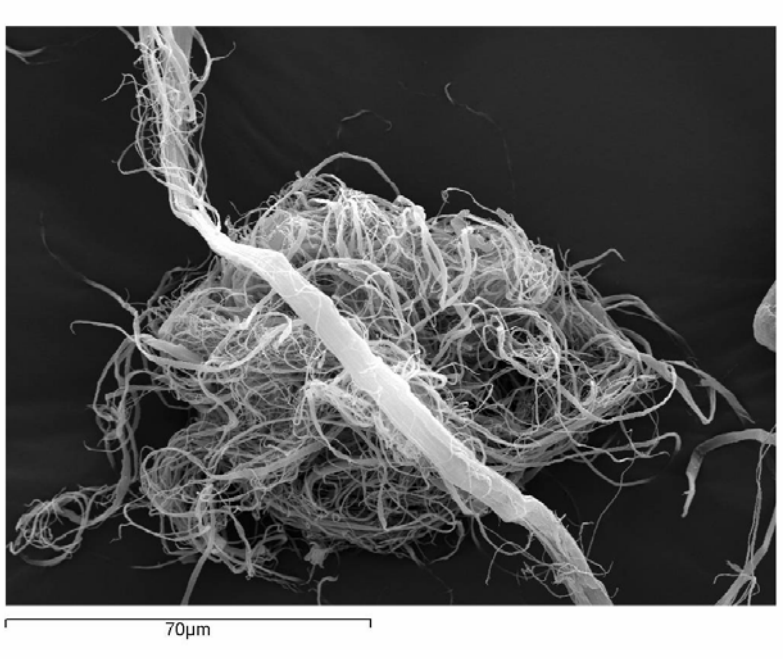

Figure 5.5 Net structure of fine Twaron fibres

Two separate length scales of aramid fibres have been shown to make up the volume of Twaron 1099 yet it is the combination of the two fibres that gives rise to the bulk mechanical properties recorded in earlier sections. Figure 5.6 shows an SEM image of a fibre structure found within the fibre pulp and illustrates the hierarchal structure of fibres found within the pulp. A larger fibre of approximately 18 µm in diameter is surrounded by an entangled network of smaller fibres of ≤ 1 µm diameter to produce a two part structure referred to from this point on as the bulk and net. The bulk volume and strength is taken from the structural rigidity of the larger fibre that supports the net like structure of finer fibrils. Figure 5.6 also shows a number of fibrils attached to the larger fibres indicating towards the origin of the smaller fibres. Certainly a proportion of the net structure will have come from other separate fibres as shown in figure 5.5 yet they combine with a larger fibre to produce a structure with bulk volume to aid mixing and green strength of friction materials and a net like structure that to aid dispersion and dust suppression of small particulates as demonstrated in later sections 5.3.1, 5.3.3.1 and 5.3.4.2.

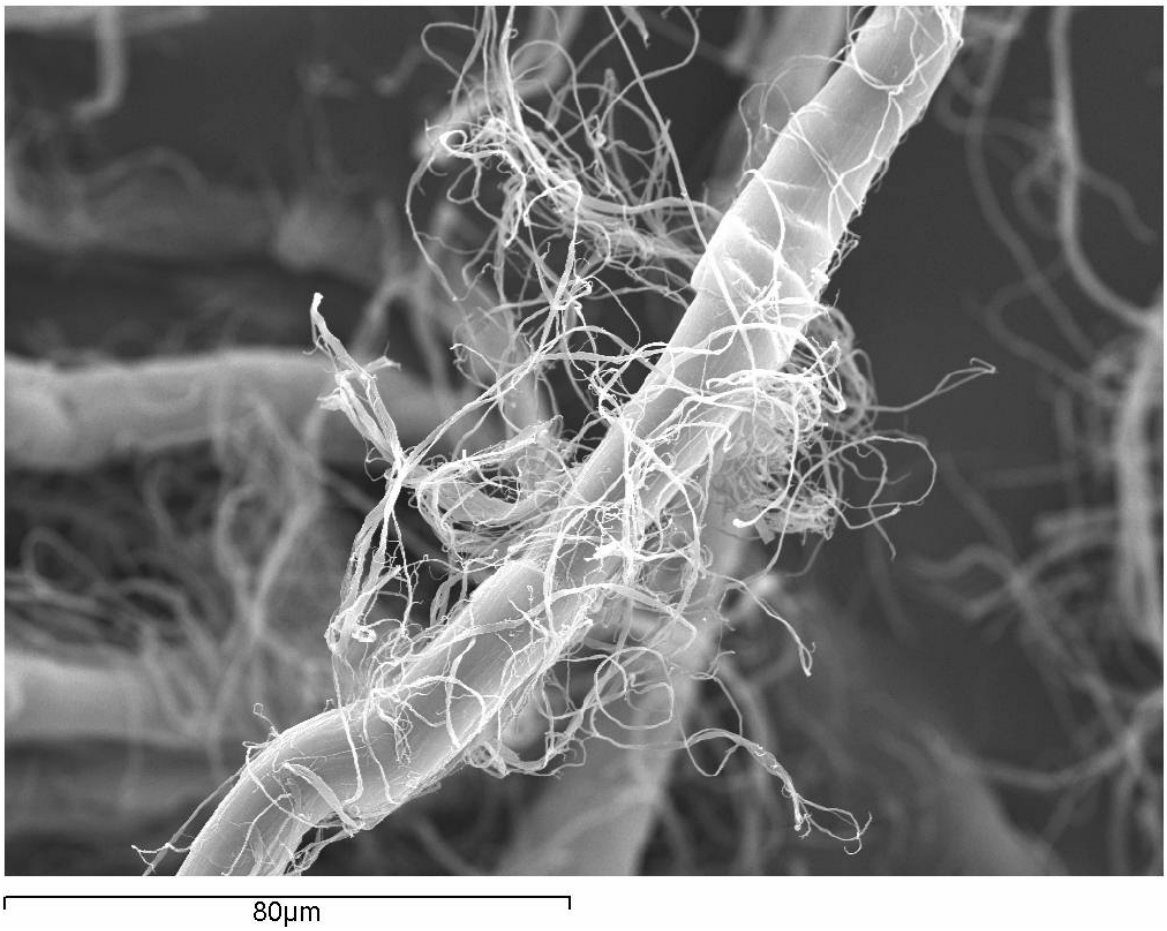

Figure 5.6 Hierarchal fibre structure of Twaron 1099 pulp

SEM images taken of aramid pulp demonstrates the toughness and resilience of the fibres as can be seen below in figure 5.7 A larger fibre from the pulp has clearly experienced damage from an external force yet with sustained plastic deformation the fibrous appearance remains, indicating the toughness of aramid fibres and their suitability to high speed mixing of friction materials.

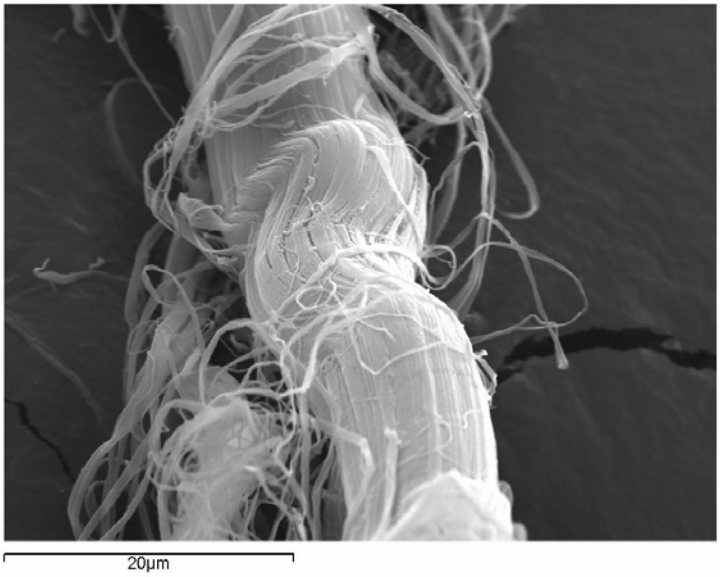

Figure 5.7 Toughness of Twaron fibres

A further example of the resilience of aramid fibres is shown in figure 5.8 as an image of a fibre that has most likely failed in the transverse fibre direction under compressive loading due to the anisotropy of aramid fibres as discussed in 2.1.4. From a fracture mechanics perspective the fibre has failed catastrophically to produce a ballooned net formation along the fibre length yet with a view to hierarchal structures shows how a single

Figure 5.8 Hierarchal structure generated from single aramid fibre

aramid fibre of less than 10 μm in diameter can generate both a bulk and net structure as shown in figure 5.6.

The combination of a bulk and net structure obtained from the aramid fibres is the key to the effective performance of the fibre pulp in friction materials. This statement is reinforced by the images taken of a Twaron sample prepared with graphite that clearly show the mechanism behind material dispersion and dust suppression in friction materials. Figure 5.9 clearly shows one of the large fibres supporting an entwined net structure which itself is supporting graphite particles that have been entrapped within the net.

Further investigation of the same sample at higher magnification shown in figure 5.10 shows the same effect of the net structure capturing graphite particles in an open fibre structure of high volume, supported by larger structural fibres.

Figure 5.9 Graphite flakes with Twaron hierarchal fibre structure

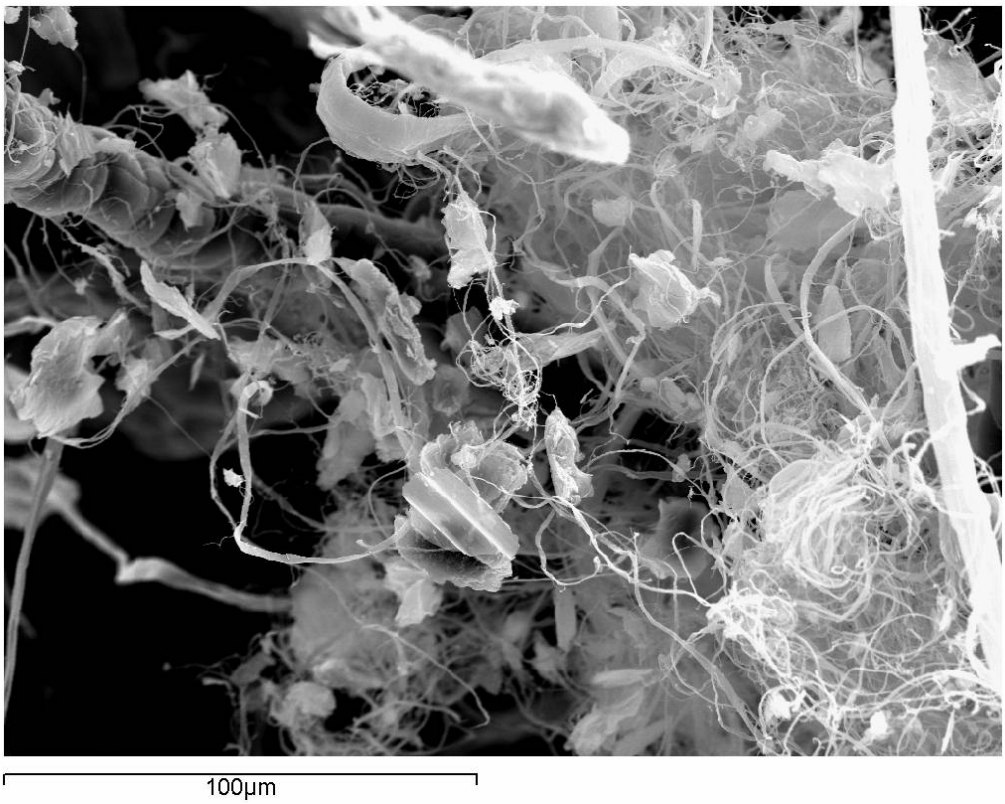

Figure 5.10 Graphite flakes within open bulk fibre structure

The bulk volume and complex fibre network structure is produced by highly fibrillated aramid fibres combining to form a hierarchal structure as previously discussed. The intentional fibrillation of aramid fibres during the manufacture of aramid pulp was covered in 2.1.4 and it is the small fibrils that form the net structure that holds friction particles in suspension thus aiding dispersion and dust suppression.

Figure 5.11 shows an SEM image of a large aramid fibre taken from the Twaron pulp that on closer inspection shows the generation of the fine ribbon like fibres from the surface of the larger fibre. The smaller fibres previously identified, that constitute the net component of the hierarchal structure are clearly formed from the surface layer of the larger fibres in the pulp due to the high degree of molecular orientation in the skin that encourages continuous ribbon fibres . A high magnification image shown in figure 5.12 shows the generation of numerous fibrils and illustrates the size differential between bulk and net fibres and also the number of smaller fibres that can potentially form from one larger fibre.

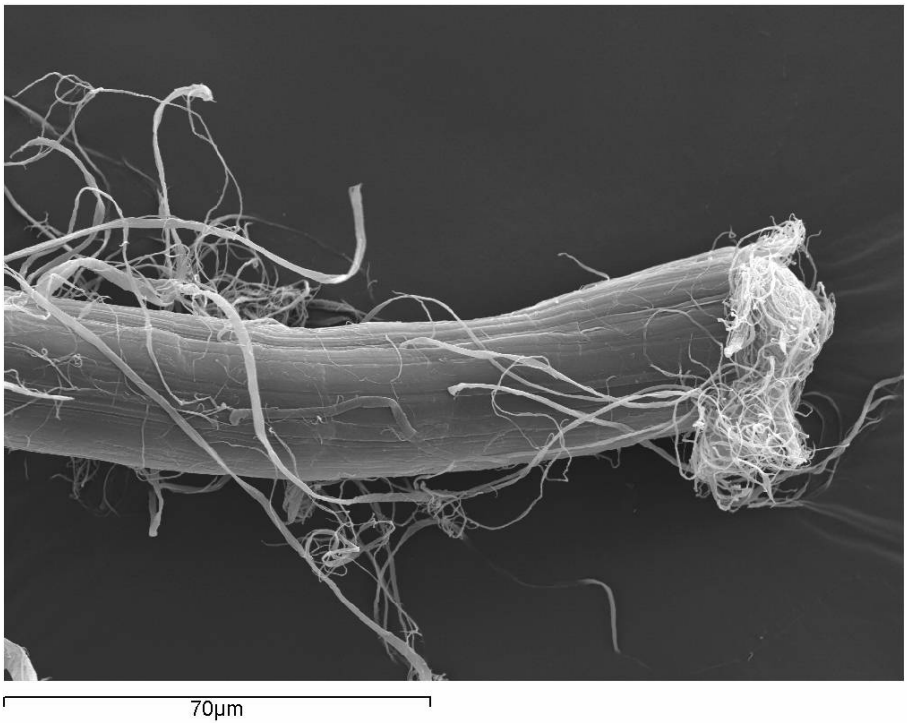

Figure 5.11 Generation of Twaron fibrils

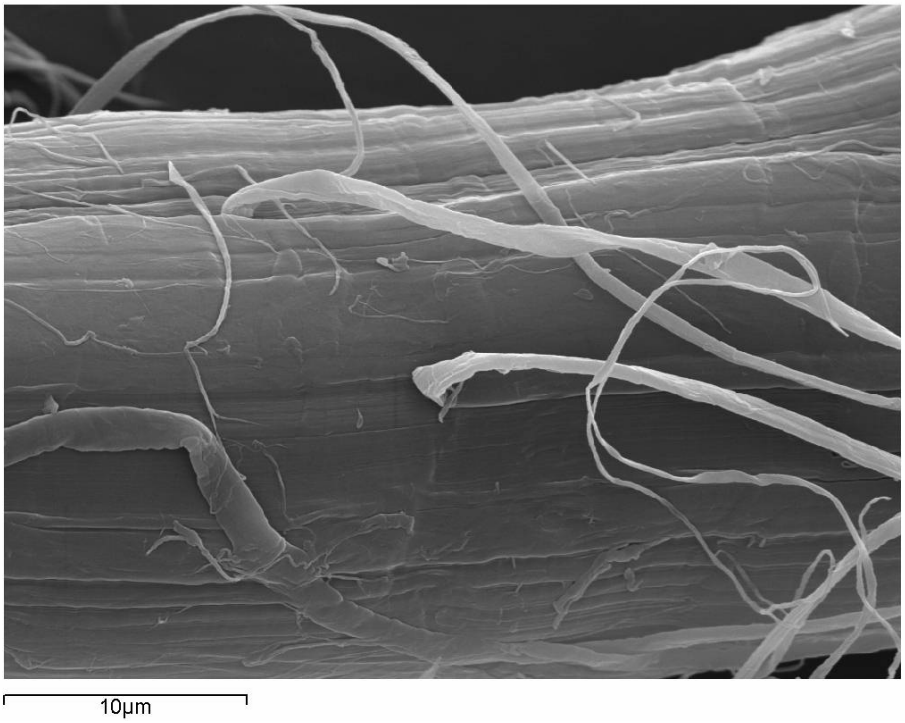

Figure 5.12 Fibrillation mechanism of Twaron fibres

It is proposed that the majority of fibre fibrils are produced from the skin layer on the larger aramid fibres, however figure 5.13 shows that due to the highly aligned molecular structure in aramid fibres, fibrils can be produced from deeper within a large fibre thus increasing the propensity for a single fibre to generate a large number of fine fibrils.

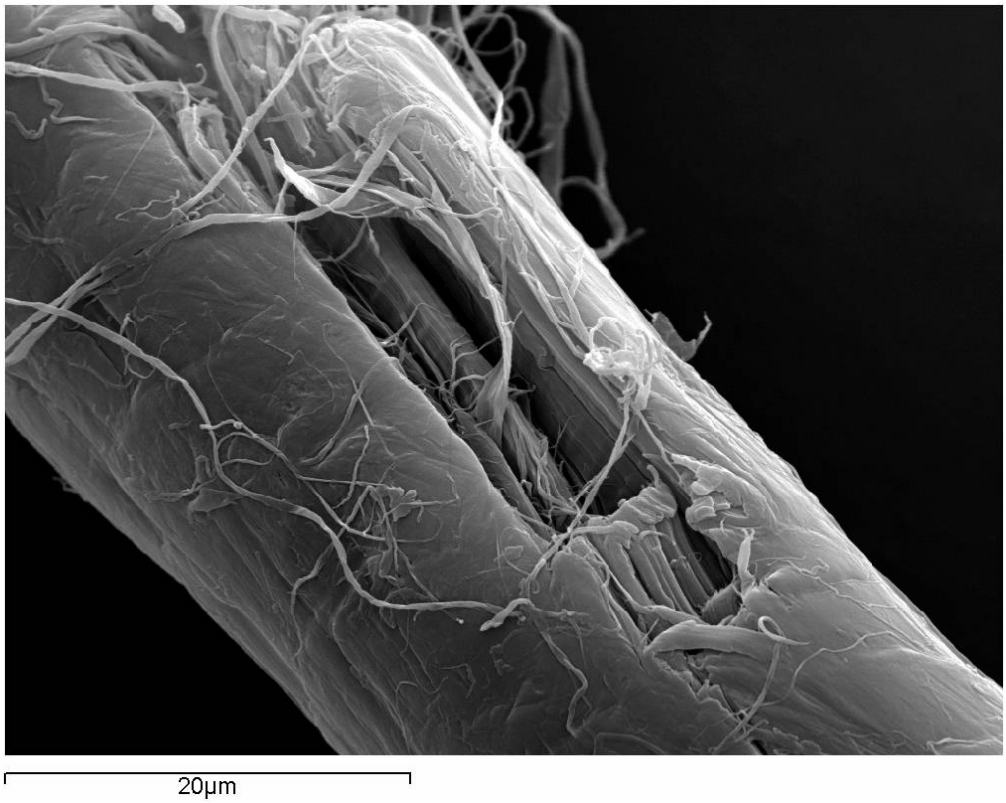

Figure 5.13 Internal and external fibrillation of a large Twaron fibre

Recycled aramid is used in friction materials to offset the high cost of virgin aramid pulp yet the lack of processing performance compared to the virgin material is marked, leading to only partial substitutions of virgin fibre. Figures 5.14a and 5.14b show SEM images of Goonvean aramid and Sterling aramid respectively – two forms of recycled material readily available to friction manufacturers. The source of the Sterling fibre is undetermined however the Goonvean material is produced from recycled fire blankets – commonly manufactured from meta-aramid. Both types of fibre are much smoother and uniform in surface finish and the pulp has a noticeable lack of net component to complement the bulk

fibres. This clearly highlights the difference in morphology between aramid fibres intentionally manufactured as processing fibres for the friction industry.

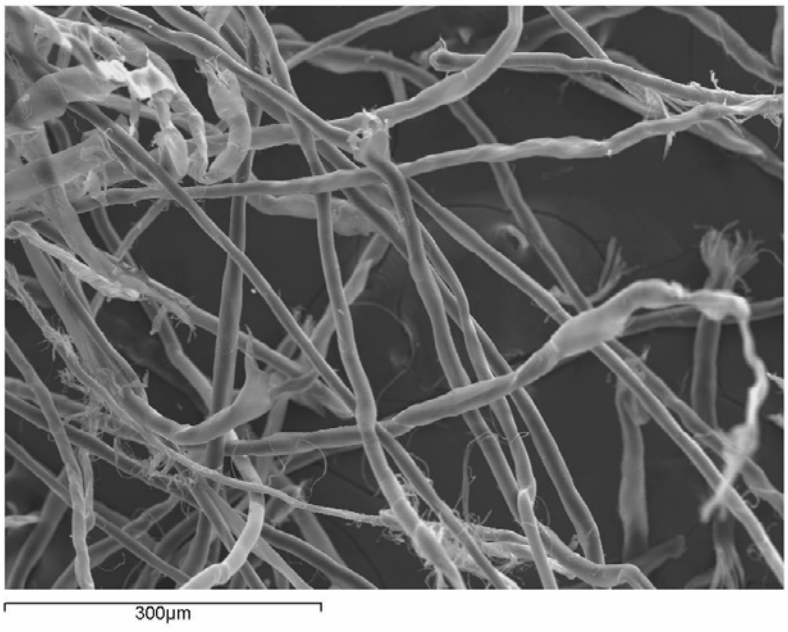

Figure 5.14a Goonvean aramid

Figure 5.14b Sterling fibres aramid

SEM images of the natural fibres used in this research were produced to compare with the morphology of the aramid fibres. Figure 5.15 shows a selection of hemp fibres and a large bundle of hemp fibres still held together by the amorphous polymers – pectin and lignin. Note the scale bar showing fibre sizes up to 10 times larger in width compared to the largest fibres in aramid pulp.

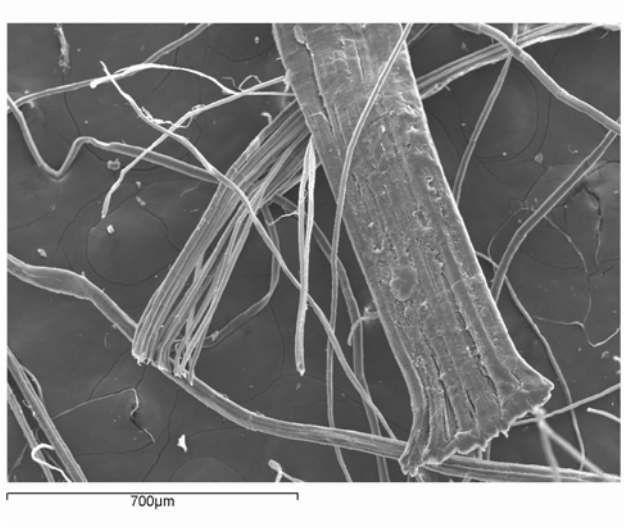

Figure 5.15 Hemcore FC fibre

High magnification images of a similar bast fibre – flax – are shown below. Figure 5.16a shows the cross section of a typical flax fibre bundle with smaller fibre bundles starting to separate. Figure 5.16b shows the cellular structure of the woody shive material frequently found alongside natural fibres. As part of the natural plant the shive has entirely different physical properties to the fibres classifying such particles as contaminants.

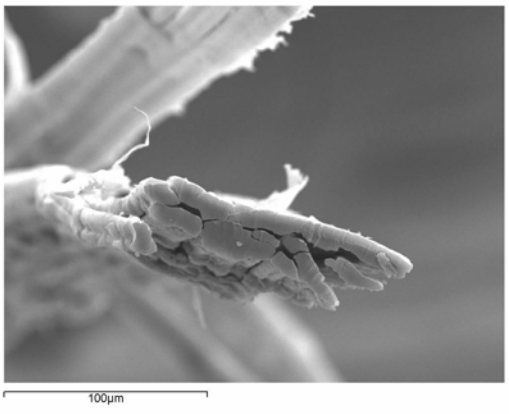

Figure 5.16a Flax fibre

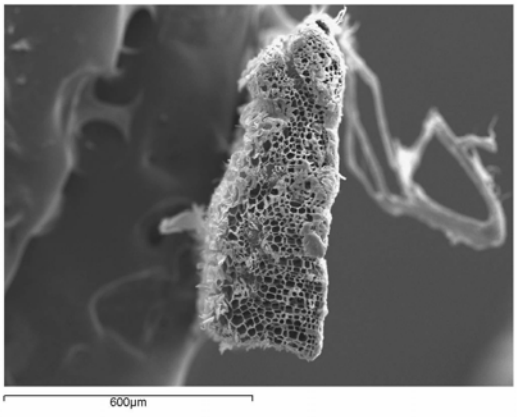

Figure 5.16b Flax contamination

The cross section of a fibre from the sisal plant is shown in figure 5.17. Much larger in size than the bast fibres, and on a similar scale to bast fibre bundles, sisal fibres did not show evidence of fibrillation after mechanical processing and predominantly fractured across the main fibre axis to produce progressively shorter sisal fibres.

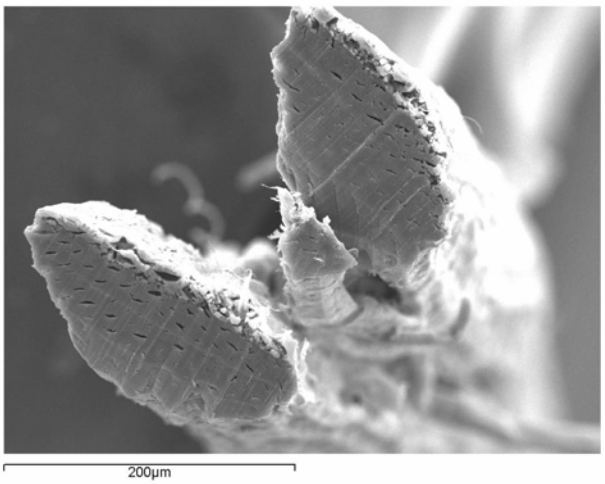

Figure 5.17 Cross section of leaf fibre sisal

In contrast to the fibre length shortening fracture of sisal fibres, hemp fibres were observed to initiate fibrillation especially at the ends of the fibres giving a brush like appearance. Figure 5.18 shows an example of an end fibrillated hemp fibre showing the formation of numerous fibres from a single hemp fibre albeit on a larger scale compared to aramid fibres.

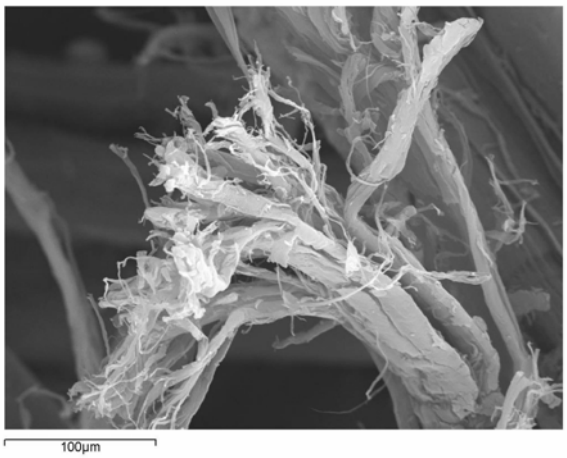

Figure 5.18 Fibrillated end of hemp fibre

No evidence of long slender hemp fibres was found indicating the inability of low diameter, high aspect hemp fibres to form due to fibre length reduction by fracturing transverse to the main fibre axis.

The mechanically fibrillated hemp fibres FC+2-4 were imaged to show fibre morphology and shown to have improved fibrillation whilst retaining the desired fibres length. Figure 5.19 shows an example of a FC+4 fibre showing fibrillation along the length of the fibre whilst still retaining the fibril to the main fibre trunk in a similar manner to aramid fibres.

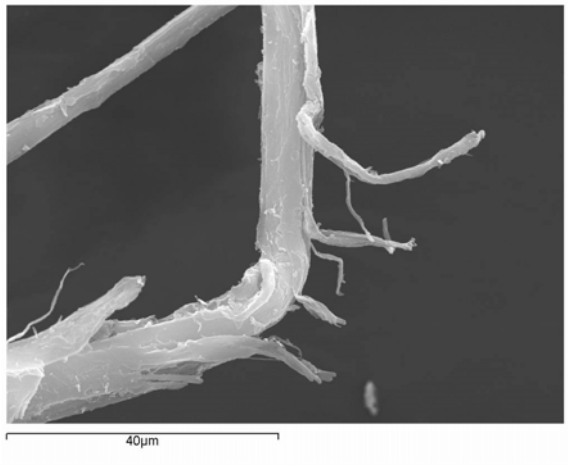

Figure 5.19 Fibrillation of FC+4 hemp fibre

Although on a different scale of fibre size and degree of fibrillation compared to Twaron 1099, the images show an increase fibre fineness and surface area compared to the hemp fibre image in figure 5.15.

5.2.2 Aramid fibre length

Of the 21 large bulk fibres randomly selected from the Twaron 1099 pulp an average fibre length of 5.82 mm was calculated with a standard deviation of 0.93 mm. In the absence of automated fibre analysis software this result, although taken from a small sample of fibres, gives an accurate length of the large bulk structural fibres found in the fibre pulp. This value was used as a length guide for natural fibres that were processed for use in the formulations.

Figure 5.20a and 5.20b show two examples of structural fibres mounted on a microscopy slide, scale bar is equal to 500 µm.

Figure 5.20a Large structural aramid fibre

Figure 5.20b Large structural aramid fibre

5.2.3 Dynamic mechanical testing

The dynamic mechanical test was employed to evaluate the bulk visco-elastic properties of dry fibre networks made from current and prospective processing fibres for friction materials and is based on the work of Askling et al [110] who employed a dynamic mechanical test to evaluate the visco-elastic response of dry formed fibre networks.

The effect of strain rate was identified in section 4.2.3.2 as an additional variable parameter in the fibre network tests. All samples were subject to the same test configuration so the test parameters are comparative for all samples.

The two measured parameters taken from this dynamic mechanical work are the elastic component of the shear modulus (G') which is used to identify the interaction of the inter-fibre contacts and the strain levels sustained before a permanent strain is imposed. The second parameter is the critical (γ_{crit}) strain level at which the onset of permanent strain is recorded. It is proposed that this strain level defines the onset of damage to the fibrous structure however further testing and microscopic inspection would be required to confirm this.

5.2.3.1 Sample preparation and loading

A series of preliminary tests were used to refine the test procedure, which furthered the work by Askling et al [110]. Due to the form of the fibrous samples used in friction materials a new method of sample loading was devised using double sided tape. The repeatability between tests was established by running 3 identical samples and plotting the results as shown in figure 5.21. The graph of elastic shear modulus versus applied strain for 3 aramid pulp samples is shown below and demonstrates an excellent correlation between runs especially for the key critical strain value when the elastic recovery of the network is reduced.

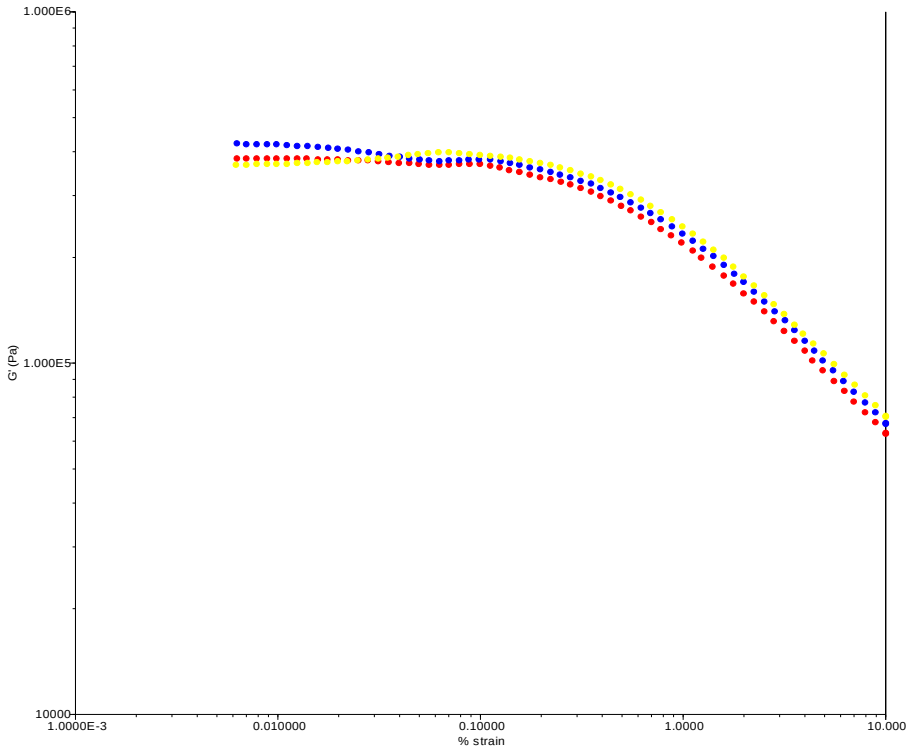

Figure 5.21 Repeatability of dynamic oscillation test

5.2.3.2 Fatigue tests

Inducing permanent structural damage to the fibrous structure by repeatedly applying cyclic strains was a concern addressed by employing a fatigue test. A fixed strain was applied to samples at a frequency of 1 Hz for a 1 hour period – over twice the duration of a standard frequency sweep test. Figure 5.22 shows a stable elastic modulus as a function of time ruling out any fatigue associated effects with the test results.

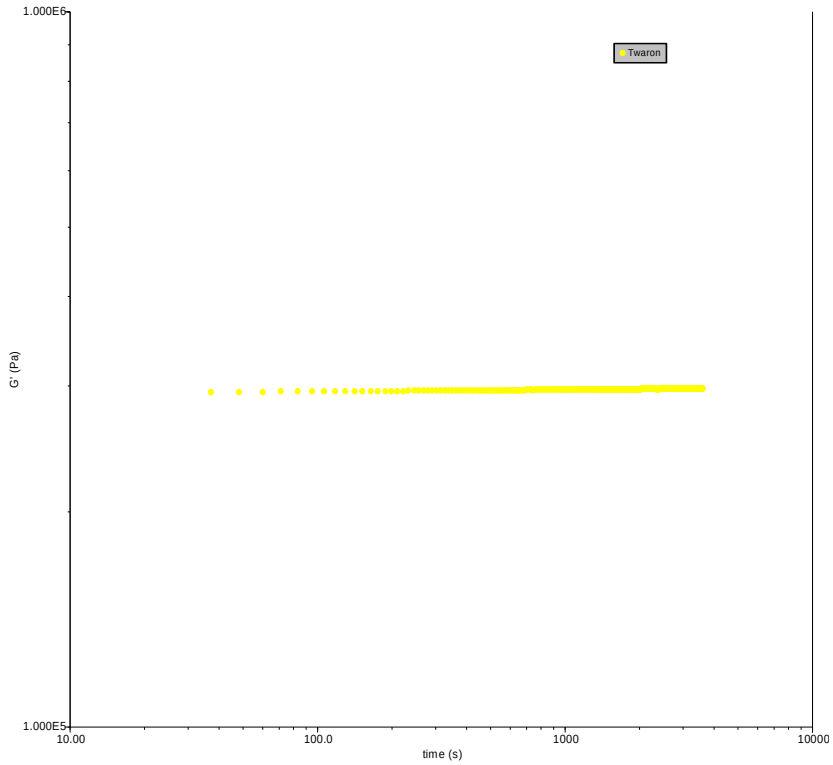

Figure 5.22 Oscillation fatigue analysis of Twaron pulp

5.2.3.3 Oscillation Tests

Having established a consistent and accurate test procedure free from repeated cycling effects, a strain sweep program was used to analyse the elastic response of various fibre networks structures to an increased level of strain at a fixed frequency.

Figure 5.23 shows the result from the Twaron sample and represents the baseline performance target for any candidate processing fibre. The two key values taken from the graph are the initial elastic shear modulus, taken from a tangent through the initial 4 low strain data points, and the critical strain value calculated using the intersection of the two tangents taken against the start and end linear sections.

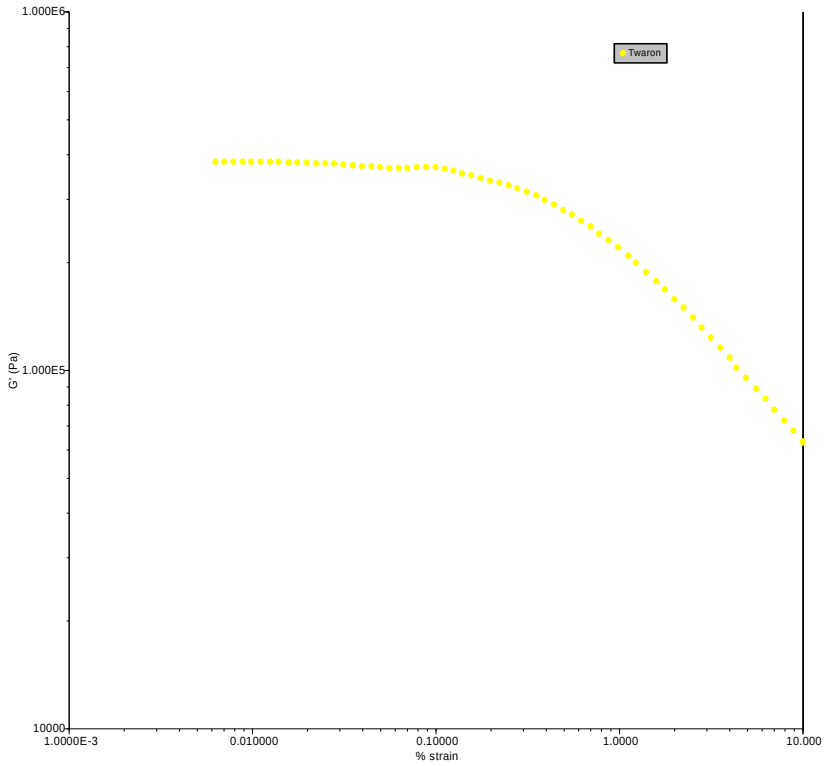

Figure 5.23 Oscillation strain sweep of Twaron pulp

Samples prepared from Sterling and Goonvean recycled aramid fibres were analysed and compared to virgin Twaron in figure 5.24. From the result it is clear that both recycled aramid fibres have comparable initial elastic shear modulus and critical strain values – which are far inferior to the highly fibrillated Twaron 1099. A lower initial elastic shear modulus is evident for both fibres and more importantly a significantly lower critical strain level equating to a much lower physical displacement is required to produce the measured critical strain level.

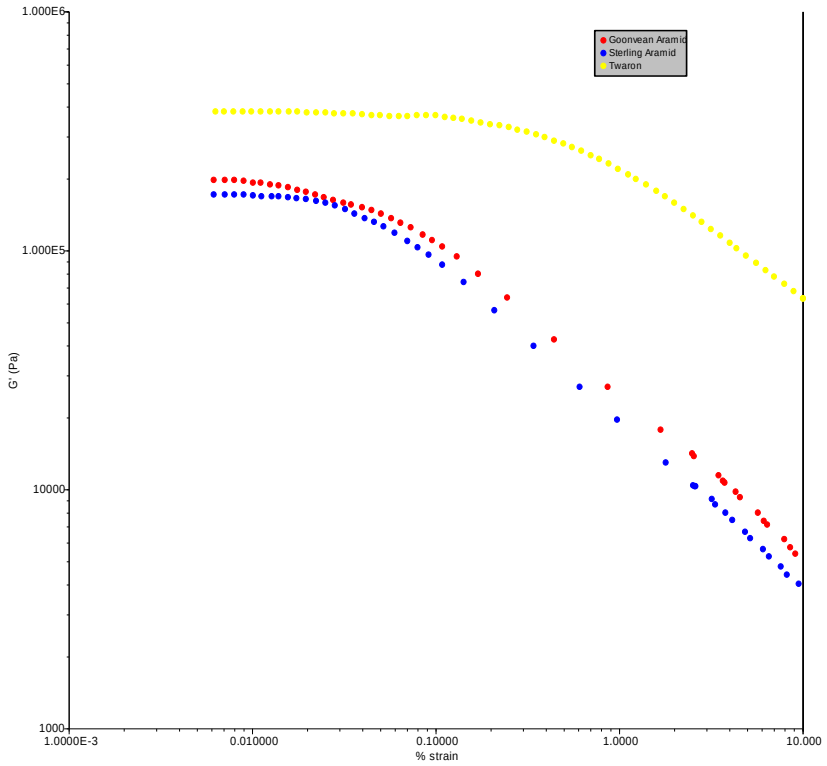

Figure 5.24 Oscillation strain sweep of Twaron and recycled aramid

Moving away from aramid fibres, two other commonly used fibres in friction materials were analysed using the oscillation frequency sweep to establish the elastic shear modulus of other fibrous materials not primarily used as processing aids. Cellulose fibres are a cheap raw material commonly added as a bulking agent and to aid other processing fibres in the formulation. Rockwool is synthetically manufactured to produce very short uniform mineral fibres used in friction materials for thermal stability. The data is shown in figure 5.25.

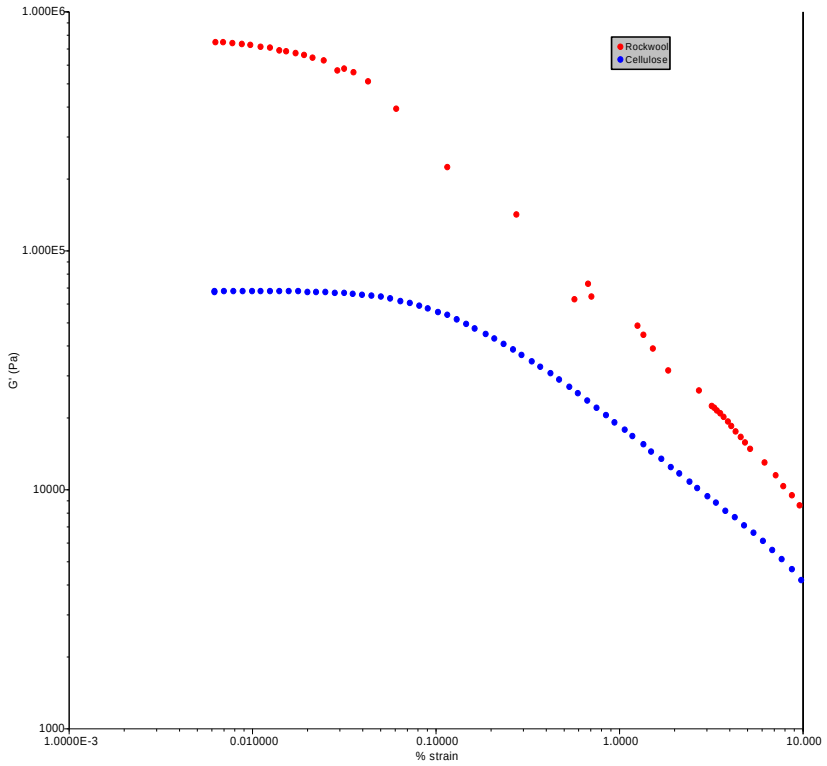

Figure 5.25 Oscillation strain sweep of Rockwool and cellulose fibres

Blends of aramid fibres and hemp fibres have proved a major part of this research as it has been shown that the unique morphology of Twaron pulp is required to manufacture friction materials to the required performance levels. The oscillation test was used to determine the optimum ratio of hemp and aramid blends to produce a dry fibre network with the highest critical strain level before network failure. It is proposed that large critical strain values are achieved through highly entangled fibre networks with numerous inter-fibre contacts/entanglements.

To determine the optimum natural fibre to use in the blends, the oscillation test was employed to evaluate the highly processed hemp fibres FC+2 through to FC+5. A summary of the results can be found in table 5.2.

Fibre type	Initial Elastic shear modulus (Pa)	Critical Strain
Twaron 1099	3.89×10^5	0.472
Sterling aramid	1.683×10^5	0.06574
Goonvean aramid	1.841×10^5	0.04075
Cellulose	6.939×10^4	0.1418
Rockwool	6.454×10^5	0.08993
FC+2	1.22×10^5	0.06052
FC+3	1.30×10^5	0.0665
FC+4	1.55×10^5	0.07212
FC+5	1.87×10^5	0.05949
1.5% 1099 2.25% FC+4	2.58×10^5	0.2485
2% 1099 1.75% FC+4	2.57×10^5	0.3379
2.5% 1099 1.25% FC+4	3.21×10^5	0.3377
3% 1099 0.75% FC+4	3.03×10^5	0.4158

Table 5.2 Summary of dynamic oscillation fibre network results

The optimum fibre selected was the FC+4 fibre which produced the highest critical strain level of all the processed natural fibres. This indicates that the additional mechanical processing increased the fibrillation of the hemp fibres, which in turn increased the elastic shear modulus of the fibre network and the maximum strain it can withstand before the onset of permanent strain. The fibre FC+5 showed a reduction in the critical strain level which was attributed to over processing of the hemp fibres.

Fibre blend samples were produced and the oscillation tests repeated to establish the optimum ration of aramid to hemp, having found the hemp fibre network with the highest resilience to an applied strain. The results are summarised in table 5.2.

Figure 5.26 below compares a virgin Twaron sample with an A3(FC+4)0.75 sample.

The initial elastic modulus of the fibre blend is lower than the virgin Twaron and shows a minor increase in stiffness, peaking at a strain level of 0.06. The critical strain of the fibre network is 88% of the virgin Twaron and has reduced the aramid content by 20% which

represents a major cost saving considering the relative cost of the fibres and the volumes used by the friction industry.

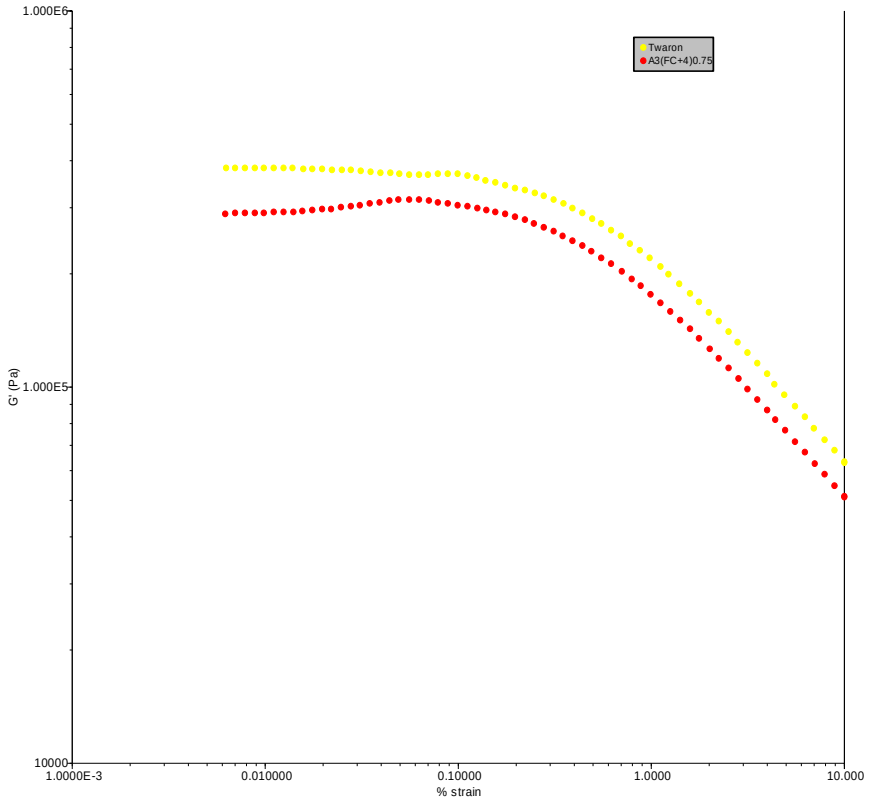

Figure 5.26 Oscillation strain sweep of Twaron and A3(FC+4)0.75

5.3 Friction material formulation

5.3.1 Dust Suppression

The sieve test results are shown in figure 5.27 together with a fitted linear regression line. A high fall though mass is a result of particulates that have not been captured by the processing fibre (Twaron) within the formulation and would manifest themselves as dust in an industrial manufacturing process. Reducing the percentage of aramid pulp from the master batch formulation level of 3.75 % by volume increases the mass of free particles in a linear manner until the formulation with 1 % by volume increases sharply with an average mass equating to a separation of 43 % by mass of particulates. As the percentage of aramid is reduced in the formulation the amount particulate materials held together in suspension also declines indicating the effect of Twaron pulp as a dust suppressing fibrous network. The spread of data increases with the reduction of aramid content resulting not only in a lower performance but also a less predictable performance in terms of particulate suspension and dust suppression.

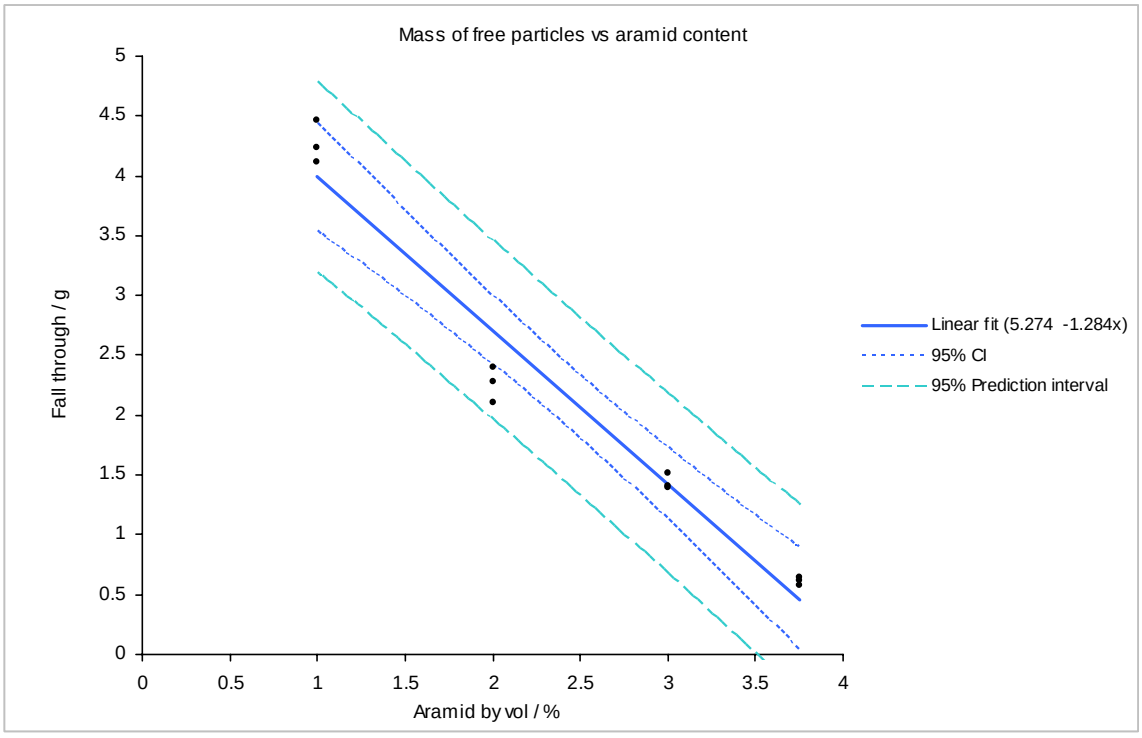

Figure 5.27 Mass of separated particle from formulation versus aramid content

The probability values calculated for the regression line slop and intercept equalling zero are shown below. Both values are very low indicating a direct relationship between aramid content and dust suppression.

P_{slope} = < 0.0001

$P_{intercept}$ = <0.0001

5.3.2 Bulk density

The bulk density of a friction formulation describes the mass per unit volume of a friction formulation. The processing fibre provides the volumetric bulk to the formulation therefore the bulk density is a key measure of the performance of the processing fibre. The processing fibre is solely responsible for adding volume to a formulation that is otherwise composed of dry powders and particulates, and undergoes a rigorous mixing process that can easily destroy a delicate fibrous structure.

Table 5.3 shows the measured bulk density of formulation as a function of fibre content, starting with the baseline value of 3.75 % aramid by volume. Reducing the aramid content in the formulation increases the bulk density which equates to a low volume "flat" friction formulation which is undesirable during subsequent compression and pre-forming stages. As the aramid content is further reduced by a drop of 2 % by volume the bulk density of the formulation has increased by over 40 % indicating the substantial affect of aramid pulp on the bulk density value. The effect of Aramid pulp is further highlighted by comparing the measured bulk density against the apparent bulk density values calculated using the volume fractions and densities of constituent materials in the formulation as show in table 4.1.

Data shown in table 5.3 is represented graphically below in figure 5.28.

The probability of the slope of the line fitted to the data set equalling zero is very low indicating a direct relationship between aramid content by volume and bulk density measurements. The probability of the intercept equalling zero is also very low, indicating this relationship will not pass through the origin of the graph.

P_{slope} = < 0.0001

$P_{intercept}$ = <0.0001

Fibre inclusion (% by vol)	Bulk density (kgm^{-3})	% increase on Master Batch	% increase in apparent density
aramid 3.75	431	0	0
aramid 3	469	8.8	0.7
aramid 2	505	17.2	1.8
aramid 1	607	40.8	2.9
aramid :FC+4 50:50	474	9.9	1.8
Hemcore short 3.75	774	79.6	0

Table 5.3 Bulk density of friction formulations

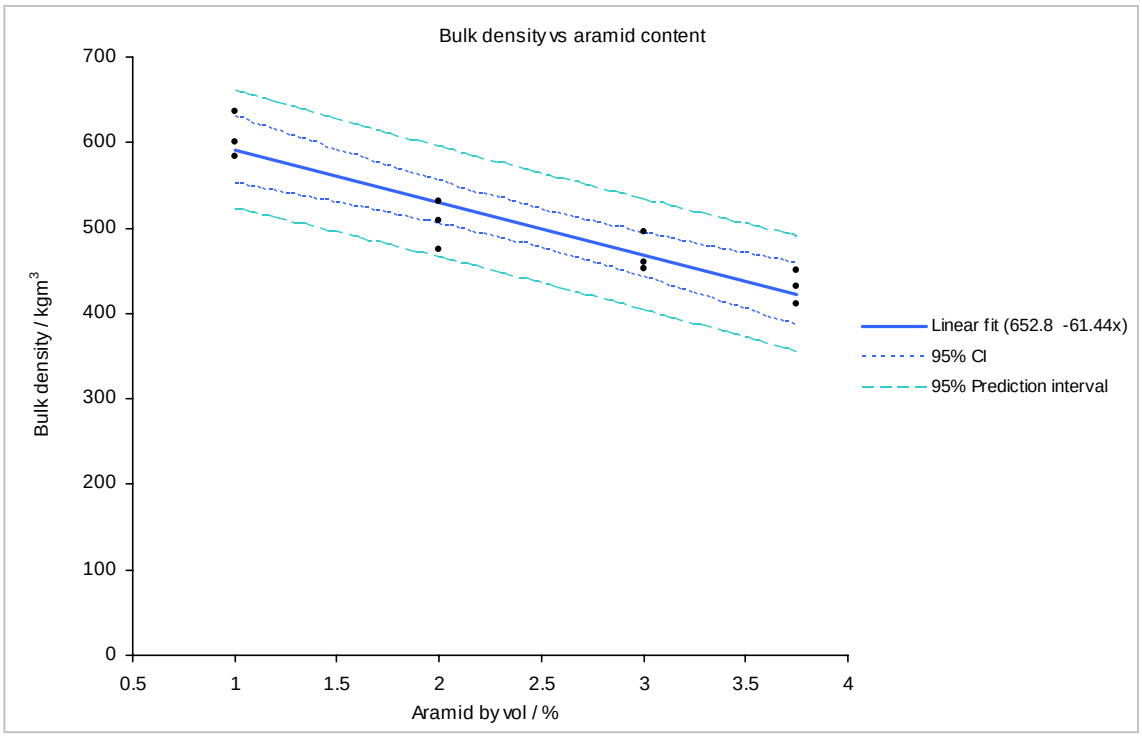

Figure 5.28 Bulk density versus aramid content

Two additional measurements were taken on formulations containing hemp fibres and hemp and aramid blends to show the effect of processing fibre on the bulk density. Substituting 1.875 % of aramid pulp with the highly processed hemp fibre FC+4 to produce a 50:50 blend gave a bulk density lower than that of the formulation containing 2% aramid indicating the additional increase in volume gained from using a highly processed hemp fibre. The remaining bulk density calculation was taken on a formulation trialled using solely Hemcore short hemp as the processing fibre and produced the highest bulk density value of all the formulations – considerably higher than the formulation containing only 1 % aramid by volume – and a negligible processing benefit from using that type of hemp fibre alone in the formulation.

Statistical analysis of the data shown in table 5.3 using the Kruskal-Wallis rank test and the Chi square distribution function in Excel;

Kruskal-Wallis H =9.97

CHIDIST = 0.018 = 1.8% (d.o.f = 3)

As the Chi distribution is less than the critical value of 5%, it can be confirmed that the data set medians are independent of one another and that the Aramid content has a direct effect on the measured bulk density when blended with natural fibres in formulations.

The bulk density of friction formulations is highly sensitive to the both the processing fibre and the inclusion levels of that fibre. Aramid pulp is a high performance processing fibre that greatly increases the volume of a friction formulation and is able to withstand the high speed mechanical actions subjected during mixing. Bulk density measurements of aramid pulp before and after mixing were taken to demonstrate the effect of the mechanical action of mixing on the bulk structure of the pulp and to determine the volume fraction of fibres in the Twaron 1099 pulp. Table 5.4 shows the bulk density of a theoretical solid block of aramid compared to the Twaron 1009 pulp as received and post mixing.

TWARON FORM	BULK DENSITY (KG/M^3)	VOLUME FRACTION OF FIBRES (%)
Solid Twaron	1440	100
1099 pulp as received	32.356	2.247
1099 pulp 5 mins mixed	12.416	0.8622

Table 5.4 Bulk density and volume fraction of aramid pulp

This result demonstrates the low bulk density and volume fraction of aramid fibres found in this form of Twaron pulp produced from monofilament tows. The compression history of the fibre pulp introduced during packaging and transportation is removed once the pulp is mixed in a laboratory mixer to increase the bulk density by over 250 %. This demonstrates the low volume fraction of fibres within the pulp bulk density but also the resilience of the fibre structure to the high speed cutting action of the mixing blades and the effect an initial mixing stage has on the bulk volume of the resultant formulation.

5.3.3 Manufacture of Pre-forms

5.3.3.1 Green Strength

The green strength of pre-forms is crucial to friction manufacturers using the pre-forming stage to manufacture brake pads. Pre-forms must demonstrate a high geometric stability and be resilient to handling by the factory operatives. Figures 5.29a and 5.29b show the difference in geometric integrity of pre-forms produced using formulations incorporating 1% and 3.75% aramid by volume respectively.

Figure 5.29a Pre-form 1 % aramid pulp

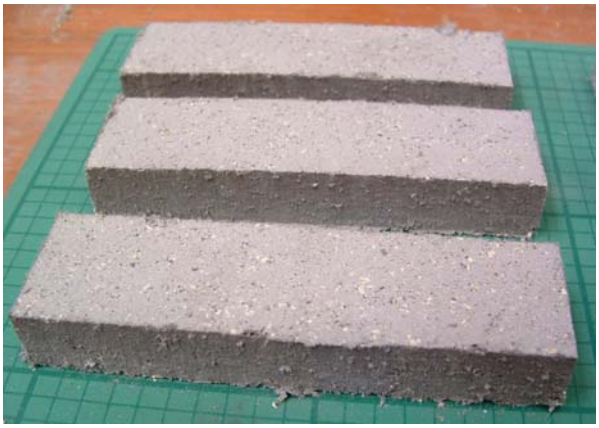

Figure 5.29b Pre-form 3.75% aramid pulp

It is clearly evident from figure 5.29a the lack of structure and edge definition to a pre-form manufactured using 1% aramid by volume. Manufacturing brake pads from this formulation is unfeasible due to high wastage of material and a geometric integrity varying widely from the design shape. Structural integrity of the pre-forms is achieved through a highly dispersed network of fine aramid fibres that once compacted provide a skeletal structure to support the remaining raw materials and a bulk volume to produce well defined angular edges and three dimensional pre-form structures. The indentation test designed to replicate manual handling by factory operatives provides a further insight into the

mechanical strength of pre-forms as a function of the aramid content. A typical force/deflection curve from a test, used to calculate the peak load is shown below in figure 5.30.

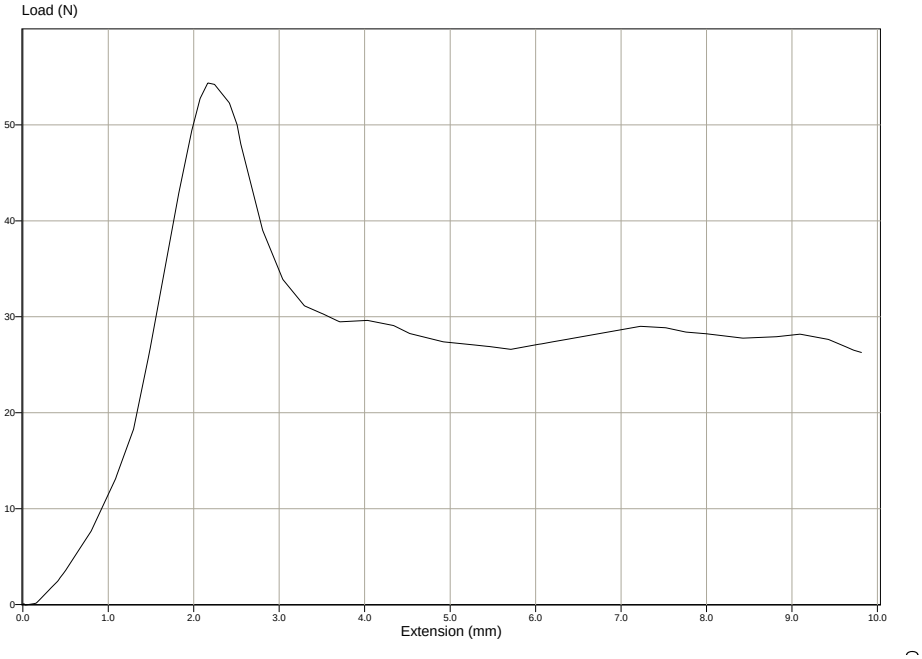

Figure 5.30 Load/deflection curve for pre-form indentation

The complete data set from the pre-form indentation tests is shown in figure 5.31 together with a fitted linear regression. The mean maximum indentation load recorded before structural failure of the pre-forms shows a near linear relationship with the volumetric aramid content. The test produced a failure of the pre-forms typically seen by a manual handling error and so represents a fast and accurate method of evaluating the green strength performance of a processing fibre. The spread is the data for each formulation is relatively high with little appreciable strength gain between 2 % and 3% aramid by volume. There is a noticeable performance advantage achieved by using the master batch level of 3.75 % producing an average maximum load of 50.2 N and a minimum target for future candidate formulations.

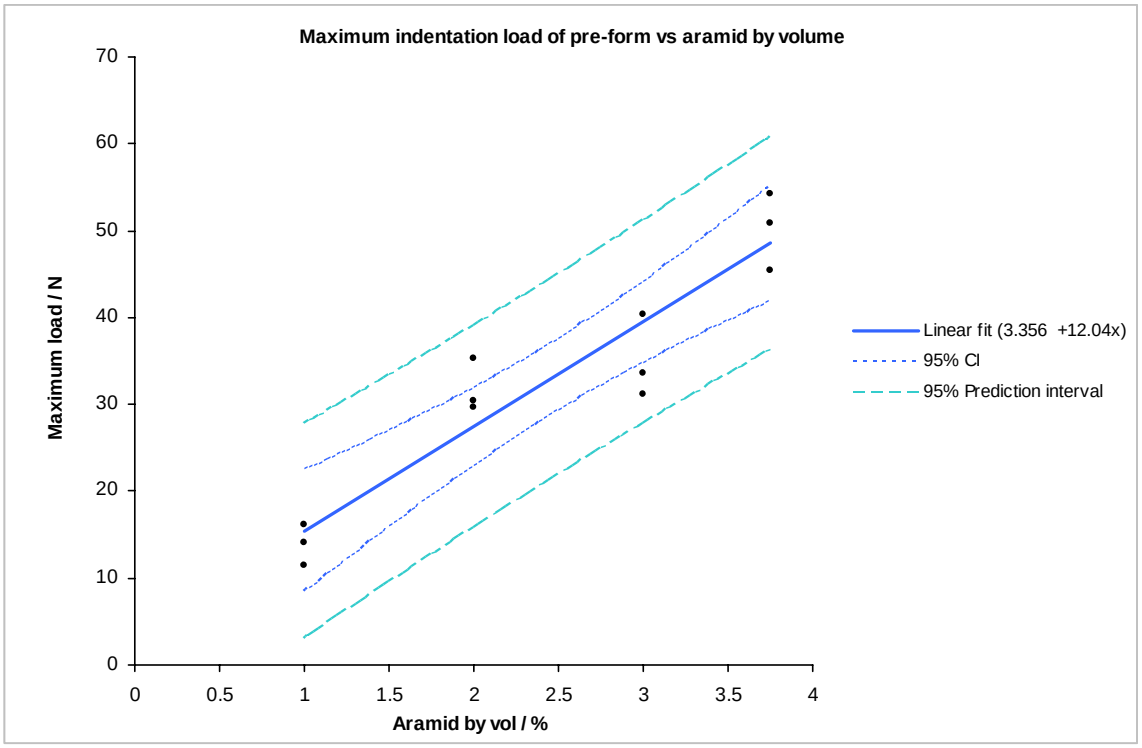

Figure 5.31 Maximum indentation load of pre-form vs aramid content

Statistical analysis of the data shown in figure 5.31 using a linear regression returns the following probability values for the intercept and slope equalling zero;

P_{slope} = <0.0001

$P_{intercept}$ = 0.3826

The probability results clearly show the slope is not equal to zero however the probability is high that the intercept is and will occur at the origin of the data plot.

Numerous formulations using natural fibres as a direct replacement for aramid were produced yet no variant of natural fibre type or morphology could impart the equivalent green strength of even 1% aramid by volume. This result focused attention towards the physical structure of aramid pulp and the morphology of the individual fibres that combined to produce the complex fibre pulp structure that provided the skeletal structure to the friction formulations. The next stop was to investigate the effect of partial replacement of aramid using natural fibres on the pre-form green strength. Three formulations were

produced using different morphologies of hemp fibres on an equal volumetric ration with aramid pulp. Figure 5.32 shows the maximum load of indentation of pre-forms made using the aramid natural fibre 50:50 ratio in addition to the master batch result take from figure 5.31.

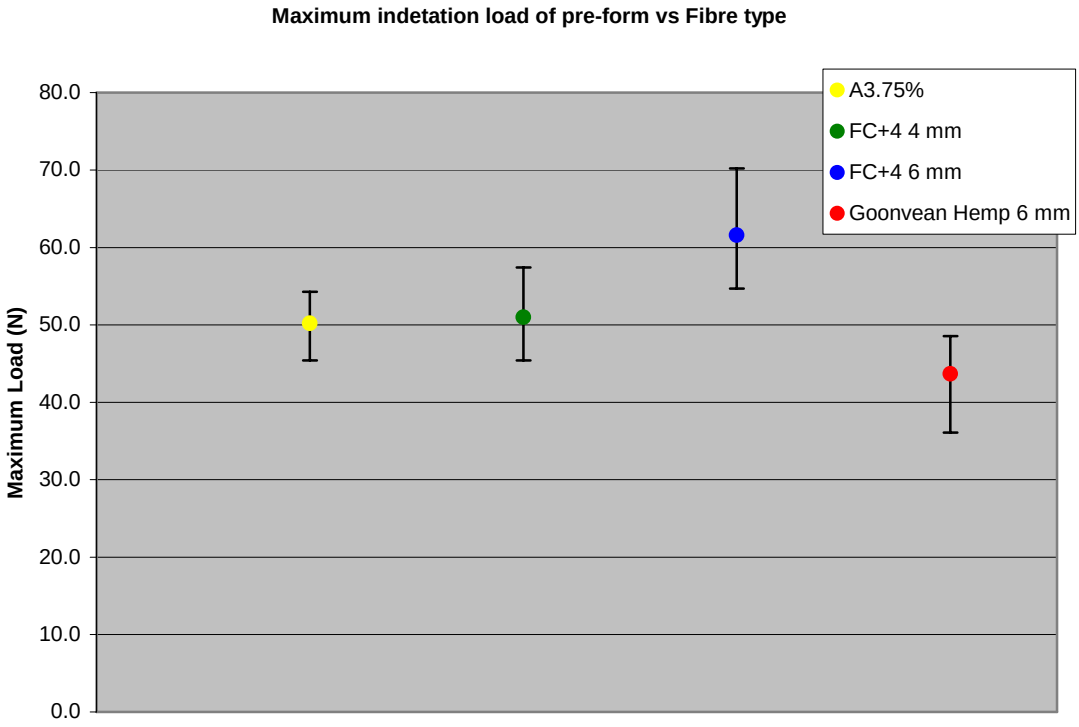

Figure 5.32 Maximum indentation load of pre-form vs fibre type

The results in Figure 5.32 show that the highly processed and fibrillated hemp fibre FC +4 in 4mm length, combined with aramid, produces a comparative mean green strength with the Master batch formulation. Introducing 6mm length hemp fibres into the formulation demonstrates a further increase in the mean pre-form strength. The Goonvean hemp fibres, obtained from recycled fibre sources, smooth in surface morphology and comparable in fibre length, demonstrate a marked reduction in reinforcing strength to the pre-forms, highlighting the effect of fibre fibrillation on the performance of processing fibres in friction materials. The variations in mean pre-form strength are closely related and require statistical analysis to make further conclusions regarding the relationship between data sets.

Statistical analysis of the data shown in figure 5.32 using the Kruskal-Wallis rank test and the Chi square distribution function in Excel;

Kruskal-Wallis H = 6.45 (d.o.f = 3)
CHIDIST = 0.091

As the Chi distribution is greater than the critical value of 5%, it can be confirmed that the data set medians are equal and the variation in data spread lie within experimental error. This shows that a pre-form strength equivalent to the standard formulation can be achieved by substituting half the aramid fibres by volume with hemp fibres in either 4 mm or 6 mm lengths.

5.3.4 Manufacture of Friction composites

5.3.4.1 Flexural Strength of composite

Flexural tests were employed on cured friction composites to evaluate the reinforcing effect of aramid pulp on the economy friction formulation used in this research. Samples were manufactured and tested as described in 4.2.6. Five samples for each formulation were tested, each one failing in a tensile fracture mode on the underside face of the sample. Figure 5.33 shows the maximum flexural stress within the samples at failure as a function of aramid content.

Figure 5.33 clearly shows a comparable flexural strength for each formulation as a function of aramid content. The linear regression shows there is no statistically significant relationship between aramid percentage and flexural strength. This is a key result and contradicts the published benefit [66] of Twaron in friction formulations as a reinforcing fibre that imparts mechanical strength to composite brake pads. The relationship is confirmed using the linear regression analysis to return the probability values for the slope and intercept of the linear fit.

P_{slope} = 0.7125
$P_{intercept}$ = <0.0001

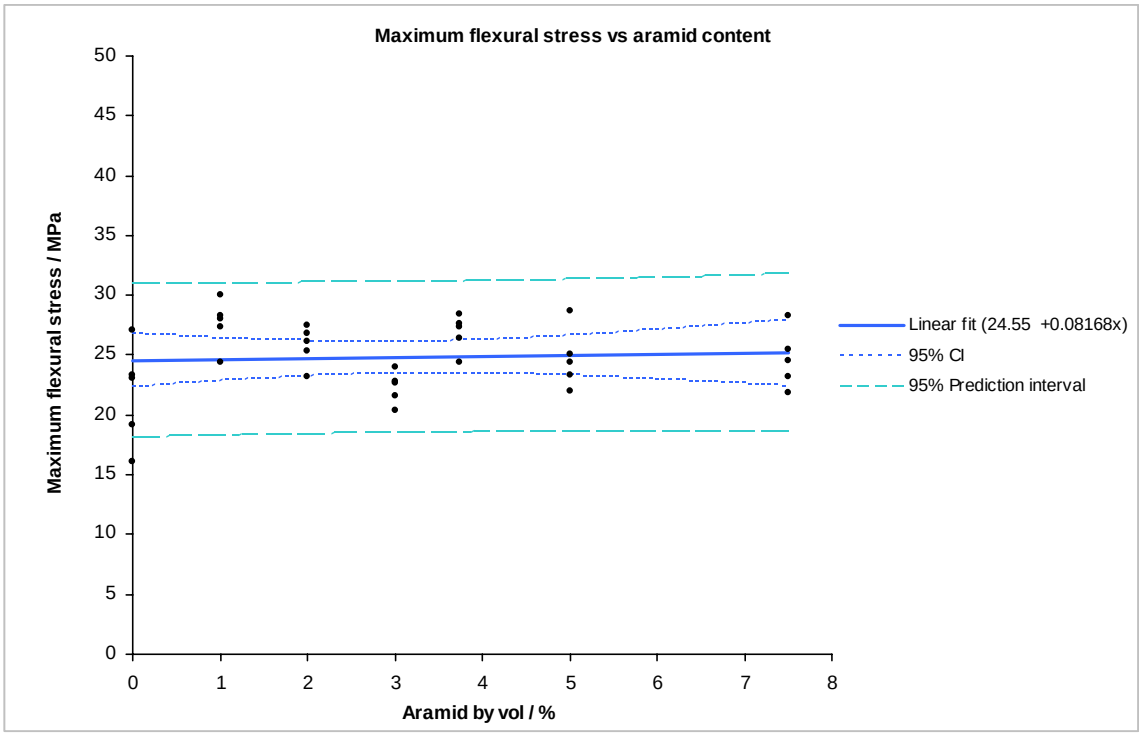

Figure 5.33 Flexural strength of friction composite versus aramid content

Having demonstrated no appreciable reinforcing benefit at ambient temperature it is possible that a similar result will be witnessed at elevated temperatures, thus any assumption made regarding the thermal stability of aramid can be negated in terms of mechanical strength.

5.3.4.2 Dispersion of materials

EDX

Safe and predictable performance of composite friction materials requires a composite material with a three dimensional homogenous distribution of raw materials. Energy Dispersive X-ray analysis (EDX) was used to produce elemental maps of the surface of a friction composite to show the dispersion of raw materials. Figure 5.34 shows an SEM image at low magnification taken of a composite manufactured from A0 formulation. Light areas correspond to materials with a high atomic contrast and vice versa for darker regions.

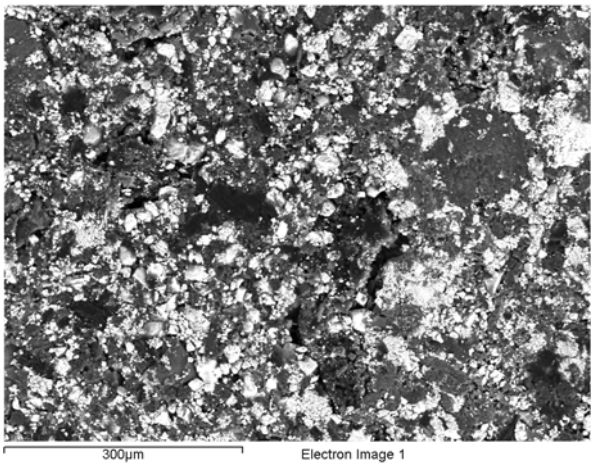

Figure 5.34 SEM image of A0 formulation surface

The EDX maps of the same image, at the same scale showing the distribution of elements antimony and barium are shown in figures 5.35a and 5.35b respectively. Selecting these elements allows for the clear identification of the raw materials antimony tri-sulphide and barium sulphate.

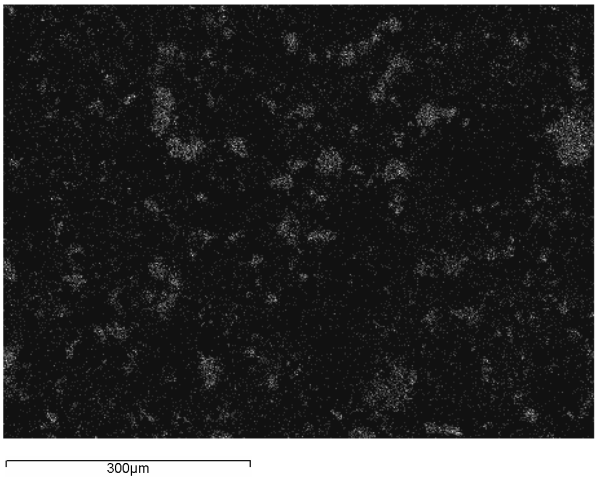

Figure 5.35a Antimony distribution across A0 composite surface

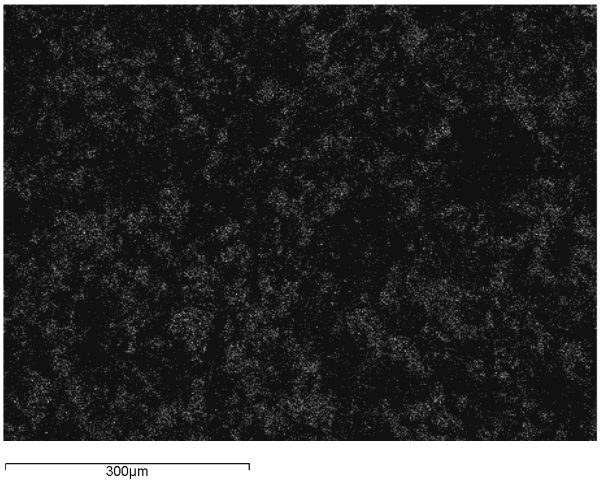

Figure 5.35b Barium distribution across A0 composite surface

Figure 5.35a clearly shows antimony tri-sulphide particles agglomerating together and an uneven distribution across the scanned area and to a lesser extent the same can be said for the barytes particles which although present in larger quantities, still shows a tendency to form patched areas without the presence of aramid pulp in the formulation.

The EDX process was repeated for a friction composite manufactured from A3.75 – master batch formulation – to compare the dispersion of the same raw materials with aramid pulp present. The EDX maps produced showing the dispersion of elements antimony and barium shown in figures 5.36a and 5.36b respectively. In comparison the antimony particles are more highly dispersed and do not form antimony rich areas on the same scale as figure 5.35a. The barytes particles also show a finer distribution across the surface of the friction material compounding the statement that aramid pulp in friction formulations aids an even distribution of other particulate materials in the formulation.

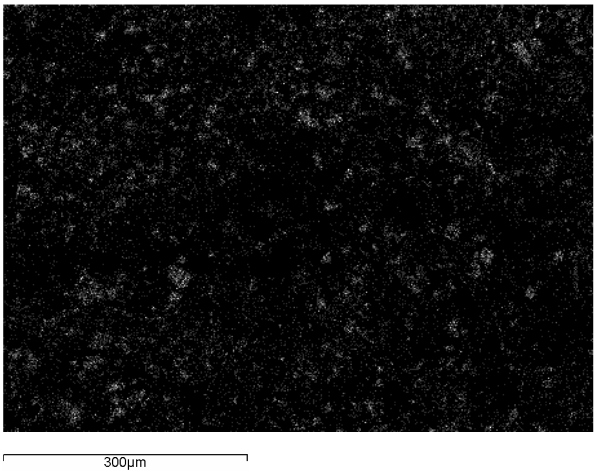

Figure 5.36a Antimony distribution across A3.75 composite surface

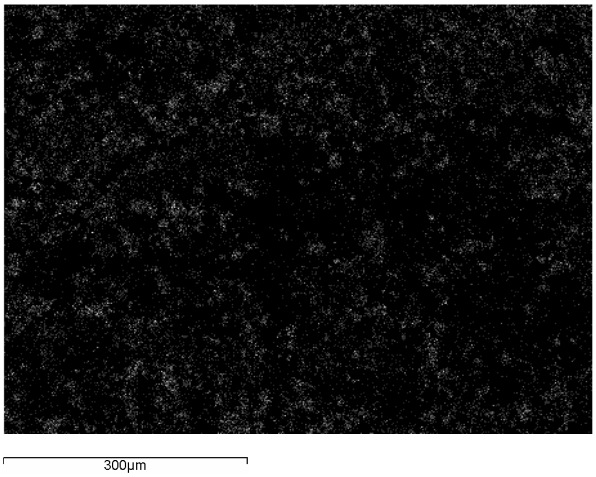

Figure 5.36b Barium distribution across A3.75 composite surface

UV microscopy

The distribution of raw materials as a function of aramid content has been shown. Therefore a complementary technique to show the distribution of aramid fibres was used. The EDX technique used to produce elemental maps can highlight the presence of the predominantly carbon rich fibres yet individual fibres are easily missed due to the mass of other carbon rich materials in the formulation. Ultra violet light excites the aromatic ring in the aramid molecular chain causing the fibres to fluoresce clearly marking their location. Figure 5.37 shows the dispersion of aramid fibres for an A3.75 sample. Scale bar is 500 µm. At this low magnification only the larger fibres in the pulp are clearly visible,

especially those in the sample plane as the composite surface, and appear to only occupy a small area in relation to the overall surface.

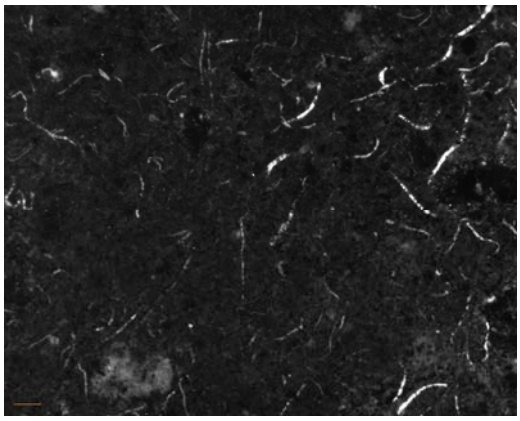

Figure 5.37 UV image of A3.75 surface

Increased magnification of the same sample reveals the small fibres within the aramid pulp network. Figure 5.38 with a 100 μm scale bar shows this. The smaller diameter aramid fibres are clearly evident, both as individual fibres and as fibrils off the main trunk of a larger fibre. At this higher magnification, the true surface area occupied by the aramid fibres becomes apparent and also that the large number of fibres are well dispersed across the surface. Figure 5.39 shows only aramid fibres fluorescing and also the fine fibrils still attached to larger fibres retaining a high surface area of the fibres giving a high degree of interaction with the resin. Scale bar remains 100 μm.

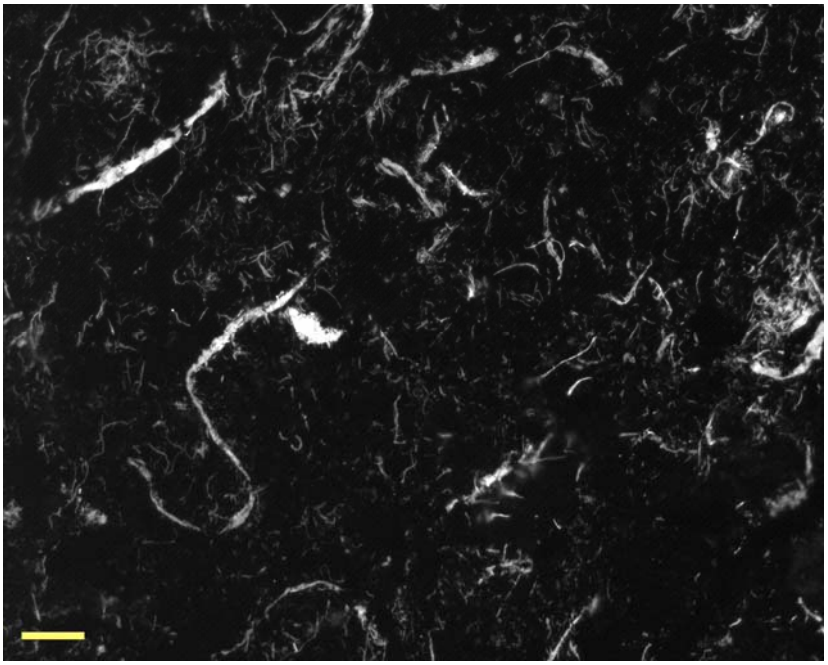

Figure 5.38 UV image of A3.75 UV dapi filter

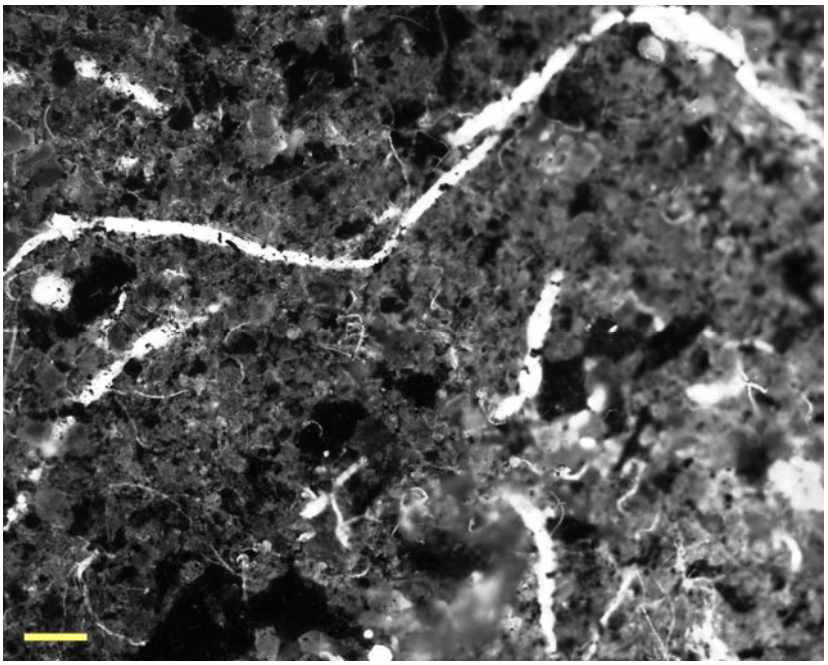

Figure 5.39 UV image of A3.75 UV dapi filter

5.3.4.3 Friction and wear testing – Chase tester

A friction and wear evaluation of friction materials as a function of both aramid content and natural fibres content was undertaken as described in 4.3.5.4. The friction performance of samples will be discussed using the dynamometer results in 5.3.5.2, this section shows the results obtained from constant speed and load wear tests performed on a sub scale friction and wear machined designed and manufactured for this research. The specific wear rate of various samples is presented below as a result of the testing performed. Detailed design and manufacturing diagrams can be found in Appendix 3.

The specific wear rate of each sample was calculated using equation (4.3). Figure 5.40 shows the specific wear rate of samples A0, A1, A2, A3 and A3.75.

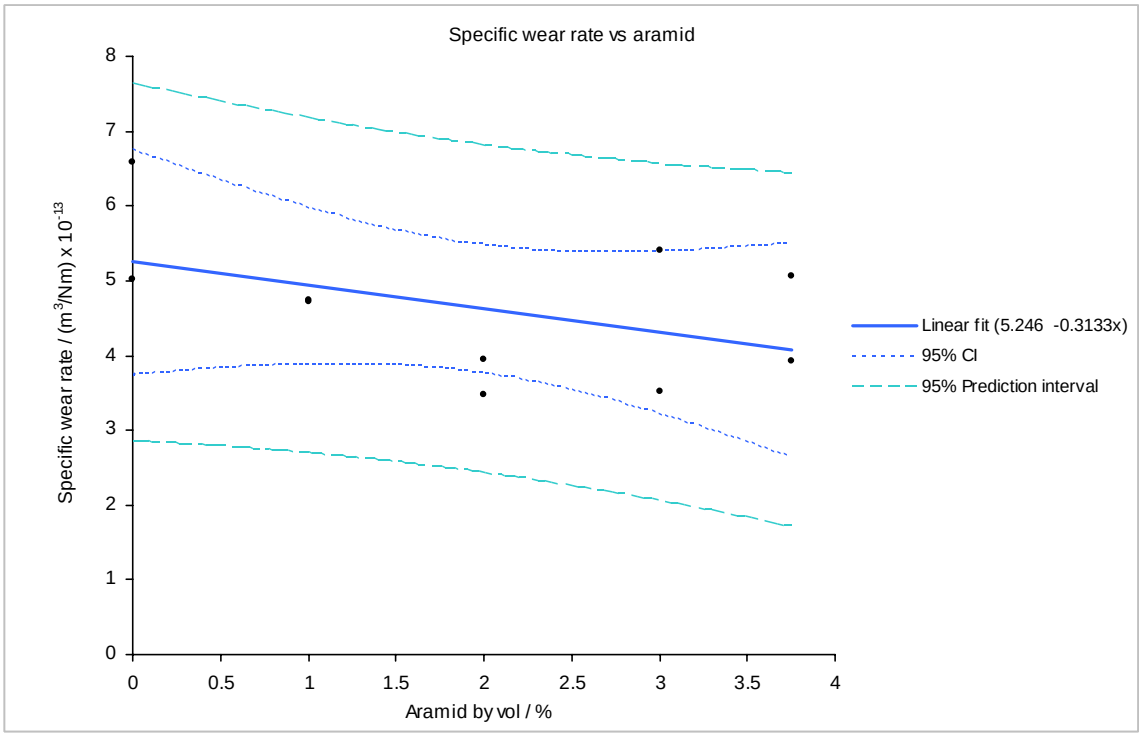

Figure 5.40 Specific wear rate of friction materials vs aramid content

Formulation A0 exhibits the highest average specific wear rate of the samples. As the volumetric inclusion of aramid in the formulation is raised, the specific wear rate decreases to a minimum at a level of 2 % by volume. Increased aramid levels in Formulations A3 and A3.75 produce an increase in the specific wear level in addition to a greater variation from

the mean value. The upper value for the specific wear rate of these two formulations was recorded in the first wear test with the significantly lower wear result recorded as a result of the second wear test – wear runs 11 to 20. This lower value obtained from the second wear test is comparable between samples A2, A3 and A3.75, pointing towards an asymptotic wear rate for this formulation. This indicates towards a possible reduction in wear rate as a function of contact time between pad and disc. The linear regression slope and intercept probability calculations are shown below indicating an 18% probability that the slope is equal to zero and clearly showing that the intercept is not equal to zero.

$P_{slope} = 0.1797$

$P_{intercept} = <0.0001$

The specific wear rate of the hemp and aramid fibre blends is shown in figure 5.41.

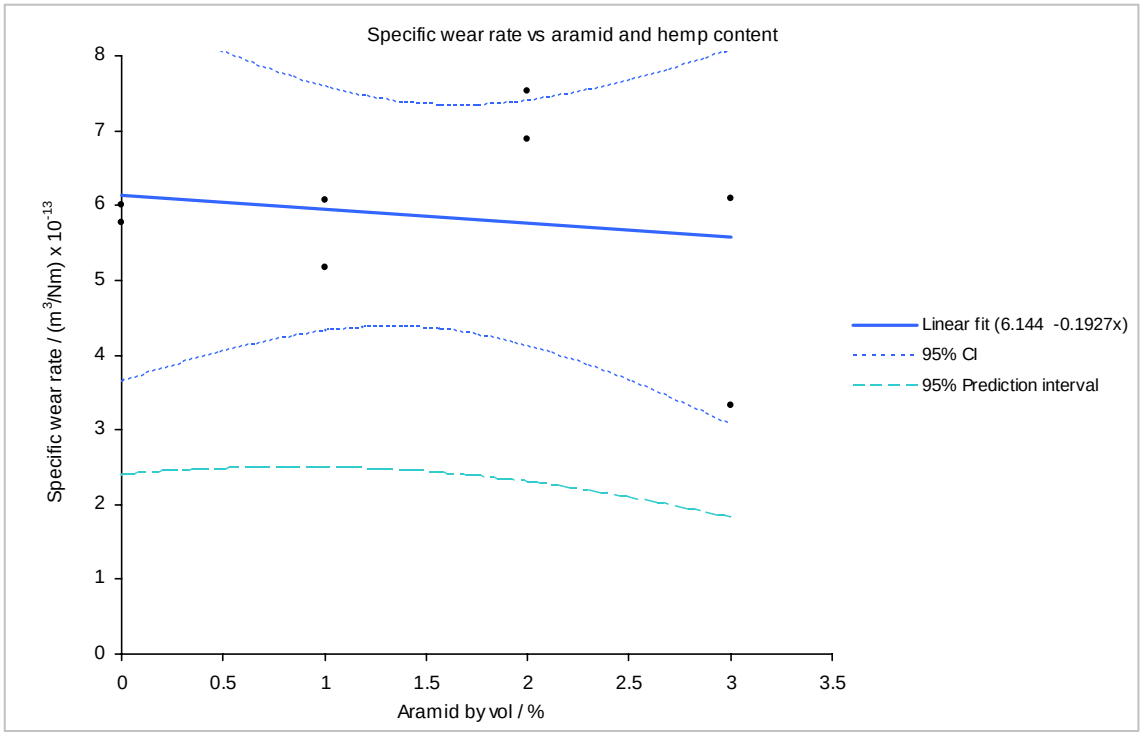

Figure 5.41 Specific wear rate of friction materials vs aramid and hemp content

The inclusion of hemp fibres in the formulations produced a higher average specific wear irrespective of fibre inclusion levels. No clear correlation between hemp fibre inclusion levels and the wear rate of the formulations was observed. Formulation A2(FC+4)1.75 produced the highest specific wear rate of all the formulations

A significant result is the specific wear rate of formulations A0 and FC+4 – both represented as 0% aramid on figure 5.41 – as the wear rate does not increase with the addition of only hemp fibres with respect to A0. The formulations containing both hemp and aramid show higher wear levels than samples with equivalent aramid levels and also greater variation between the formulations. When aramid is blended with hemp, the linear regression shows a stronger probability that the wear rate is independent of the aramid content as shown below.

$P_{slope} = 0.6603$

$P_{intercept} = 0.0002$

Figures 5.42 and 5.43 show the average coefficient of friction recorded during the 20 drag tests for each sample as a function of the content of aramid pulp and aramid blended with hemp respectively.

The operating coefficient of friction for samples A0 to A3.75 is shown to be independent of Aramid content. Average friction values for all samples remain close to 0.5 irrespective of aramid content, yet the addition of the fibres does give indications of a higher spread of friction levels for formulations A3 and A3.75.

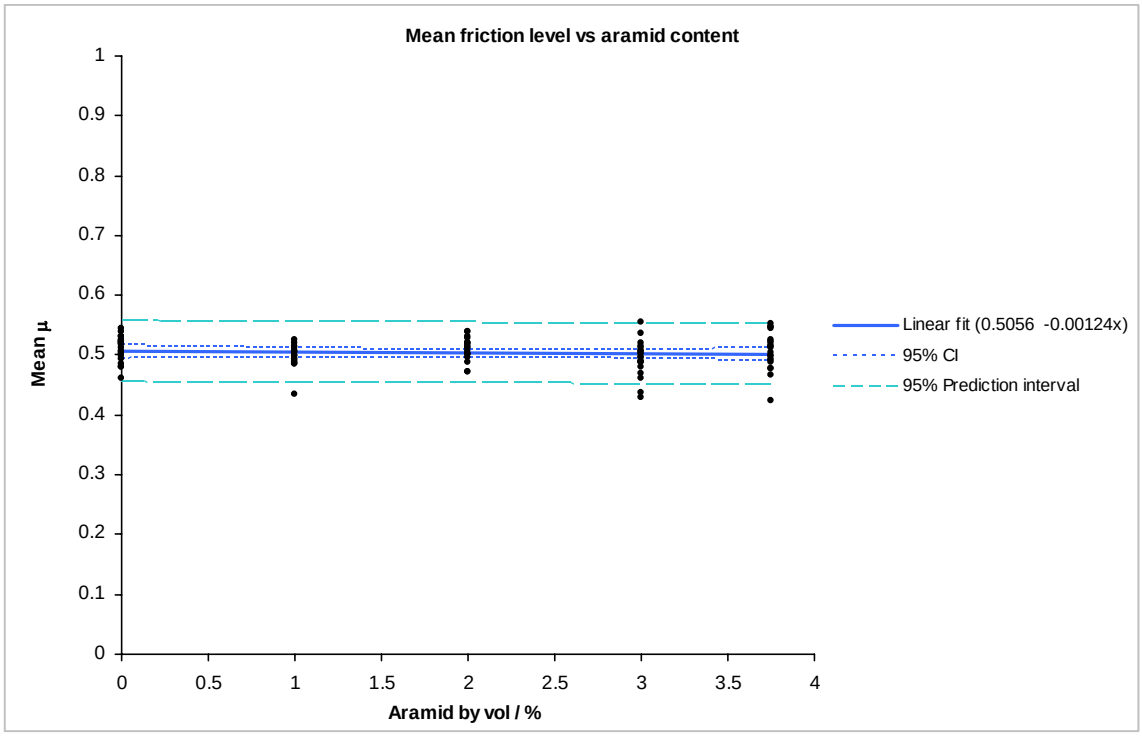

Figure 5.42 Mean friction level vs aramid content by volume

The independence of aramid on friction level can be confirmed by the linear regression probability values shown below.

P_{slope} = 0.5122

$P_{intercept}$ = <0.0001

The addition of hemp fibre to the formulations has the net effect of lowering the operating coefficient of friction during the Chase machine testing as shown in figure 5.43. A stable linear trend between average friction levels shows the addition of hemp in the formulation reduced the value in the region of 0.03. A comparable spread of data for each formulation was recorded showing that the addition of hemp in the formulations fractionally lowered the operating friction level.

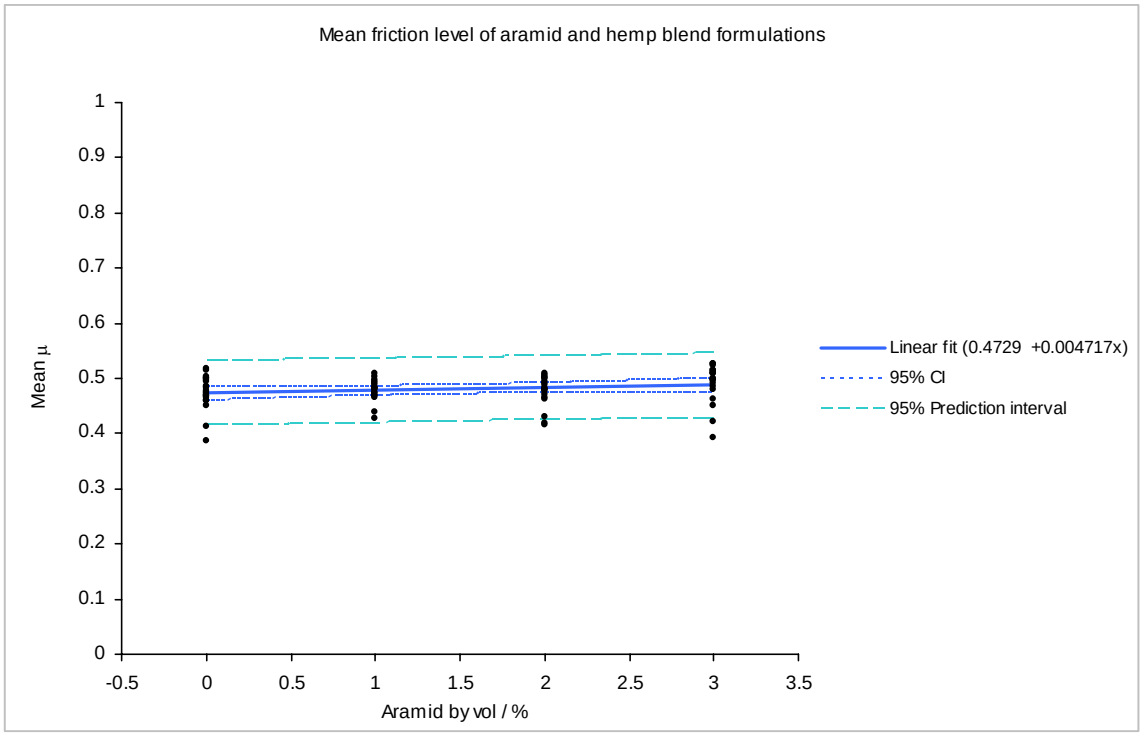

Figure 5.43 Mean friction level vs aramid and hemp content by volume

Linear regression analysis of the data set shows that the intercept is not equal to zero and there is a 10.7% probability of the slope equalling zero. This is a low probability of a statistical relationship between the variables but not as low as the data would suggest in figure 5.43.

$P_{slope} = 0.1073$

$P_{intercept} = <0.0001$

In addition to the average friction levels presented in figures 5.42 and 5.43, the coefficient of friction at the early stages of the wear tests are presented below in figure 5.44a, b and c to show the performance experienced in a real life short braking application. For clarity only wear tests 1, 10 and 20 have been plotted for comparison showing the friction level for friction materials A0, A2 and A3.75 for the first 10 seconds of the respective wear tests. Applications of the normal load produces an initial rise in the friction level which settles to a steady state or variable level depending on the formulation and wear test number. Sample

A0 demonstrates a rise in friction followed by a steady state operating level or a drop in friction for wear test 20. There is disparity in both initial and operating friction across wear runs for sample A0.

Formulation A2 shows a tighter correlation between wear runs for both friction levels and initial stability. Wear tests 1 and 10 show near identical performance for the initial 5 seconds before a separation in the coefficient of friction. The result for sample A0 was replicated as wear test 20 produced the highest operating friction level of the wear tests.

Sample A3.75 showed the greatest correlation in friction performance over the initial 10 seconds over the 20 wear test procedures. Initial friction levels did not show the marked drop as shown in formulations A0 and A2 and the operating friction showed a smooth gradual increase over the initial 10 seconds, repeatable across all wear tests.

These results indicate towards increased levels of aramid pulp in the formulation producing greater repeatability and predictability in friction levels during a short braking interval and also a higher friction level for the same time period.

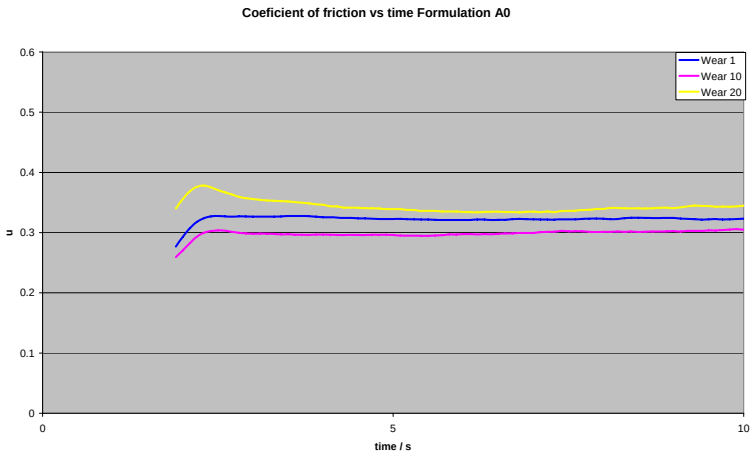

Figure 5.44a Friction level of formulation A0 versus wear test

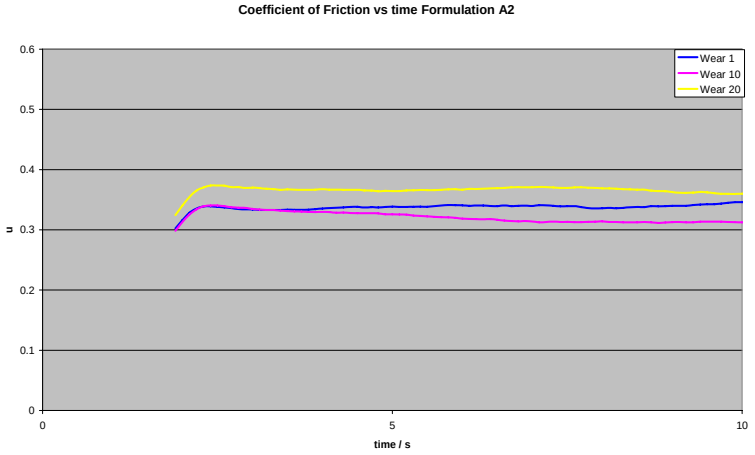

Figure 5.44b Friction level of formulation A2 versus wear test

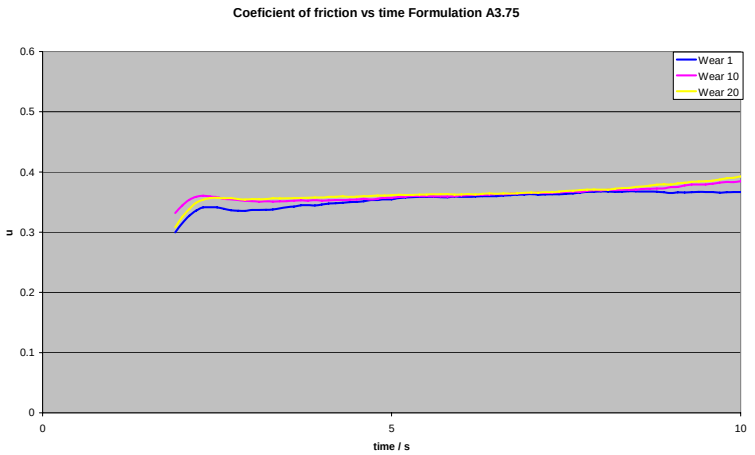

Figure 5.44c Friction level of formulation A3.75 versus wear test

The surface temperature of the cast iron disc was recorded during the wear tests to discuss the rise in disc temperature over a test as a function of the friction material used. Increased levels of aramid in the formulations produced a greater variation between the recorded rise in mean disc temperature, resulting in a greater spread of data. Friction materials containing higher levels of aramid pulp demonstrated cooler running temperatures yet the values recorded were not frequent enough to significantly change the mean temperature rise over the 20 wear tests. Figure 5.45 shows the average rise in disc temperature over the 20 wear tests as a function of aramid content.

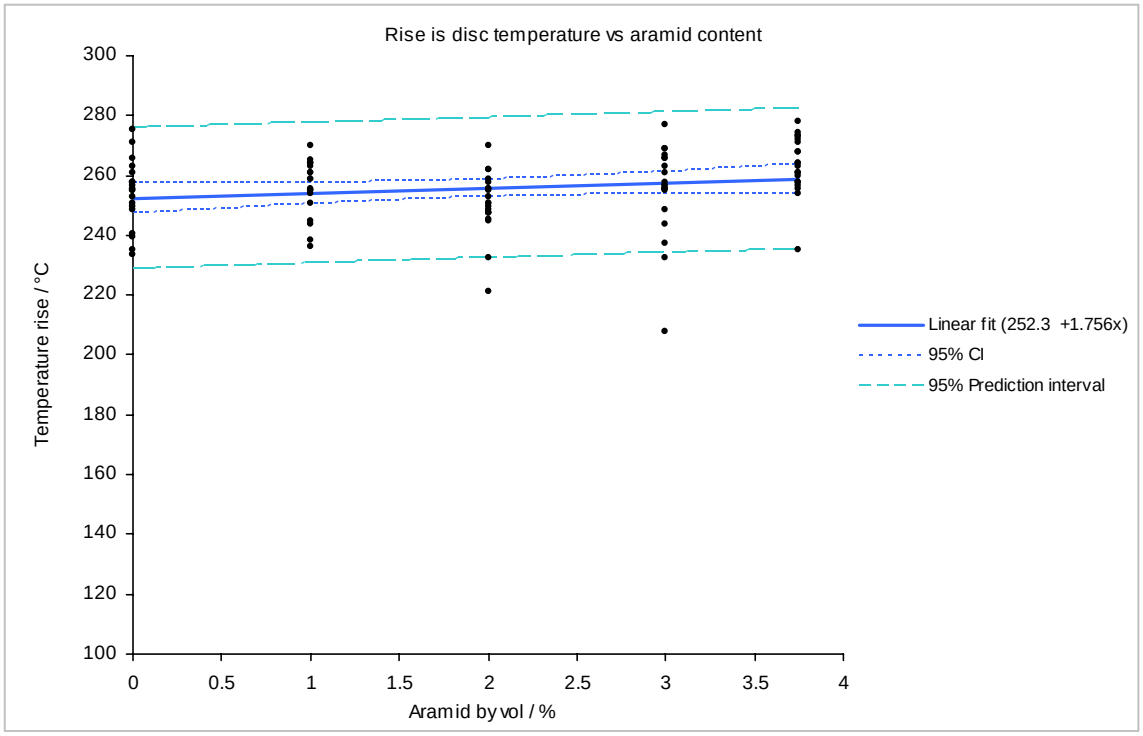

Figure 5.45 Rise in disc temperature versus aramid content

The linear regression analysis of the data confirms that the temperature rise is not equal to zero and shows a probability of the slope equalling zero to be marginally below the specified confidence interval of 5%.

$P_{slope} = 0.0470$

$P_{intercept} = <0.0001$

The regression therefore shows a probability for the slope to not equal zero and as such a correlation between aramid content and disc operating temperature. Further analysis would be required to confirm this statement due to the calculated low probability of the event.

The effect of hemp fibres on the average rise in disc temperature is shown in figure 5.46. Hemp fibres have a notable effect on the mean operating temperature and maximum temperature in formulations A2(FC+4)1.75 and A3(FC+4)0.75.

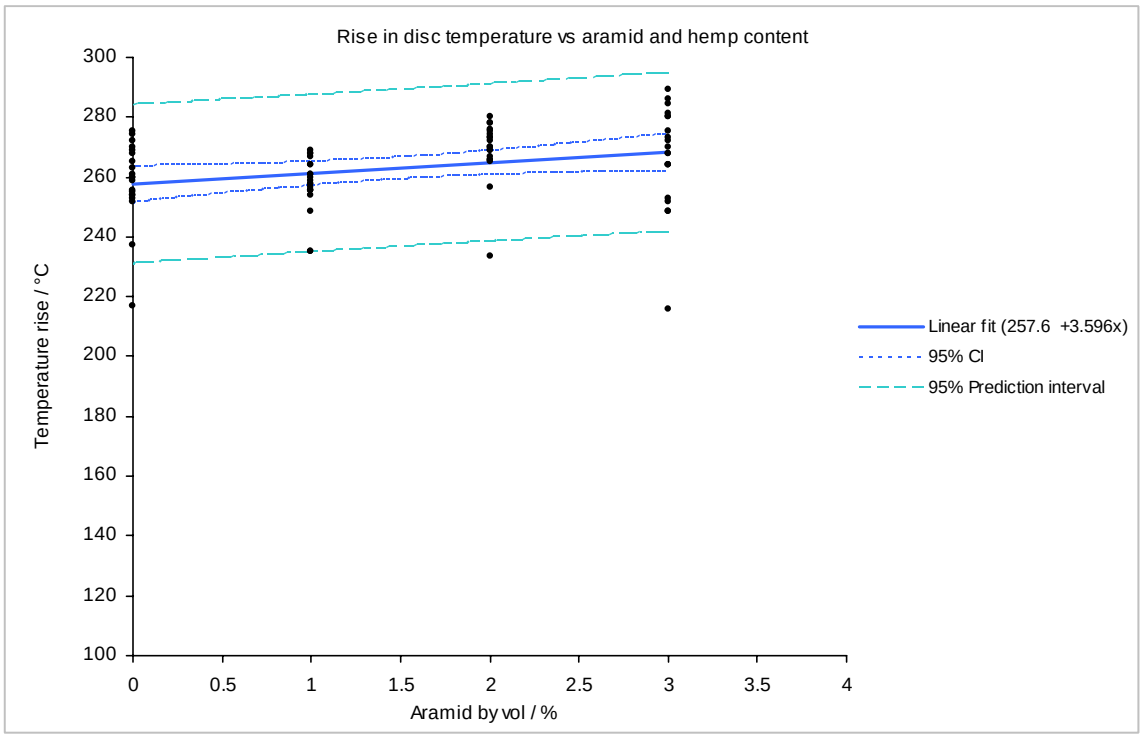

Figure 5.46 Rise in disc temperature versus aramid and hemp content

The linear regression probability values for figure 5.46 are shown below and indicate that both the intercept and slope of the linear fit are not equal to zero.

P_{slope} = 0.0076

$P_{intercept}$ = <0.0001

5.3.5 Manufacture of Brake pads

Brake pads were manufactured as described in 4.3.6 using a powder moulding technique as opposed to the desired pre-forming route. All formulations produced brake pads that passed a rigorous visual inspection focusing on dimensional and structural integrity. Common moulding problems such as delamination, uneven curing of the resin and edge definition were not identified on any of the pads made.

5.3.5.1 Back plate interfacial bond

Regulation 90 [68] specifies the shear strength between the friction material and back-plate must exceed a minimum level of 2.5 MPa in order for a brake pad to be legally sold.

In addition to the performance requirements specified in Regulation 90 friction manufacturers include voluntary safety factors in the range of 2 – 4 to ensure these critical safety requirements are well exceeded. Table 5.5 lists the results obtained performing an interfacial bond test on VW Golf brake pads.

Formulation	Shear test MPa
DM1070	10.21
Hemp short	8.43
Kenaf	9.76
Jute	10.74
Sisal	10.51
Hemp Unretted	9.74
Flax	9.77

Table 5.5 Maximum shear strength of interfacial bond of VW brake pads

The interfacial shear strength between back plate and friction material is a key safety result for any friction formulation. It can be concluded from the results in table 5.5 that the addition of varying types of natural fibres, all 6 mm in length, had little detrimental effect on the shear strength of the brake pads with all fibre types exceeding the Reg 90 specification by a minimum safety factor of 3. The spread of results between natural fibre types is higher than would be expected for a single fibre type indicating that the variance in natural fibre does have an influence on the interfacial bond yet well exceed the specified minimum safety requirements. This is another key result, demonstrating that the natural fibres listed in table 5.5 can be incorporated in friction formulations at 3.75 % by volume and will successfully mould under hot pressing conditions brake pads with high interfacial bond strength between friction material and back plate without adjustments to the manufacturing process.

5.3.5.2 Friction and wear testing –Dynamometer

Dynamometer testing of friction materials is the industry accepted method of evaluating new friction materials and the crucial test for evaluation new formulations as the fully instrumented dynamometers can produce identical test runs for different materials using full scale brake assemblies that subject the brake pad to the temperatures, pressures and stresses found in service conditions.

The AK Master test is the most comprehensive dynamometer procedure used by European Friction Industries, a break down of the individual test procedures in addition to the test results can be found in appendix 1

The constant torque dynamometer procedure was employed as a screening procedure to evaluate the effect of natural fibre type of the coefficient of friction of full size brake pads. A description of the test procedure stages together with the full set of results can be found in appendix 2.

AK master test

The extensive friction analysis procedure known as the AK Master test uses 20 separate test procedures totalling 276 brake applications to evaluate the performance of brake pads over a wide range of operating speeds, temperatures and braking pressures. The testing procedure is based around a characterisation stage that is repeated throughout the test and replicates a VW Golf decelerating from 80 to 30 km/h at constant brake pedal pressure. Separating the characterisation stages are procedures to evaluate the coefficient of friction, at varying operating speeds, rates of deceleration, applied pressures and disc temperatures. A full explanation of the test procedure together with graphical results can be found in appendix 1. A summary of the test results is given in table 5.6.

Test Stage / Formulation	A3.75	A2(FC+4)1.75	Jute
Characterisation 1 (mean μ)	0.52	0.40	0.44
Speed series no2 (mean μ)	0.42	0.34	0.37
Speed series no4 (mean μ)	0.32	0.33	0.34
Characterisation 2 (mean μ)	0.49	0.44	0.48
Cold Stop (mean μ)	0.31	0.34	0.40
Highway stop (mean μ)	0.31	0.30	0.36
Characterisation 3 (mean μ)	0.49	0.45	0.46
Fade 1 (minimum μ)	0.28	0.30	0.30
Characterisation 4 (mean μ)	0.41	0.45	0.51
High temp effectiveness (minimum μ)	0.35	0.36	0.40
Characterisation 5 (mean μ)	0.45	0.48	0.5
Fade 2 (minimum μ)	0.32	0.29	0.36
Characterisation 6 (mean μ)	0.40	0.43	0.48
Operating Friction (mean μ)	0.41	0.40	0.43

Table 5.6 Summary of Coefficient of friction from AK Master tests

All three materials showed a near identical friction performance for the very first braking application. However over 30 stops, the friction level of the mater batch pad progressively increased to levels in excess of 0.5 and remained stable through out the bedding and initial characterisation stops. Pads containing natural fibres showed a lower friction level from the start but did maintain a constant value throughout the first characterisation stage.

The addition of natural fibres also showed an increased sensitivity to the applied pressure during the slow and medium speed braking stages in addition to an overall lower average friction level. All samples showed a comparable friction level throughout the high speed stops highlighting a sensitivity of the A3.75 formulation to high speed brake applications due to the previous high operating levels. In comparison to the first characterisation, the second run showed a 5% reduction in the friction level of the master batch pad but a 10% rise for both pads containing natural fibres. Characterisation stage 2 and 3 were separated by cold performance stops and high deceleration brake applications which showed negligible effect on the operating friction.

The high temperature fade procedure produced an interesting result in a comparable operating friction level as shown in table 5.6 but a reduced fade effect for pads containing natural fibres. The post fade characterisation showed operating levels for the natural fibre pads equal to and exceed the preceding characterisation, indicating a change in operating friction as a result of the elevated temperatures experienced in the fade test.

In a similar manner to the fade result, the high temperature effectiveness stage showed a greater fade level from the master batch pad and higher friction levels from the pads containing natural fibres. Friction levels for the next characterisation were elevated on the previous comparative for pads containing aramid and of an equally high level for the jute fibre pad showing little sign of recovery or effects from the high temperature characterisation.

The final temperature induced fade stage demonstrated a drop in friction levels for all pads but of a lower magnitude compared to the first fade. The jute pads replicated the previous fade test by recording both the highest average and most stable friction level for the stage.

The average operating friction level for the complete AK master test for each pad are within 7% of one another with the jute pads demonstrating the highest value of 0.43 compared to 0.4 and 0.41 of the aramid/hemp blend and master batch respectively.

Constant torque

A detailed description of the constant torque test procedure together with graphical results for each test procedure can be found in appendix 2.

A summary of the measured coefficient of friction of brake pads as a function of the natural fibre content is shown in table 5.7. The master batch formulation DM1070 is included for reference. The operating coefficient of friction is an average of all the recorded values during the test and is very comparable for all natural fibre types. The correlation of friction between natural fibre types – over 110 braking applications encompassing three separate temperature driven procedures – shows that the natural fibre type has minimal effect on the operating coefficient of friction in the chosen friction formulation. All natural fibre pads showed a lower operating friction level compared to DM1070 and also a more contained variation between maximum and minimum recorded values.

Additional information can be taken from the test results by comparing the performance of the natural fibre pads over individual stages of the test.

Natural fibre	Operating μ	Maximum μ	Minimum μ
DM1070	0.465	0.626	0.189
Hemp short	0.424	0.528	0.235
Kenaf	0.424	0.521	0.226
Jute	0.432	0.525	0.245
Sisal	0.425	0.521	0.258
Hemp Unretted	0.422	0.523	0.263
Flax	0.427	0.504	0.246

Table 5.7 Friction summary of constant torque test on natural fibres

The bedding-in procedure is a 30 application procedure used to ensure a high contact area between pad and disc and also evaluate the “off the shelf” performance. A minimum of 10 braking applications were required to achieve a stable operating coefficient of friction for all pads with the jute formulation settling noticeably faster. Minor fluctuations in the friction level were observed for all pads as the disc temperature reached the maximum at the end of each stage.

Greater variance in the friction level was observed for each pad during the first heating stage with maximum disc temperatures of 350 °C inducing minor brake fade and a corresponding increase in brake line pressure to maintain torque levels.

The first hot performance procedure increased disc temperatures to 500 °C and induced large brake fade for each material, which as shown in the last column of table 5.7 is of a comparable magnitude.

The 20 braking applications after the hot performance known as the recovery demonstrated that each pad quickly recovered to a stable operating coefficient of friction levels, giving smooth, predictable performance.

The second hot performance stage generated the same high temperatures as the first run yet the scale of induced brake fade was not recorded for any of the pads. A drop in friction of approximately one third of that recorded in the first hot performance run can be observed for a number of pads. This phenomenon is thought to occur as a result of evolved volatile materials during the first hot performance in the form of gaseous products lubricating the friction interface and producing the brake fade observed. This would agree with the conclusions observed by Savage when investigating fade resistance of friction materials [5]. Subsequent temperature ramps do not experience such fade as the bulk of the volatile compounds have been previously liberated.

The overall friction performance of natural fibre pads during the constant torque dynamometer run are very comparable to one another and can be attributed to the similarity in chemical structure between the fibre types, primarily the high percentage of cellulose molecules that will dominate the thermal and frictional stability of the fibres.

6 Fibre Network model development

The role of aramid fibres has been demonstrated to be fundamental to the processing performance of the chosen friction formulation. Key results are demonstrated in sections 5.2.1, 5.2.3, 5.3.1, 5.3.2 and 5.3.3. This complex fibre network structure formed by the highly fibrillated individual fibres provides a combination of bulk volume to encourage mixing and dispersion of raw materials and a net structure of fine fibres that hold particulates in suspension. The SEM images in section 5.2.1 clearly show this complex structure. A network model has been developed to describe both of these physical attribute that are key to the performance of the fibres in friction materials. Initially the "net" structure of the pulp is modelled to describe the particulate retention performance of aramid fibres as a function of fibre and particulate geometry. This is followed by a simple structural analysis describing the rigidity of the fibre network and hence the bulk volume of the pulp. In addition to processing fibres for friction materials this model has numerous applications due to the variety of fibrous materials and applications.

Many natural and synthetic materials use threadlike or fibrous structures to form the bulk material assembly. Example materials listed below are classified based on the architecture of the fibres within the bulk material. Applications for the materials range from everyday household products to high performance engineering materials at the forefront of materials science.

- cellular materials – foams, bone, wood
- fibre scaffolds – sintered metallic mats and bio-polymers
- random fibre networks – paper, filtration
- woven and twisted fibres structures – textiles and rope
- Entangled random fibres – Wool, insulating wool, polymers

The vast number of fibrous and cellular materials show wide ranging physical and thermal properties that depend on the structural detail. Cellular materials use a reticulated network of interconnected ribs, fibre scaffolds and random fibre networks consisting of high aspect ratio fibres connected by inter-fibre bonds and entangled random fibres use semi-flexible fibres entwined together. Light fibrous structures such as wools and fibre mats typically

demonstrate low density structures providing light weight and thermally insulating materials. aramid pulp used in friction materials can be classed as a light fibrous material as the highly fibrillated fibres produce a lightweight, high volume fibre pulp that excels in the manufacture of friction materials. Current research has focused on correlating the performance of constituent fibres to bulk material properties [112-116]. The ability to predict and quantify the bulk mechanical properties of fibrous materials has a key impact on the manufacturing processes of materials such as paper, filters, wool and composite fibre pre-pregs especially with regards to the compressibility and elastic recovery of such structures [117-119].

The mechanical performance of cellular materials such has foams has been well documented [120] and analogies can be made between the random distribution of open or close cells observed in foams to light fibrous materials [114]. The elastic properties of fibrous mats were investigated by Askling et al [110,121] who performed dynamic mechanical measurements on samples to obtain the elastic modulus and critical strains values for different fibre morphologies. These tests provided the foundation for the results obtained in chapter 6 and will be used as a comparison to the structural model developed here.

The hierarchal structure displayed by aramid pulp produces a fibre pulp structure with a netlike structure to entrap small particles and a larger fibre framework giving the bulk volume and elasticity to the fibre pulp.

The smaller fibres produce a net like structure to capture the dry powdered materials used in the friction formulation and the large fibre framework provides the fibre bulk structure supporting both the smaller fibres and the entrapped particulates. Two separate models have been developed to investigate the different structures viewed in aramid pulp.

Figure 6.1 shows the proposed fibre structure of a large fibre structure supporting a smaller fibre network, itself supporting particulate materials.

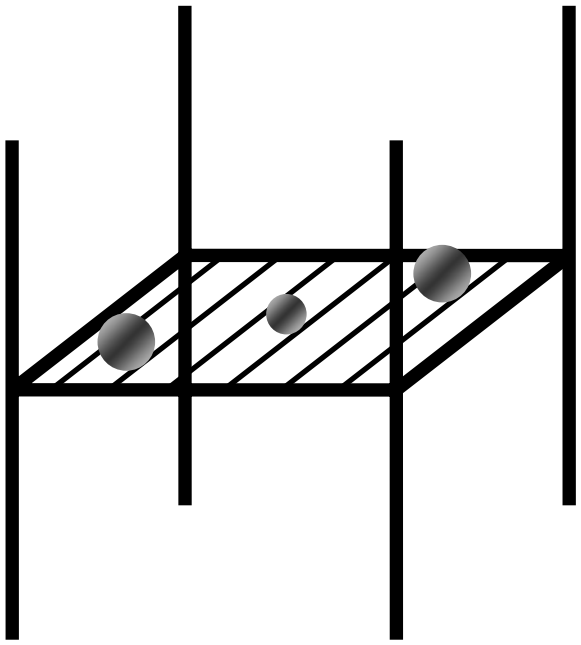

Figure 6.1 Large framework structure supporting “net” structure

6.1 Small net like structure

It has been shown in section 5.2.1 that small fibres within the aramid pulp form the net structure that entraps small particles, holding them in suspension, providing dust suppression and material dispersion. This section of the network model aims to predict this performance as a function of fibre and particle geometry.

The simplest configuration required to trap an individual particle can be modelled as two fibres of diameter d separated by an initial span of S. The fibres are simply supported at the ends and other end effects such as frictional forces, fibre rotation and twisting are ignored. A spherical particle of diameter D and density ρ is equally supported by each fibre and will induce a deflection δ in each fibre. Only in-plane deformation of the fibres is assumed, such that fibre deflections due to loading increase the initial span as shown in figure 6.2.

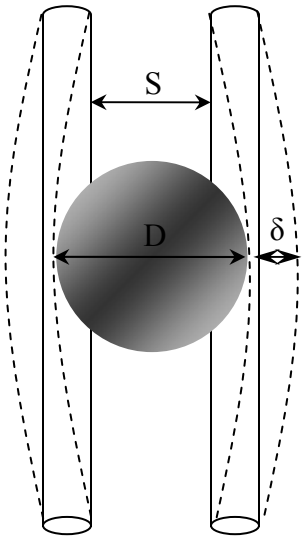

Figure 6.2 Two small fibres supporting a spherical particle

In order for the particle to remain supported, the total fibre separation must remain less than the diameter D. The maximum fibre separation is equal to the initial fibre span plus the bending deformation induced by the particle mass. Equating the maximum fibre separation to the particle diameter gives;

$$D = S + 2\delta \tag{6.1}$$

Standard beam mechanics can be used to calculate the deflection δ of a fibre of length L_{sf}, Young's Modulus E and diameter d subject to a point loading as shown in equation 6.2

$$\delta = \frac{PL_{sf}^{\ 3}}{48EI} \tag{6.2}$$

Where

P = Load (N)

L_{sf} = Fibre length (m)

E = Young's Modulus (Nm^{-2})

I = Second moment of Area (m^4)

For a circular section fibre of diameter d_{sf}, the second moment of area I_{sf} as shown in figure 6.3 is given by equation (6.3)

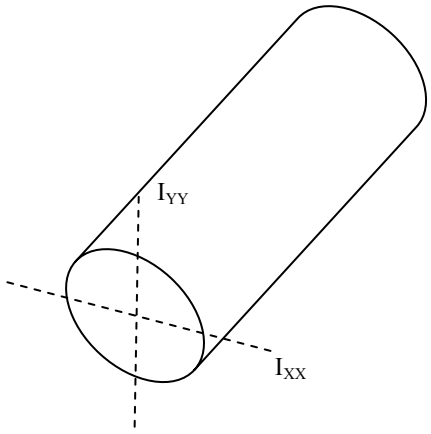

Figure 6.3 Second moment of area of cylinder

$$I_{sf} = \frac{\pi d_{sf}^{\ 4}}{64} \tag{6.3}$$

The load (P) acting on the fibres can be calculated as a function of the particle density ρ and diameter D_{par} which for a spherical particle is given by;

$$P = \frac{\pi g \rho D_{par}{}^{3}}{6} \tag{6.4}$$

Where

P = Load (N)

g = acceleration due to gravity (ms^{-2})

ρ = density of particle (kgm^{-3})

D_{par} = diameter of particle (m)

Combining equations (6.2) (6.3) and (6.4) gives the deflection of one fibre subject to static loading from a particle.

$$\delta_{sf} = \frac{\rho D_{par}{}^{3} L_{sf}{}^{3}}{9 E d_{sf}{}^{4}} \tag{6.5}$$

The maximum initial span S_{sf} between two small fibres required to support a particle of diameter D_{par} can therefore be calculated by combining (6.1) and (6.5) and rearranging to give.

$$S_{sf} = D_{par} - \frac{2\rho D_{par}{}^{3} L_{sf}{}^{3}}{9 E d_{sf}{}^{4}} \tag{6.6}$$

Thus for a given initial fibre separation for fibres of fixed length and diameter, the maximum single particle size for a given material can be determined. The particle retention

ability of a fibre couple depends on various dimensional parameters of both fibre and particle.

Figure 6.4 plots the relationship described in equation for fibres of varying diameter for a fibre length of 10 μm.

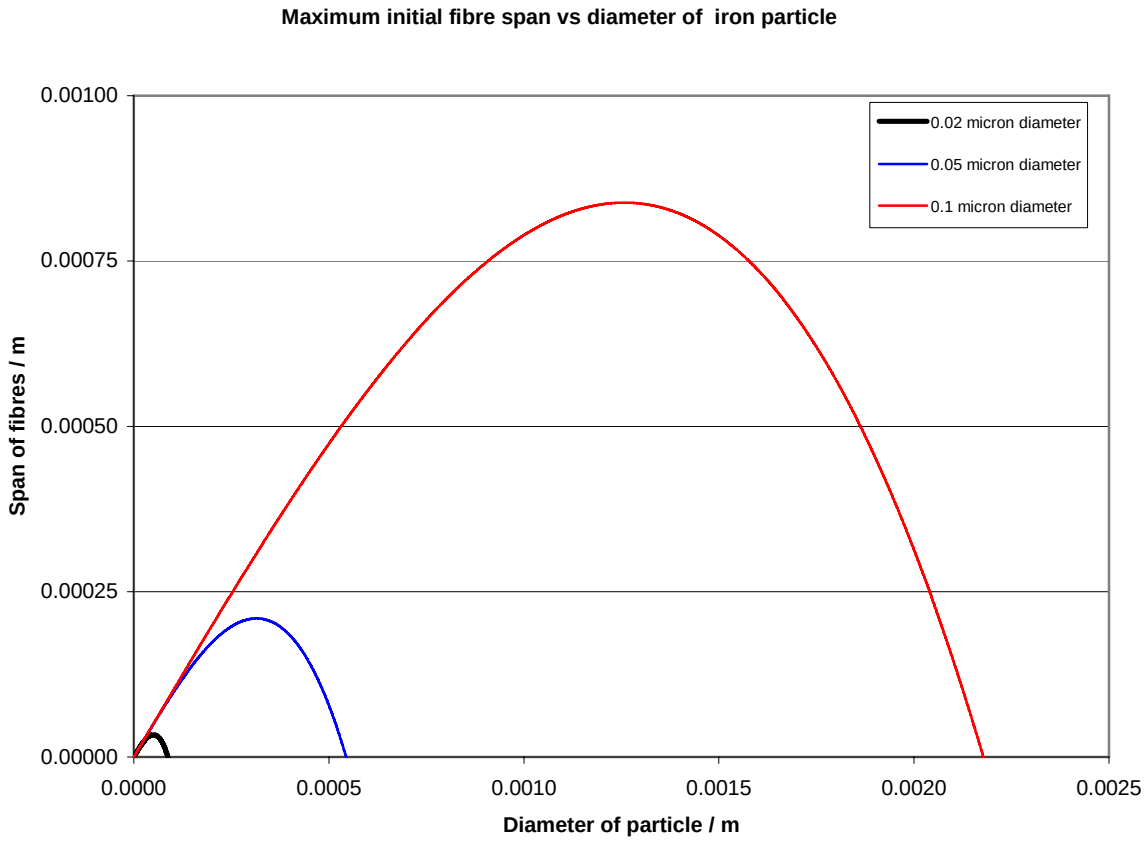

Figure 6.4 Fibre span versus particle diameter as a function of fibre diameter

Positive fibre separations are only valid for this model therefore the maximum initial fibre span can be determined for all positive fibre separation values. Increasing the fibre diameter has a significant effect on the maximum particle diameter as shown in figure 6.4, this is because the fibre diameter is raised to the forth power and so is a dominating variable in equation 6.6. The fibre free length and the particle density are constants for figure 6.4.

Equation 6.6 gives the fibre span as a function of the particle diameter, initially raised to the power unity followed by the second term in which the particle diameter is a cubic. For a given fibre diameter and length, the initial relationship between span and particle diameter

is linear before a critical particle diameter is reached and the cubic term in the equation dominates, reducing the fibre span. The maximum particle diameter is therefore calculated by differentiating equation 6.6 with respect to the particle diameter as shown below.

$$\frac{dS_{sf}}{dD_{par}} = 1 - \frac{6\rho D_{par}{}^{2} L_{sf}{}^{3}}{9E d_{sf}{}^{4}} \tag{6.7}$$

As the gradient of the curve is equal to zero at the maximum this can be entered into equation 6.7 and rearranged to give the maximum particle diameter D_{MAX}.

$$D_{MAX} = \sqrt{\frac{9E d_{sf}{}^{4}}{6\rho L_{sf}{}^{3}}} \tag{6.8}$$

For a given fibre length and particle density, the maximum particle diameter can be calculated as a function of the fibre diameter. Entering the values obtained from equation 6.8 into 6.6 allows this value to be plotted against the fibre span and combined with figure 6.4 as shown below in figure 6.5.

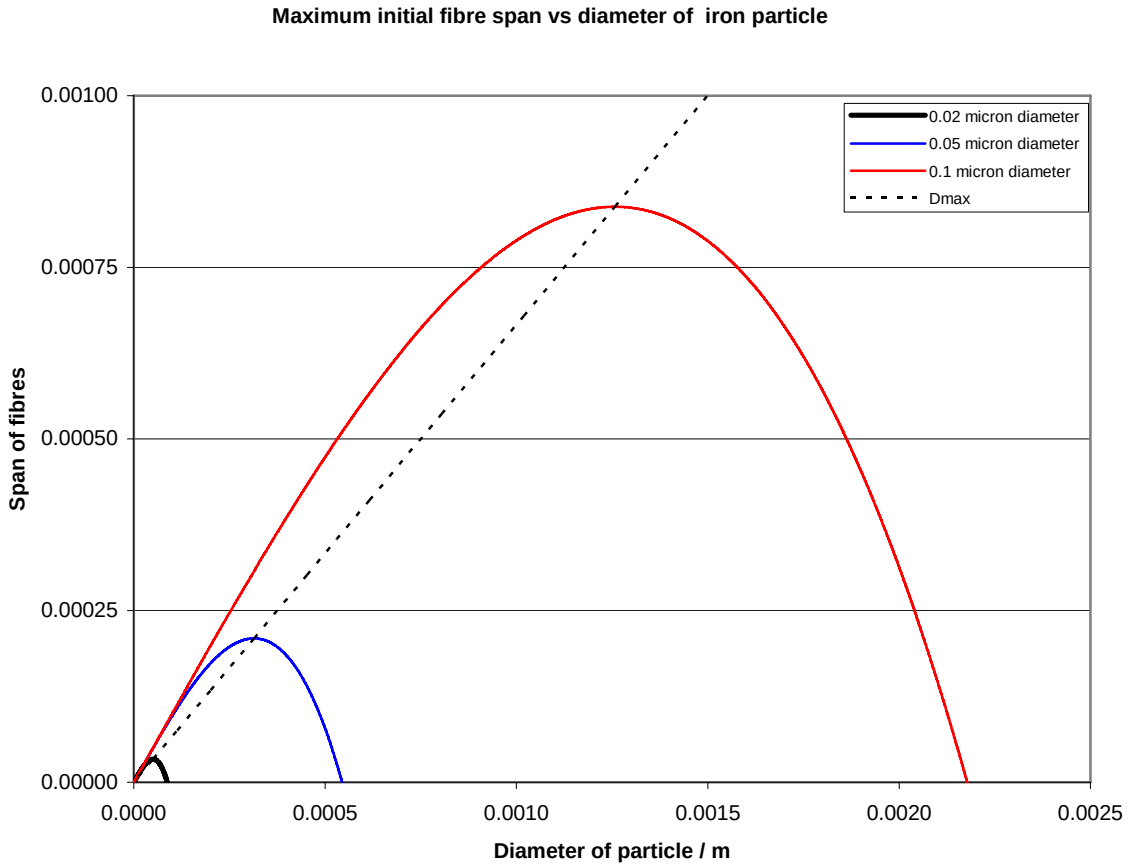

Figure 6.5 Fibre span versus particle diameter as a function of fibre diameter

The maximum particle diameter for a given material and fibre length can also be shown as a function of the fibre diameter. Using equation 6.8 and retaining the same particle density and fibre free length, the relationship is shown below in figure 6.6.

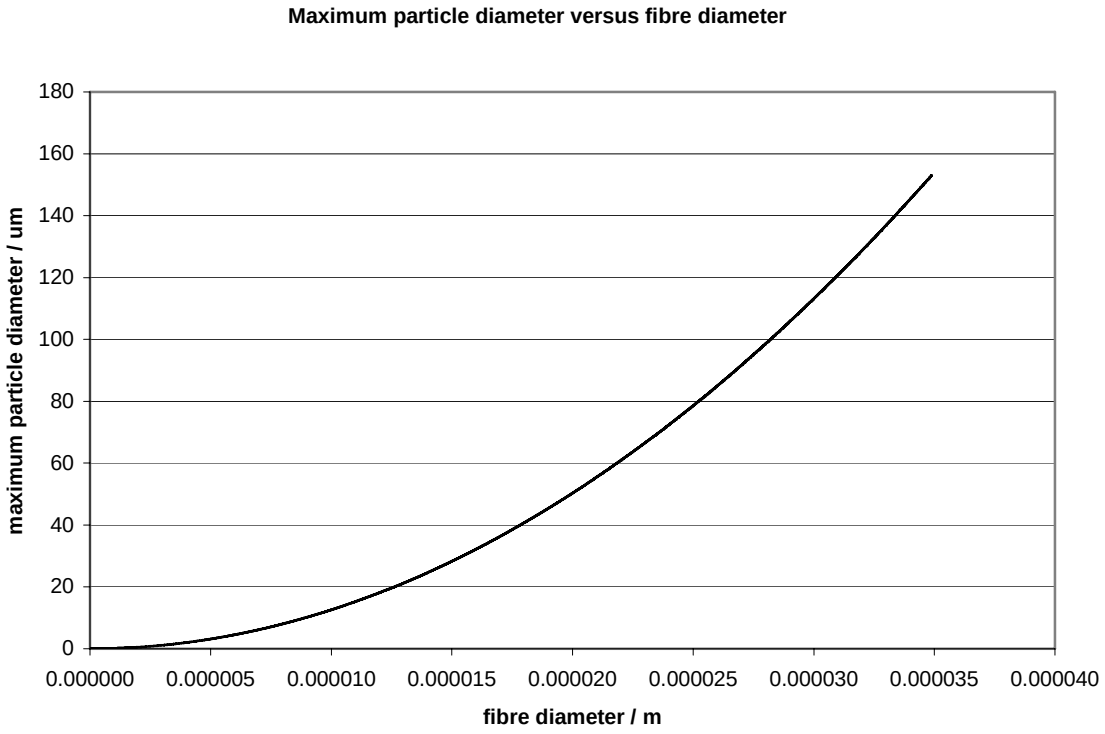

Figure 6.6 Maximum particle diameter versus fibre diameter

The fibre length – equivalent to the free length of the simply supported beam affects the degree to which particles are retained by the net structure. The stiffness of a fibre supporting a point load – in this case a particle – has an inherent stiffness that varies as the cube of the fibre length as shown in equation 6.5 therefore changes in this value will significantly affect the maximum particle size that a fibre pair can support. This is shown in figure 6.7, fibre diameter and particle densities remain constant.

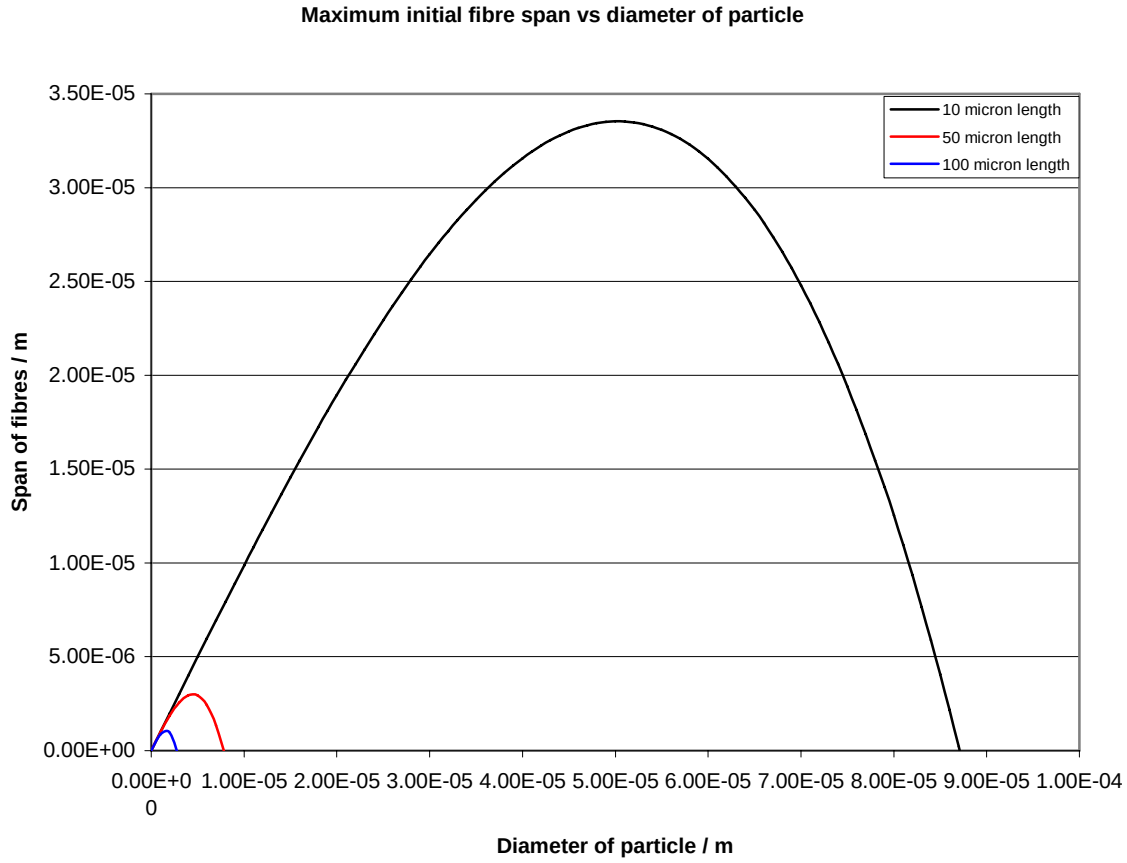

Figure 6.7 Fibre span versus particle diameter as a function of fibre free length

The models presented so far have only considered the fibre geometry as variables yet in reality, 12 different particulates are entrapped by the aramid pulp net structure. Materials of increasing densities will produce a greater loading on the fibre couple therefore reducing the maximum size of particle. This relationship is plotted in figure 6.8 and clearly shows the two competing components of equation 6.6 with respect to the particle diameter. The values entered for fibre diameter and length are 2 μm and 10 μm respectively.

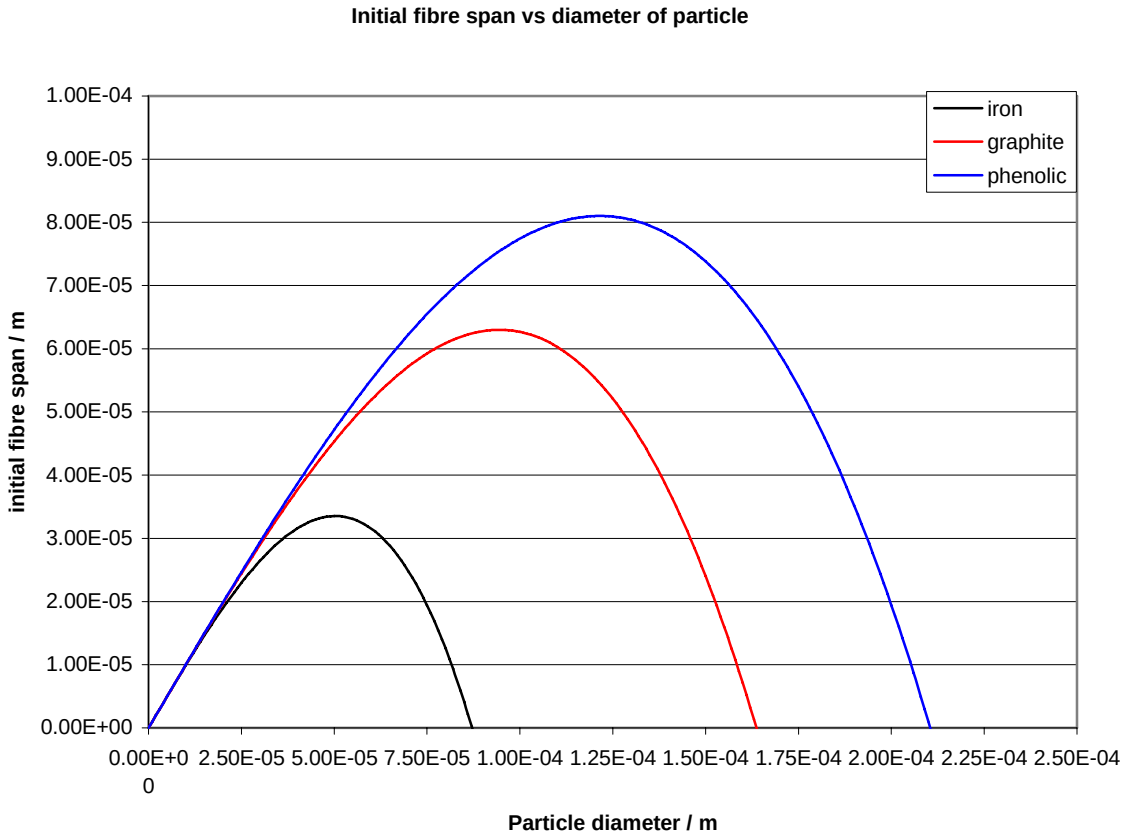

Figure 6.8 Fibre span versus particle diameter for varying density particles

6.2 Large fibre framework

The second part of the fibre network model is concerned with the larger fibres within the fibre pulp and the structural integrity that they impart to the fibre network. The aim is to model the rigidity of the large fibre network, determine the buckling load and compare this to the actual loading from the other raw materials. It is proposed that the large fibres provide the bulk volume and structure to the fibre pulp. The large fibre framework is subjected to two loading conditions.

- Supporting the smaller fibre network as virgin aramid pulp
- Supporting the small fibre network with entrapped friction particles during the manufacture of brake pads.

The initial model will assume the large fibres arranged in a regular rectangular grid arrangement, supporting a mass of smaller fibres. The mass of smaller fibres will be determined for a given large fibre deflection. One square from a grid of fibres is shown in figure 6.9. The fibres are equally spaced by a distance L_{lf} and are of uniform circular cross section with a diameter d_{lf} . The fibres are assumed to be simply supported at each end and all other end effects are ignored. A point loading P is applied in the midpoint of the fibre to give maximum deflection

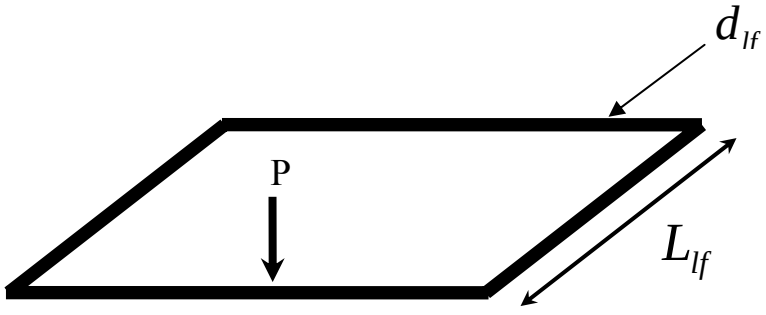

Figure 6.9 Single fibre square grid

It is assumed that all large "structural" fibres are rigid for all bending deflections less than 1% of the fibre diameter, e.g a 0.3μm deflection.

Using standard beam mechanics, the deflection of a simply supported fibre subject to a point load is given by.

$$\delta_{lf} = \frac{4PL_{lf}^{3}}{3E\pi d_{lf}^{4}} \tag{6.9}$$

Where;

δ_{lf} = Maximum fibre deflection (m)

P = Load (N)

L_{lf} = Fibre length (m)

E = Young's modulus of fibre (Nm^{-2})

d_{lf} = fibre diameter (m)

Entering a nominal load of 1μN into (6.9), the fibre deflection as a function of the fibre spacing can be calculated as shown in figure 6.10.

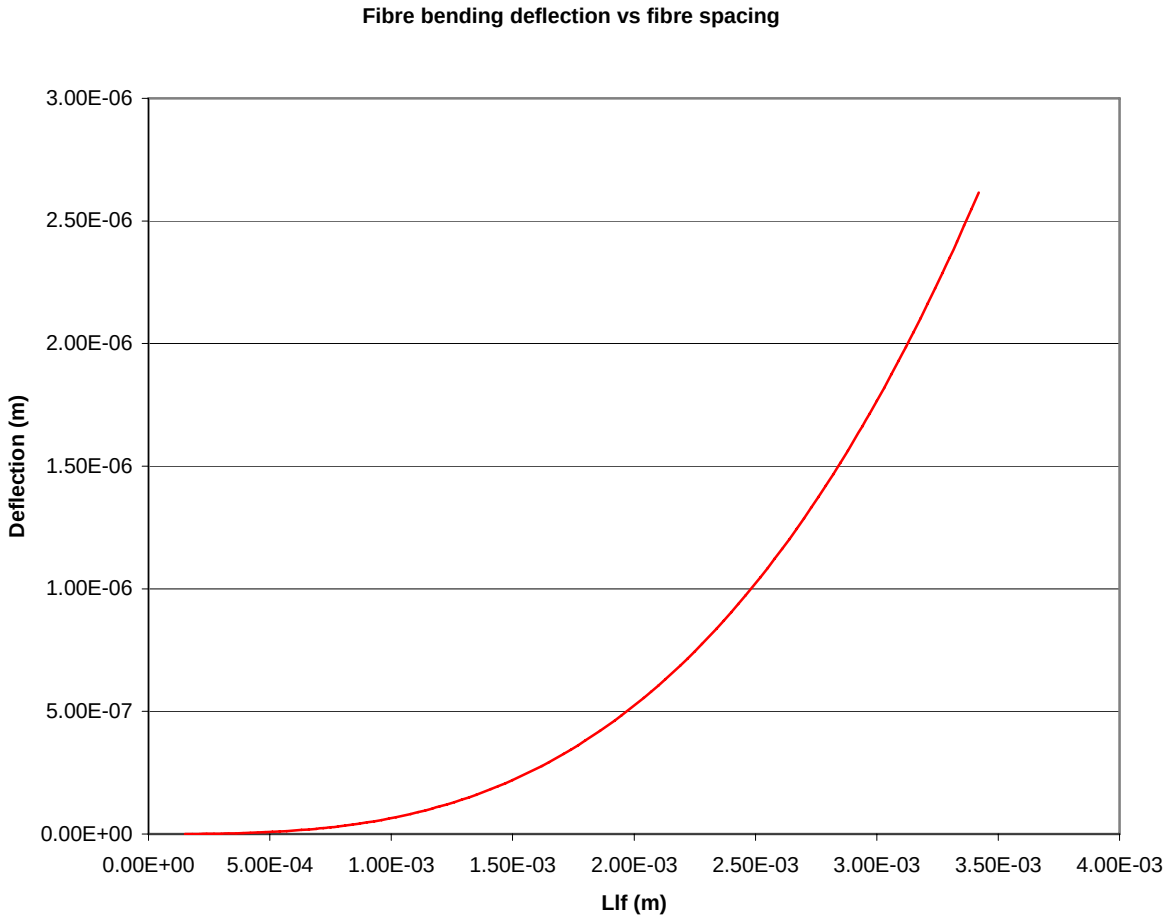

Figure 6.10 Bending deflection of structural aramid fibre versus fibre spacing

The load (P) applied to the large fibres is due to the mass of small fibres being supported. Assuming the small fibres occupy a percentage V_{frsf} of the total fibre pulp of volume fraction V_{frac}, the volume of small fibres V_{sf} supported by one large fibre in a regular grid arrangement for a given deflection is given by equation (6.10).

$$V_{sf} = \frac{3\pi E d_{lf}^{\ 4} \delta_{\max} V_{frsf} V_{frac}}{4 \rho g L_{lf}^{\ 3}} \qquad (6.10)$$

One large fibre is assumed to support one quarter of the load applied over the grid surface area A_G, therefore the height of fibre pulp h_f supported for a given fibre deflection of 1% diameter can be calculated using;

$$h_f = \frac{V_{sf}}{4L_{lf}^{\ 2}} \tag{6.11}$$

Combining equations (6.10) and (6.11) enables the linear height of small fibres supported by one large structural fibre to be calculated. The solution for a fibre diameter d_{lf} of 30 μm and a deflection of $0.01\,d_{lf}$ gives the relationship shown in figure 6.11.

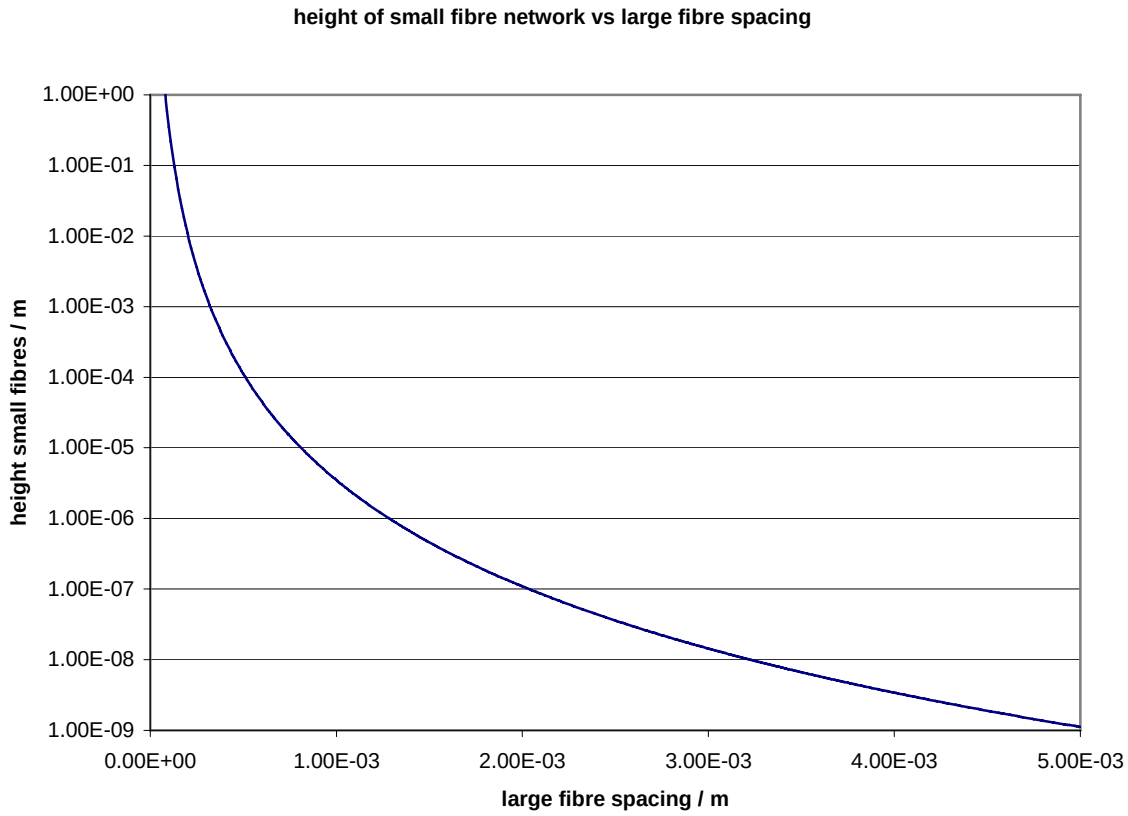

Figure 6.11 Loading capacity of large fibres as a function of fibre spacing

Figure 6.11 shows the rigidity of the fibre network especially at low fibres spacing where large heights of fibre pulp can be supported by the proposed structural framework.

To further the analytical model in this section, an estimate of the fibre spacing is required. Using the experimental data calculated in section 5.3.3.3, an estimation of the fibre spacing may be taken using additional theoretical equations. Analogies between the bulk mechanical properties of fibre pulps and open cell foams have been previously discussed. Gibson and Ashby [120] presented a model for the shear modulus of open cell foams, using a bending deflection of the cells in response to an applied stress. For low strains in which the bending deflection is well below the Euler buckling criteria, the Shear modulus G is given as;

$$G = \frac{\tau}{\gamma} = \frac{C_2 EI}{l^4} \tag{6.12}$$

Where;

C_2 = proportionality constant ≈ 3/8

E = Elastic modulus (Nm^{-2})

I = Second moment of Area (m^4)

l = strut length (m)

Combining equation (6.12) above with (6.3) and rearranging to give the fibre length produces;

$$l = \left(\frac{3\pi E d^4}{512 G} \right)^{\frac{1}{4}} \tag{6.13}$$

The experimental results obtained from chapter 6.3.3.3 gave a shear modulus for aramid pulp at low strains as 3.89 x 10^5 Pa. Entering this value together with a fibre diameter of 30 μm gives a fibre free segment length of 744 μm.

Assuming the structural fibres form a regular lattice structure, this fibre spacing can be used to confirm the structural integrity of the framework by first calculating the theoretical buckling load of the fibres and subsequently calculating the actual load applied and comparing the two values. Figure 6.12 Shows the cubic structure with a single unit cell identified, loading the vertical supporting fibres.

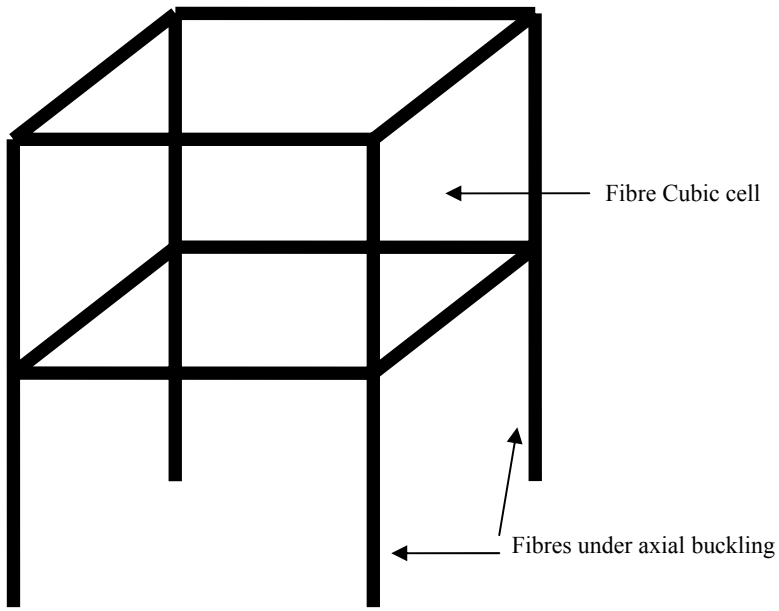

Figure 6.12 Lattice structure of large framework

Assuming the particles are evenly distributed throughout the aramid fibre structure in the friction formulation, the load L_c supported by one unit cell in the structure is given by equation 6.14.

$$L_c = \frac{V_A L^3}{m_p m_a g} \tag{6.14}$$

Where

m_A = mass of aramid (kg)

V_A = Bulk volume aramid pulp (kg/m^3)

m_p = mass of particles per unit volume of aramid (kg)

L_{lf} = fibre spacing (m)

If the entire load is assumed to be supported by the vertical fibres – producing the greatest loading case for individual fibres – the load supported by one fibre L_{cf} will be one quarter of the total load in (6.14).

The Euler buckling load E_{cr} for a simply supported slender fibre is given by equation (6.15) which can be solved for this case giving;

$$E_{cr} = \frac{\pi^3 E d_{lf}^{\ 4}}{64 L_{lf}^{\ 2}} \tag{6.15}$$

There are now two equations that calculate the real axial loading of the fibres using (6.14) and the theoretical buckling load of the fibres using (6.15).

Solving both equations gives real versus theoretical axial fibre loadings of;

Real loading $L_{cf} = 6.37 \times 10^{-7}$ N

Theoretical buckling $E_{cr} = 56.7 \times 10^{-3}$ N

Comparing the theoretical loading of a single slender fibre strut in the framework to the critical buckling loading shows that the static loading is well within the buckling limit and as such as rigid fibre framework can be demonstrated.

7 Discussion

7.1 Thermal stability of materials

The thermo-gravimetric analysis (TGA) results show a wide variance in the thermal stability of individual raw materials in the friction formulation. Most materials demonstrated a thermal stability above 400 °C, giving a good thermal stability to the composite brake pad. The friction formulation demonstrates a degradation onset temperature of 379 °C which can be attributed to the pyrolosis of the least thermally stable organic material – rubber crumb – followed shortly after by the second rubber compound in the formulation. Higher temperatures induce a thermal degradation of aramid fibres and the phenolic resin which, combined with the rubber compounds and the partial mass loss of the magnesium oxide, represent a maximum of 17% by mass of the formulation. This correlates well with the recorded TGA mass loss.

Further increases in temperature produces a competing effect between the mass loss of organic materials and mass gains from the metallic compounds. The net result is only a small change in the total mass of the formulation. Barytes was chosen as the replacement material of aramid in the friction and wear test due to its high thermal stability and this was confirmed from the TGA results.

Twaron fibres demonstrated a high thermal stability for an organic fibre, confirming the values stated by the manufacturer [66]. A 48 °C difference in mass loss onset between oxygen and inert atmospheres was observed. It is assumed that oxygen is present at the bulk of the friction interface and therefore this condition is assumed for thermal degradation studies.

Natural fibres demonstrated a similar thermal stability amongst one another in terms of onset temperature and rate of thermal degradation. Mass losses for flax, sisal, kenaf and jute were observed from 100 °C onwards and are attributed to evaporation of both surface and bound moisture within the fibres. Up to 5% by mass is lost during this initial phase indicating greater moisture content than aramid fibres and confirming cellulose fibres' affinity for water. The onset of the main thermal degradation at around 250 °C is dominated by the high cellulose content of the fibres and demonstrates a comparable thermal stability between all natural fibres trialled in this research. This result demonstrates that natural

fibres in friction formulations will be the lowest thermally stable materials along with the rubber particles. This work agrees with the temperature limitations of using natural fibres in brake pads identified by Xin [57].

In addition to the elevated temperatures, high mechanical stresses on the friction material imposed during service will affect the stability and presence of raw materials at the friction interface. TGA does not quantify the mechanical strength however the thermal stability as a function of the mass change has allowed the presence and stability of each raw material in this particular friction formulation to be discussed.

7.2 Fibres as processing aids in friction materials

7.2.1 Aramid

The results from sieve tests in section 5.3.1 demonstrate a direct correlation between the aramid content and the mass of particles retained by the fibre network structure. The test provided a consistent and quantitative measure of the dust suppressing performance of the aramid pulp in a friction formulation. As the sole processing fibre within the formulation the aramid fibre structure captures and retains the large number of particles. A baseline value for the formulation A3.75 represents an acceptable performance for industrial manufacture. Reducing the volumetric inclusion of aramid by only 0.75 % increased the particulate separation by 236 % and reducing aramid levels 1% by volume increased the separation by 700 %. The volumetric percentage of aramid pulp in this economy friction formulation clearly controls the retention of all other raw materials. Reducing the volume of aramid pulp decreases the number of fibres in the formulation, the density of net structure and hence the number of inter-fibre contacts. This reduces the ability of the fibre structure to capture and retain particulate materials and produces greater static loading due to the reduced number of fibres.

The sieve test clearly demonstrates that aramid pulp provides the physical structure and mechanism behind the dust suppression in this friction formulation.

Bulk density is a measure of the mass per unit volume of a friction material formulation. The only raw material in the formulation capable of producing a high volume, low density structure and hence influencing the bulk density of the formulation are the processing

fibres. In the chosen formulation aramid is the only processing fibre therefore changes in bulk density can be directly attributed to aramid.

The observed increase in bulk density in relation to the reduced levels of aramid pulp agrees with the previous statement attributing bulk volume solely to the processing fibres. A linear increase in bulk density is observed for formulations A3 and A2 however formulation A1 containing only 1% aramid by volume produces an increase in bulk density of over 40%. The justification is that reducing the volume fraction of aramid produces a higher loading per unit area of fibre and hence a weaker fibre structure that deforms and yields under the mass of raw materials. Reducing the aramid pulp from A3.75 to A1, i.e. by 2.75% by volume, produces a 400% increase in the static loading placed on the fibres and so reducing the stability of the aramid fibre network structure.

Bulk density measurements of virgin aramid pulp show the low volume fraction of the material. Values were calculated for the fibre pulp as supplied and also after processing in a high speed mixer. Twaron 1099 is able to withstand the mechanical cutting action of steel blades in a high speed mixer as mixing reduces the bulk density by a factor of over 2.5 compared to the original starting fibre pulp. It is proposed that this resilience to high speed mixing and increase in volume of the fibre bulk is derived from a combination inherent material properties and the physical structure of the fibre pulp network. Tough resilient aramid fibres withstand high speed impacts from cutting blades by either additional fibrillation or deflection due to lack of restraint from other fibres. The highly entangled fibre network allows externally imposed forces to be absorbed and distributed through the fibre pulp, increasing the separation distance of individual fibres without destroying the number of inter-fibre contacts. Increased separation of fibres will produce a higher volume fibre structure. This volume can only be sustained if the number of fibre interactions is retained to transfer the load throughout the fibre structure. Aramid pulp provides such a structure, ideally suiting the material to friction material processing and manufacture.

Pre-forms are a key stage in the manufacturing process of brake pads and in parallel to dust suppression rely solely on the processing fibre for enhanced performance. The indentation test developed provided an accurate reflection of the real life failure mode of the pre-forms and a rapid method of obtaining quantitative data for the green strength of a pre-form. The maximum load recorded on indentation of formulation A3.75 represented the minimum

acceptable value for industrial manufacture of brake pads. Exceeding the value would be of minor benefit. Geometric integrity of pre-forms is fundamental to the shape of the final brake pads and a determining factor in the quality control process. Minor adjustments in the volumetric percentage of aramid pulp in the formulation produce large changes in the physical number of aramid fibres present. The high volume, highly compressible fibre network structure provides the skeleton structure to the pre-forms, observed in the resistance to indentation and also geometric integrity such as edge definition. The fineness of the aramid fibres produces an evenly distributed bulk of fibres that compress, taking up the form of the pre-form mould. The resistance to indentation is taken from the inter-fibre contacts, which are numerous within the friction mix and increased in density further during compression of the pre-forms. A linear reduction in green strength can be observed with respect to aramid content. Additional similarity with dust suppression and bulk density results can be seen in the marked drop in performance with respect to formulation A1. It is proposed that at a 1% level, the low volume of aramid fibres, contain a low number of fibre interactions that are progressively destroyed through the manufacturing process due to overloading of the aramid fibre network structure.

7.2.2 Natural fibres

Partially substituting aramid pulp with a variety of natural fibres demonstrated that natural fibres used in conjunction with aramid pulp produce pre-forms of equal strength to the master batch formulation. The indentation test provides a comparative study for the green strength. Pre-form strength can be maintained using an aramid fibre and fibrillated hemp fibres in a 50:50 ratio. Statistical analysis showed the increase observed between the fibrillated fibre types lay within experimental variance. Pre-form strength were not maintained if aramid levels were reduced by more than 50% of the original percentage volumes.

7.3 Fibres in composite friction materials

7.3.1 Shear strength

A key result for trialling natural fibres in friction materials was the successful production of full size brake pads incorporating 100% natural fibres. The pads showed a high structural integrity with no visual evidence of material defects such as delamination, voiding, cracks or inhomogeneous appearance. The formulations containing 100% natural fibres did not pre-form but successfully passed through the hot pressing and post baking stages. The minimum shear strength between friction material and back plate required to meet the safety standards specified in Regulation 90 was exceeded by all brake pads containing natural fibres as a direct replacement for aramid. The interfacial bond derives strength from a combination of mechanical keying of friction material into the back plate and the bond strength between the heat activated adhesive applied to the back plate and friction material. All pads failed at shear strengths greater than the minimum specification by a safety factor in excess of 3. Interfacial bond failure for all materials produced a similar result by leaving an even thickness of friction material attached to the back plate. This shows that natural fibres do not affect the bulk shear strength of the brake pad or the method of failure through the material. Greatest interfacial bond strength was observed for the jute and sisal samples which also exhibited greater bond strength than the master batch pads. The observed shear strength of brake pads containing natural fibres demonstrates that short cellulose based natural fibres can be incorporated in this formulation at 3.75% by volume and produce a brake pad with a back plate bond strength exceeding the minimum Regulation 90 standards by a factor of safety of greater than 3.

7.3.2 Flexural strength

The flexural strength results showed no gain in the average flexural strength with the addition of aramid fibres. This was confirmed by the statistical analysis of the data sets. This result is only valid for this formulation however there are many economy friction formulations on the market using very similar raw materials. It is proposed that the absence of gain in flexural strength with increased aramid is due to the steel fibres and vermiculite particles within the composite dominating the fracture mechanics. The relatively large steel

fibres and vermiculite particles sit amongst a composite of highly compacted fine powders bound together with a thermosetting resin providing the surface flaws and the sites for crack propagation upon the application of an applied stress. Having proved no appreciable reinforcing benefit at ambient temperature it is possible that a similar result will be witnessed at elevated temperatures.

7.3.3 Material dispersion

Using EDX analysis the location of fine powdered raw materials could be clearly shown on the surface of a friction material. Barium sulphate and antimony trisuphide were chosen as marker compounds to track the distribution of fine powders across the surface of a friction composite as a function of aramid content.

Formulation A0 produced a friction surface in which antimony trisulphide particles agglomerated together producing a patchy distribution across the surface. Formulation A3.75 showed a much finer distribution of the same particles across the surface..

This same result is replicated to a lesser degree for the barium sulphate particles showing an improved distribution of fine particles as the aramid content is increased.

This elemental mapping technique views a two dimensional distribution however it could be inferred from these results that material distribution through the thickness of the pad follows the same trend. An inhomogeneous material is undesirable for predictable friction and wear performance throughout the life of the pad.

Ultra Violet excitation of virgin aramid fibres is a tool to identify their location across the friction composite surface. Images obtained show aramid fibres randomly distributed across the friction surface with small fibrils clearly attached to larger fibres within the resin matrix.

7.4 Friction and wear

7.4.1 Dynamometer testing

For the inertial dynamometer testing, formulations A3.75, A2(FC+4)1.75 and jute showed a near identical friction performance for the initial braking test of 30 stops. This dynamometer test represents the “off the shelf” performance of a friction material and is an

important result for both safety consideration and consumer expectation. The friction level of the A3.75 pad progressively increased to levels in excess of 0.5 and remained stable through out the bedding and initial characterisation stops. Pads A2(FC+4)1.75 and jute, containing natural fibres, showed a marginally lower friction level from the start yet maintained a constant value throughout the first characterisation stage.

The addition of natural fibres in the pads showed an increased sensitivity to the applied pressure during the slow and medium speed braking stages. A marginally lower operating friction level was observed across the variable pressure tests for pads containing natural fibres indicating a sensitivity of the formulations to both speed and pressure.

All samples showed a comparable friction level during the high speed decelerations from 200 to 170 km/h, highlighting the only speed sensitivity observed for the A3.75 formulation.

In comparison to the first characterisation, the second run showed a 5% reduction in the friction level of the master batch pad but a 10% rise for both pads containing natural fibres. Characterisation stage 2 and 3 were separated by cold performance stops and high deceleration brake applications which showed negligible effect on the operating friction.

The high temperature fade procedure produced a comparable operating friction level between all samples as shown in table 5.10 but a reduced fade effect for pads containing natural fibres. The mechanisms for this result are unclear yet a pad containing jute fibres – with a thermal stability 214 °C lower than aramid – can demonstrate a greater friction stability throughout the high temperature fade test. The high temperatures experienced in the fade test far exceed the thermal degradation of both fibre types, therefore producing a charred material at the friction interface or leaving voids previously occupied by the fibres. Jute fibres are physically larger in comparison to the aramid and would leave larger voids on the friction interface. Brake fade is known to occur when high temperatures liberate volatile gasses that lubricate and apply a back pressure to the friction material [11]. Voids in the friction surface could act as expansion chambers for the trapped gasses, reducing the pressure at the friction interface and also the mechanism behind brake fade.

The post fade characterisation showed operating levels for the natural fibre pads to equal and exceed the preceding characterisation, indicating a possible change in operating friction as a result of the elevated temperatures experienced in the fade test. High fade temperatures

would carbonise the friction surface leaving thermally stable material prominent such as metallic and mineral particles. Steel fibres and abrasive silica particles rubbing against the brake disc could account for this rise in friction levels.

In a similar manner to the fade result, the high temperature effectiveness stage showed a greater fade level from the master batch pad and higher friction levels from the pads containing natural fibres. Friction levels for characterisation 5 were elevated on the previous comparative for pads containing aramid and of an equally high level for the jute fibre pad showing little sign of effect from the high temperature characterisation.

The sustained increase in friction level for the jute pads compounds the previous discussion of thermally stable mineral and metallic particles dominating the friction levels.

The final temperature induced fade stage demonstrated a drop in friction levels for all pads but of a lower magnitude compared to the first fade. This result agrees with the expulsion of volatiles producing a primary brake fade and also the work of Savage [11]. Jute brake pads replicated the previous fade test by recording both the highest average and most stable friction level for the stage.

The average operating friction level for the complete AK master test for each pad are within a 7% of one another with the jute pads demonstrating the highest value of 0.43, an average value that is raised by the elevated friction levels after the first fade test. Average friction levels for the aramid/hemp blend and master batch were 0.4 and 0.41 respectively.

Constant torque dynamometer procedures are a fast and cost effective method of evaluating friction materials on the full scale inertial dynamometer. The natural fibre friction formulations produced comparable operating friction levels in agreement with the AK master test results. Comparing the friction data for all fibre types it can be shown that all natural fibres pads produced comparable results in both coefficient of friction levels and fade and recovery performance after temperature fade tests. The repeat of high temperature performance echoed the fade results from the AK master test as the magnitude of the second fade in friction levels was reduced by approximately two thirds, highlighting that the largest fade experienced in a dynamometer fade test will be the first. Visual inspection of the post tested pads showed no signs of crumbling, delamination or surface pitting indicating that the brake pads containing 3.75 % natural fibres by volume show a good mechanical integrity after the rigours of a dynamometer test.

7.4.2 Chase friction and wear testing

Friction and wear results from the Chase machine produced friction and wear data for friction materials as a function of both aramid and natural fibre content. Data obtained from sub-scale friction and wear machines complement the dynamometer results but is not directly comparable for reasons discussed earlier.

The specific wear rate of friction material was observed to reduce as a function of aramid levels where a 2 % by volume inclusion of aramid pulp reduced the average specific wear rate by 36%. Increasing the aramid content in formulations A3 and A3.75 displayed an increase in the average wear rate with a greater offset between the two specific wear calculations. The reasons for this variation in wear levels are unclear however both samples produced substantially lower wear rates during the second wear test indicating the wear rate of these surfaces to be sensitive to contact time. This shows a reduction in the wear rate of the formulation reaching a minimum value for aramid levels of 2% by volume and above.

No clear correlation between hemp fibre inclusion levels and the wear rate of the formulations was observed. Formulation A2(FC+4)1.75 produced the highest specific wear rate of all the formulations. Specific wear values were obtained as the mean value over 10 runs, therefore only 2 specific wear rates were calculated for each friction material. Additional data would be required to confirm any relationship using statistical analysis.

The average friction levels recorded for the formulation did not significantly vary as a function of aramid content, yet the addition of hemp fibres indicated a small reduction across all fibre inclusion levels. Low mechanical shear strength of the natural fibres, providing a weaker frictional interface is a possible mechanism behind the minor drop in coefficient of friction observed for the formulation. Analysis of variance for the friction levels for all friction materials show that the mean values recorded for all material are equal and therefore the fibres in the friction materials tested are independent of the measured level of friction.

Data presented for the operating friction of formulations A0, A2 and A3.75 during the early stages of individual wear test shows increased aramid levels to stabilise the coefficient of friction and produce a repeatable value for short braking applications. This result agrees with previous research [3,47] that identified the contribution of aramid fibres in friction

materials to develop a stable continuous friction film that stabilised the friction level and increased repeatability between runs.

The rise in disc temperature was plotted as a function of fibre type for both aramid content and aramid:hemp blends. The data recorded indicated towards an influence in the temperature rise due to both fibre type and inclusion level. Statistical analysis showed that a null hypothesis can be rejected for the data recorded – indicating the data sets are not equal – however additional data needs to be obtained before confirming this statement. Measuring the rise in bulk disc temperature as a result of a small tribological contact patch requires a large number of data point before any solid conclusions may be drawn.

7.5 Fibre structure

High magnification SEM images of Twaron 1099 have illustrated the hierarchal structure of aramid fibre pulp in which large fibres provide support to smaller fibres that in turn entrap particulate materials. Identifying this fibre structure explains the observed performance benefits of dust suppression, pre-form strength, bulk volume and fibre resilience. The small fibre network entitled the “net structure” has been observed in operation as part of the hierarchal fibre arrangement. The molecular arrangement of aramid, controlled during manufacture, has been shown to dictate the fibrillation process of the fibres giving a highly flexible material in terms of fibre morphology. The weak directional skin structure of aramid fibres allows the formation of micro fibrils along the fibre length, which can be further increased by mechanical processing, contributing to the net structure. This agrees with the literature review in section 2.1.4. The net structure can be an integral part of the large aramid fibres or separate ribbon like fibres that combine with the large fibre via fibre entanglements. The performance of the net structure was clearly demonstrated by blending the fibres with graphite particles, and provided the starting point for the subsequent fibre models.

Recycled aramid products do not demonstrate such a high degree of fibrillation and fibre entanglement as these forms of aramid are not manufactured to intentionally fibrillate by means of the discrete skin and core molecular structure.

Natural fibres were nearly two orders of magnitude larger in size compared to aramid in the received state from suppliers. All natural fibres examined exhibited a much greater variance in structure with respect to aramid which can explain the difference in fracture mechanics that manifests as a reluctance of natural fibre to fibrillate to the same degree. Mechanical processing of hemp fibres produced smaller diameter fibres with a high aspect ratio but on a scale much larger than aramid. Fibrillation along the fibre length was observed for processed hemp fibres however the fibrils were not able to attain high aspect ratios as they would fracture producing small discrete fibres. Hemp and other natural fibres do not have the directional molecular order of aramid and so cannot fibrillate in the same manner to produce the desired dry fibre network.

7.6 Dynamic mechanical analysis

The dynamic mechanical testing employed to characterise the fibres pulps proved to be an accurate and repeatable method of characterising the onset of changes in delicate dry fibre pulps. This method is a valuable addition to researchers wishing to understand and quantify processing fibres for friction materials. The material parameters obtained from the test – elastic shear modulus and critical strain – are key properties that describe the performance of dry fibre pulps in the processing of friction materials. The data obtained quantifies the fibre structures in a format never used by friction formulators previously and offers a test for both fibre developments and routine quality control. Repeatability between tests was confirmed and the fatigue effect of the test procedure negated. The elastic shear modulus recorded for aramid pulp was larger that the majority of fibrous materials tested and the critical strain – possibly indicating the breakdown of inter-fibre bonds – far exceeded all other materials. It is the critical strain of the aramid pulp that is the key measure from the test and the benchmark value for other fibre types and blends.

Mineral fibres routinely used in friction materials showed a very high initial modulus and a very low critical strain. The high initial modulus could be attributed to the dense network of stiff mineral fibres which short in length, and high in number, produce a larger number of inter-fibre contact points. It is proposed that the low critical network strain is due to the lack of inter-fibre elasticity, either through inter-fibre bonding and entanglements, or the

physical curl and spring like behaviour of individual fibres. The smooth melt spun mineral fibres can freely slide over one another on the application of an external strain without a mechanical means of recovering from the applied strain.

Cellulose fibres demonstrate the lowest elastic shear modulus but this is maintained to greater strain levels than the Rockwool. The cellulose fibres are inherently more flexible than the mineral fibres yet the fibre network shows a consistent elastic response over nearly twice the strain range indicating a greater degree of elastic interaction within the cellulose fibre network.

This test was used to identify the elastic properties of fibrillated hemp fibres as a function of mechanical processing. An increased critical strain of hemp fibres was observed until fibre type FC+4, after which critical strain levels dropped for FC+5. It is proposed that progressive mechanical processing increased fibre fibrillation which was observed in the critical strain values. After four cycles through the mechanical carding machines it is thought that hemp fibre no longer fibrillate and begin to physically break down. For this reason fibre type FC+4 was chosen to blend with aramid in subsequent fibre trials.

The optimum fibre blend identified using the dynamic mechanical test was A3(FC+4)0.75.

7.7 Fibre network model

The fibre network model developed in this work allows the observed hierarchal structure of aramid to be predicted as a function of fibre and particle geometry. The model is based on a number of assumptions that allows the complex dry fibre pulp to be simplified into a two component structure. The equation produced to model the particle retention performance of small aramid fibres highlights the dominating effects of fibre geometries such as diameter and free length. The equation produced has allowed the maximum fibre span of a net structure to be determined as a function of fibre diameter, length and also particle density.

Differentiation of the equation allows the maximum particle diameter to be predicted as a function of the fibre geometry and particulate density. Also the maximum particle diameter retained by a fibre pair as a function of fibre diameter has been produced. Describing this situation numerically has applications extending beyond friction materials as many

engineering systems and process involve particle capture by fibres or threadlike structures either intentionally or not.

The large network structure has also been modelled to describe the deflection of the large framework as a function of the grid fibre spacing. The stiffness of the grid structure is a cubic function of the fibre length, and as such an key value for the structural rigidity. Making an analogy between the structure fibre network and open cell foam structure has allowed the actual fibre spacing to be predicted using experimental values in an empirical equation. This is an initial step in quantifying the geometry of a complex fibre network from viscoelastic data obtained experimentally.

The large fibre framework was modelled as a regular cubic lattice structure and the critical bucking loads of the vertical fibres calculated. Comparing this value to realistic loadings shows the structure to be well within the failure loads when used at 3.75% by volume.

8 Conclusions

The performance of aramid pulp in the form of Twaron 1099 as a processing aid in non-asbestos organic friction materials was investigated. Brake pads were manufactured replicating industrial methods and analysed at progressive intervals to quantify the effect of aramid pulp on the required level of performance. The bulk density of a friction formulation is a key parameter to measure the performance of the processing fibre and a direct correlation with aramid content was observed. Reducing the level of aramid pulp in the formulation by 2.75% resulted in a 40% increase in the bulk density, nearly 15 times greater than the predicted increase by changing material density. The processing performance of aramid pulp is further highlighted by the dust suppression tests and pre-form strength results. A clear correlation between dust suppression and aramid levels was shown which for industrial manufacture equates to a more efficient and cost effective manufacturing process and reduced health and safety concerns regarding the emission of airborne particles. The indentation test, developed to quantify the pre-form strength, proved to be a quick and accurate method of evaluation new formulations and identified a direct relationship between aramid and pre-form strength. These results correlate with those published by the manufacturer of Twaron [66]] and also in academic literature [2,3,42,47,63]. No other processing fibre trialled could successfully match the performance levels observed for aramid pulp. The physical structure of aramid pulp aids the mixing and dispersion of raw materials as shown by the distribution of heavy metal elements across the surface of brake pads.

The processing performance of aramid pulp is achieved though its physical structure, identified by the high magnification images in section 5.2.1. A skin/core structure in aramid fibres was observed, agreeing with published literature [57] and identified as the mechanism behind the high levels of fibre fibrillation which in turn are responsible for the bulk fibre structure.

Flexural strength tests identified an important finding that aramid fibres do not contribute to the flexural strength of the chosen brake pad formulation even at double the standard levels. This result contradicts one of the published benefits of using aramid [66].

A novel fibre test was developed and employed to evaluate the suitability of candidate fibres as processing aids in friction materials. The elastic recovery of fibre pulps was measured and correlated well to previous research [123] allowing fibre types to be assessed, providing a new analytical technique to develop new fibre morphologies.

Brake pads containing natural fibres as a direct substitute for aramid pulp were successfully manufactured using conventional processes. The addition of 3.75% by volume of various natural fibres did not detrimentally affect the geometric integrity of the pads, or the affinity with the resin matrix and other raw materials. This was confirmed by mechanical shear testing and is a significant result for trialling natural fibres in brake pads.

Friction and wear testing showed the friction level to be independent of both aramid fibres and hemp fibres. This is an important result and demonstrates that the organic fibre content did not affect the friction level up to 3.75% by volume in the chosen formulation. Increasing the aramid content in the formulation showed a stabilising effect on the friction levels over the first 10 seconds of a test, something that would become evident during service use as smooth predictable braking.

The proposed analytical model for aramid pulp allows the particle retention performance of aramid fibre to be predicted as a function of both fibre and particle geometry. Fibre free length, and second moment of area – itself a function of diameter, cross section and fibre curl – have the greatest influence on the fibre network retaining particles in suspension.

In terms of an aramid natural fibre replacement, the research work in this thesis points towards a fibre blend until the morphology of natural fibres can be tailored to further mimic the aramid fibre structure. Results from the dynamic properties of fibre networks in section 5.2.3.3 indicate a 20% aramid replacement with a processed hemp fibre. Friction and wear results from the sub scale Chase tester also highlight this ratio of aramid to hemp fibres as producing the lowest wear rate with good friction levels compared to the other fibre blends. This work therefore proposes that aramid pulp may be replaced by fibrillated hemp fibres at a level of 20% of the current volumetric inclusion in the friction formulation used in this work.

9 Recommendations for future work

The research work in this thesis has answered a number of questions regarding the performance of processing fibres in friction materials – especially aramid – at the same time as introducing an equal number of questions for future work. Time limitations ensure that work remains to be covered on the subject and suggested directions of research will be given here.

The structure and performance of aramid pulp in friction materials has been quantified and the fracture mechanisms behind the formation of the fibre structure identified. The scope of natural fibres could be greater furthered if their structure could be made to mimic that of aramid more closely. Additional fibrillation techniques including fibre immersion and ultra sonic should be trialled to maximise the fibrillation limits of these natural materials.

Further work is required to understand the friction and wear performance of aramid and natural fibre blends and investigating the friction surface, transfer film morphology and wear debris as a function of fibre and operating conditions will give and insight to this.

Disc wear is a prominent topic in the development of friction materials so a microscopic evaluation of the tribological couple would help identify the changes in wear mechanism that were put forward in this work.

The dynamic mechanical analysis of dry fibre pulps has proven to be a valuable insight into the performance of processing fibres in friction materials. The technique has further scope to probe the bulk properties of fibre networks using creep, stress relaxation techniques. Fibre volume fractions could also be varied to quantify the elastic of the bulk as a function of the network density.

Network modelling of the hierarchal fibre structure has developed a numerical equation to predict the particle retention performance of two fibres. There is great scope to further the complexity of the model to include the fibre geometrics that will influence the rigidity of the fibres. These include cross section area, curl, kink and twist along the fibre length. Fibre end effects will have a role in the fibre network mechanics and including parameters such as fibre friction and entanglements will further towards understand this. So far only aramid fibres have been modelled and including additional fibre types within the model will complement the fibre blends trialled in this work.

10 References

1. Bijwe, J. (1997) “Composites as friction materials: Recent Developments in Non-Asbestos Fibre reinforced Friction Materials”, Polymer composites, 18, (3), 378-395.
2. Briscoe. B.J. Ramirez, I. Tweedale, P. J. (1998) “Friction of Aramid fibre composites”, International conference on disc brakes of commercial vehicles, IMechE, 15-29.
3. Kim, S.J. Jang, H. (2000)” Friction and wear of friction materials containing two different phenolic resins reinforced with aramid pulp”, Tribology International, 33, (7), 477-484.
4. Jacko, M.G.Tsang, P.H.S. Rhee, S.K. (1984) “Automotive friction materials evolution during the past decade”, Wear, 100, 503-515.
5. Sinha, S.K. Biswas, S.K. (1992) “Friction and wear behaviour of continuous fibre as cast Kevlar-phenolic resin composite”, Journal of materials science, 27, (11), 3085-3091.
6. Spurr, R.T. (1972) “Fillers in friction materials”, Wear, 22, 367-372.
7. Tirovic, M. Voller, G.P. (2002) “Commercial vehicle brake cooling - ventilated disc or ventilated wheel carrier” IMechE international conference Braking 2002, Leeds UK, Professional engineering publishing, London UK.
8. Jimbo, Y. Mibe, T. Akiyama, K. Matsui, H. Yoshida, M. Ozawa, A. (1990) “Development of high thermal conductivity cast iron for disc brake rotors” SAE transactions, 99, (5), 1-7.
9. Cho, M.H. Kim, S.J. Basch, R.H. Fash, J.W. Jang, H. (2003) “Tribological study of gray cast iron with automotive brake linings: The effect of rotor microstructure”, Tribology International, 36, (7), 537-545.
10. Metzler, H. (1990) “The brake rotor – friction partner of brake linings”, SAE technical paper, 1990;900847
11. Savage, L. (1995) “The Tribology of friction materials at high temperatures” Doctoral Thesis, School of Materials Science, University of Bath, UK.

12. Coyle, J.P. Tsang, P.H.S. (1983) “Microstructural changes of cast iron rotor surfaces and their effects on brake performance and wear resistance”, Transactions of the society of automotive engineers, 92, (2), 2573-2586.
13. Unknown (2007) “Lapinus fibres: Rockwool for friction materials, Lapinus fibres technical literature, Lapinus fibres bv, Roermond Netherlands, 1-6.
14. Kaatz, R (2006) Private communication, SAE 24th annual brake colloquium and exhibition, 2006, General motors corporation.
15. Unknown (1999) POLMIT: Pollution of Groundwater and Soil by road and Traffic Sources: Dispersal Mechanisms Pathways and Mitigation Measures, Transport research laboratory, UK.
16. Nicholson, G. (1995) “Facts about friction: 100 years of brake linings and clutch facings”, 2nd edition, Croydon PA, P&W Price Enterprises Inc,
17. Blau, P.J. (2001) “Compositions, Functions and testing of friction brake materials and their additives”, Oak Ridge national laboratory report, Tenessee, US Department of Energy, 19
18. Unknown (2006) “Bakelite Phenolic resins”, Bakelite AG technical literature, Iserlohn-Letmathe, Germany, 80.
19. Washabaugh, F.J (1986) “EMCOR 66 Ultra short fibres for asbestos free friction materials”, Society of Automotive Engineers paper number 860630.
20. Smales, H. (1994) “ Friction materials – black art or science”, Proceedings of Institution of mechanical engineers Part D: Journal of automobile engineering, 203, (3), 151-157.
21. Longley, J.W. Gardner, R. (1988) “Some compositional effects in the static and dynamic properties of commercial vehicle disc brakes”, IMechE International conference – Disc brakes for commercial vehicles, London, Professional engineering publishing, London UK , 31-38.
22. Thompson, S.K. Mason, E. (2002) “Asbestos: Mineral and fibres”, Journal of chemical health and safety, 21-23.
23. Jang, H. Lee, J.S. Fash, J.W. (2001) “Compositional effects of the brake friction material on creep groan phenomena”, Wear, 251, (1-12), 1477-1483.

24. Cho, M.H. Kim, S.J. Kim, D. Jang, H. (2005) “Effects of ingredients on tribological characteristics of a brake lining: an experimental case study”, Wear, 258, (11-12), 1682-1687.
25. Weiss, Z. Crelling, J.C. Simha Martynkova, G. Valaskova, M. Filip, P. (2006) “Identification of carbon forms and other phases in automotive brake composites using multiple analytical techniques”, Carbon, 44, (4), 792-798.
26. Osterle, W. Griepentrog, M. Gross, Th. Urban, I. (2001) “Chemical and micro structural changes induced by friction and wear of brakes”, Wear, 251, (1-12), 1469-1476.
27. Guipu, X. Zikang, Z. (2003) “Influence of brake condition on the friction and wear properties of a low metal formulation” SAE 21st brake colloquium and exhibition, Florida USA, SAE international, 65-70.
28. Filip, P. (2002) “Friction and wear of polymer matrix composite materials for automotive braking industry”, IMechE international conference Braking 2002, Leeds UK, Professional engineering publishing, London UK, 341-354.
29. Gudmand-Hoyer, L. Bach, A. Nielsen, G.T. Morgan, P. (1999) “Tribological properties of automotive disc brakes with solid lubricants”, Wear, 232, (2), 168-175.
30. Bettge, D. Starcevic, J. (2003) “Topographic properties of the contact zones of wear surfaces in disc brakes” Wear, 254, (3-4) 195-202.
31. Osterle, W. Urban, I. (2004) “Friction Layers and friction films on PMC brake pads”, Wear, 257, (1-2), 215-226.
32. Mueller, M. Ostermeyer, G.P. (2007) “Cellular automata method for macroscopic surface and friction dynamics in brake systems”, Tribology International, 40, (6), 942-952.
33. Eriksson, M. Jacobson, S. (2000) “Tribological surfaces of organic brake pads”, Tribology international, 33, (12), 817-827.
34. Chan, D. Stachowiak, G.W. (2004) “Review of automotive brake friction materials” IMechE Journal automobile engineering Part D, 218, 953-966.
35. Kim, Y.C. Cho, M.H. Kim, S.J. Jang, H. (2007) “The effect of phenolic resin, potassium titanate, and CNSL on the tribological properties of brake friction materials” Wear, 264, (3-4), 204-210.

36. Palmer, B.P. Weintraub, M.H. (2000) “The role of engineered cashew particles on performance”, IMechE international conference Braking 2000 – Automotive braking technologies for the 21st century, Leeds UK, Professional engineering publishing, London UK, 1-11.
37. Kim, S.J. Cho, M.H. Cho, K.H. Jang, H. (2007) “Complementary effects of solid lubricants in the automotive brake lining”, Tribology international, 40, (1), 15-20.
38. Smeets, L. Segeren, M. (2007) “Improved performance of NAO/non-steel disc pads by usage of Extreme low shot (ELS) Roxul 1000 fibres”, SAE 25th annual brake colloquium and exhibition, Orlando, FL, USA.
39. McLellan, R.G. (1988) “Requirements of friction materials in commercial vehicle disc brake applications”, IMechE International conference – Disc brakes for commercial vehicles, London, Professional engineering publishing, London UK , 9-13.
40. Gopal, P. Dharani, L.R. Blum, F.D. (1994) “Fade and wear characteristics of a glass fibre reinforce phenolic friction material”, Wear, 174, (1-2), 119-127.
41. Evans, R.E. Trainor, J.A. (1990) “Acrylic fibres in non-asbestos friction materials”, In proceedings of SAE eighth annual brake colloquium and exhibition, Atlantic city New Jersey USA, SAE International, 1-15.
42. Kim, S.J. Cho, M.H. Lim, D.S. Jang, H. (2001) “Synergistic effects of aramid pulp and potassium titanate whiskers in the automotive friction material”, Wear, 251, (1-12), 1484-1491.
43. Ozturk, B. Arslan, F. Oaturk, S. (2007) “Hot wear properties of ceramic and basalt fibre reinforced hybrid friction materials”, Tribology International, 40, (1), 37-48.
44. Satapathy, B.K. Bijwe, J. (2005) “Composite friction materials based on organic fibres: Sensitivity of friction and wear to operating variables”, Composites Part A: applied science and manufacturing, 37, (10), 1557-1567.
45. Gopal, P. Dharani, L.R. Blum, F.D. (1996) “Hybrid phenolic friction composites containing Kevlar pulp Part1. Enhancement of friction and wear performance”, Wear, 193, (2), 199-206.
46. Satapathy, B.K. Bijwe, J. (2004) “Performance of friction materials based on variation in nature of organic fibres Part 1”, Wear, 257, (5-6), 573-584.

47. Mutlu, I. Eldogan, O. Findink, F. (2006) “Tribological properties of some phenolic composites suggested for automotive brakes”, Tribology international, 39, (4), 317-325.
48. Crosa, G. Baumvol, I.J.R. (1993) “Tribology of composites used as friction materials”, Advances in composite Tribology, 8, Amsterdam, Elsevier science publishers BV.
49. Subramaniam, N. Sinha, B.R. Blum, F.D. Chen, Y.R. Dharani, L.R. (1991) “Glass fibre based friction materials”, International journal of Polymer materials, 15, 93-102.
50. Hettinger, W.P. Newman, J.W. Crock, R.P. Boyer, D.C. (1986) “Ashland's new low cost carbon fibre and carbonizing products for future applications” In proceedings of SAE annual brake colloquium and exhibition, 58-68.
51. Unknown (2005) “Akebono overview and reduced copper friction material development” Akebono technical literature, Tokyo, Japan.
52. Adachi, S. Kawamura, K. Takemoto, K (2001) “A trial on the quantitative risk assessment of man-made mineral fibres”, Journal of Industrial health 9, 168-174.
53. Unknown (2005) “Guide to processing CFF type V110-1 fibrillated fiber for fiction materials” Sterling fibres technical literature, Pace Florida USA, 1-14.
54. Xin, X. Xu, C.G. Qing, L.F. (2007) “Friction properties of sisal reinforced resin brake composites”, Wear, 262, (5-6), 736-741.
55. Tong, J. Arnell, R.D. Ren, L. (1998) “Dry sliding wear behaviour of bamboo”, Wear, 221, (1), 37-46.
56. Hahn, C. (2000) “Characteristics of p-Aramid fibers in friction and sealing materials”, Journal of industrial textiles, 30, 146-165.
57. Morgan, R.J. Pruneda, C.O. Steele, W.J. (1983) “The relationship between the physical structure and the microscopic deformation and failure processes of Poly(p-Phenylene Terephthalamide) Fibres”, Journal of polymer science, 21, (9), 1757-1783.
58. Li, L.S. Allard, L.F. Bigelow, W.C. (1983) “On the morphology of aromatic polyamide fibres (Kevlar, Kevlar 49 and PRD-49)” Journal macromolecular science, B22 (2), 262-290.

59. Graham, J.F. McCague, C. Warren, O.L. Norton, P.R. (2000) “Spatially resolved nano mechanical properties of Kevlar fibres”, Polymer, 41, (12), 4761-4764.
60. Manabe, S. Kajita, S., Kamide, K. (1980) “Fine structure of poly(p-phenylene terephthalamide) fibres”, sen-i kikai gakkaishi, 33.
61. Fukada, M. Kawai, H. (1993) “Moisture sorbtion mechanism of Aromatic polyamide fibres: Diffusion of moisture in poly (p-phenylene terephthalamide) fibres 1”, Textile research journal, 63, 185-193.
62. Yeu, C.Y. Padmanabhan, K. (1999) “Interfacial studies on surface modified Kevlar fibre/epoxy matrix composites”, Composites Part B: engineering, 30, (2), 205-217.
63. Kato, T. Magario, A. (1994) “The wear of Aramid fibre reinforced brake pads - The role of Aramid fibres”, Tribology transactions, 37, (3), 559-565.
64. Bijwe, J. Awtade, S. Ghosh, A. (2005) “Influence of orientation and volume fraction of Aramid fraction on abrasive wear performance of polyethersulfone composites”, Wear, 260, (4-5), 401-411.
65. Yu, L.G. Yang, S.R. (2002) “Investigation of the transfer film characteristics and tribochemical changes of Kevlar fibre reinforced polyphenylene sulfide composites in sliding against a tool steel counterface”, Thin solid films, 413, 98-103.
66. Unknown (2000) “Twaron in brake linings and clutch facings”, Teijin technical literature, Arnhem, Netherlands, 1-6.
67. United Nations (2001) “United Nations Regulation No 90. Uniform provisions concerning the approval of replacement brake lining assemblies and drum brake linings for power-driven vehicles and their trailers” European Community, Brussels, E/ECE/TRANS/505, 39.
68. Slevin, E.J. Smales, H. (2002) “Towards more accurate brake testing”, IMechE international conference Braking 2002, Leeds UK, Professional engineering publishing, London UK, 1-10.
69. Satapathy, B.K. Bijwe, J. Kolluri, D.K. (2005) “Assessment of fibre contribution to friction material performance using grey rational analysis (GRA)” Journal of composite materials, 0, 1-19.

70. Blau, P.J. McLaughlin, J.C. (2003) “Effects of water films and sliding speed on the frictional behaviour of truck disc brake materials” Tribology international, 36, (10), 709-715.
71. Bijwe, J. Nidhi. Majumdar, N. Satapathy, B.K. (2005) “Influence of modified phenolic resins on the fade and recovery behaviour of friction materials”, Wear, 259, (7-12), 1068-1078.
72. Eriksson, M. Lord, J. Jacobson, S. (2001) “Wear and contact conditions of brake pads: dynamical in situ studies of pad on glass”, Wear, 249, (3-4), 272-278.
73. Lasa, L. Rodriguez-Ibabe, J.M. (2003) “Wear behaviour of eutectic and hypereutectic Al-Si-Cu-Mg casting alloys tested against a composite brake pad”, Materials science and engineering A, 363, (1-2), 193-202.
74. Blau, P.J. Jolly, B.V. (2005) “Wear of truck brake lining materials using three different test methods”, Wear, 259, (7-12), 1022-1030.
75. Kim, S.J. Lee, J.Y. Jang, H. (2001) “Effect of humidity of friction characteristics of Automotive friction materials”, Korean society of Tribology and lubrication engineering, 2, (2), 150-153.
76. Stanford, M.K. Jain, V.K. (2001) “Friction and wear characteristics of hard coatings”, Wear, 251, (1-12), 990-996.
77. Tsang, P.H.S. Jacko, M.G. Rhee, S.K. (1985) “Comparison of chase and inertial brake dynamometer testing of automotive friction materials”, Wear, 103, 217-232.
78. Ingo, G.M. D'Uffizi, M. Falso, G. Bultrini, G. Padeletti, G. (2004) “Thermal and microchemical investigation of automotive brake pad wear residues”, Thermochimica acta, 418, (1-2), 61-68.
79. Eriksson, M. Bergman, F. Jacobson, S. (2002) “On the nature of tribological contact in automotive brakes”, Wear, 252, (1-2), 26-36.
80. Filip, P. Weiss, Z. Rafaja, D. (2002) “On friction layer formation in polymer matrix composite materials for brake applications”, Wear, 252, (3-4), 189-198.
81. Kim, S.J. Park, S.J. Basch, R.H. Fash, J.W. Jang, H. (2004) “High temperature wear properties of multiphase composite: The role of the transfer film”, Materials science forum, (449-452), 81-84.

82. Osterle, W. (2005) “Third body formation on brake pads and rotors”, Tribology international, 39, (5), 401-408.
83. Cho, M.H. Ju, J. Kim, S.J. Jang, H. (2006) “Tribological properties of solid lubricants (graphite, Sb_2, MoS_2) for automotive brake friction materials”, Wear, 260, (7-8), 855-860.
84. Jang, H. Kim, S.J. (2000) “The effects of antimony trisulphide (Sb_2S_3) and zirconium silicate ($ZrSiO_4$) in the automotive brake friction material on friction characteristics”, Wear, 239, (2), 229-236.
85. Hutchings, I.M. (1992) Tribology – Friction and wear of engineering materials, 1st Ed, Oxford, Butterworth-Heinmann, UK, 273.
86. Archard, J.F. (1953) “Contact and rubbing of flat surfaces”, Journal of applied physics, 24, 981-988.
87. Ostermeyer, G.P. (2001) “Friction and wear of brake systems”, Forschung im Ingenieurwesen, 66, 267-272.
88. Rhee, S.K. (1974) “Wear mechanisms for asbestos-reinforced automotive friction materials”, Wear, 29, 391-393.
89. Bark, L.S. Moran, D. Percival, S.J. (1975) “Chemical changes in asbestos based friction materials during performance - a review”, Wear, 34, 131-139.
90. Herring, J.M. (1967) “SAE automotive engineers congress”, Detroit, Society of Automotive Engineers paper number 670146.
91. Tanaka, K. Ueda, S. Nogughi, N. (1973) “Fundamental studies on the brake friction of resin based friction materials”, Wear, 23, 349-365.
92. Rhee, S.K. (1971) “Wear of metal reinforced phenolic resins”, Wear, 18, 417-477.
93. Wirth, A. Eggleston, D. Whitaker, R. (1994) “A fundamental tribochemical study of the third body layer formed during automotive friction braking”, Wear, 179, 75-81.
94. Osterle, W. Klob, H. Urban, I. Dmitriev, A.I. (2007) “Towards a better understanding of brake friction materials”, Wear, 263, (7-12), 1189-1201.
95. Ostermeyer, G.P. (2003) “On the dynamics of the friction coefficient”, Wear, 254, (9), 852-858.
96. Various (2000) “Handbook of technical textiles”, 3rd ed, Cambridge, Editors Horrocks, A.R. Anand, S.C, Woodhead publishing Cambridge UK, 576.

97. Mwaikambo, L.Y. Ansell, M.P. (2003) “Hemp fibre reinforced cashew nut shell liquid composites”, Composites science and technology, 63, (9), 1297-1305.
98. Wambua, P. Ivens, J. Verpoest, I. (2003) “Natural fibres: can they replace glass in fibre reinforced plastics?”, Composites Science and Technology, 63, (9), 1259-1264.
99. Zafeiropoulos, N.E. Williams, D.R. Baillie, C.A. Matthews, F.L. (2002) “Engineering and characterisation of the interface in flax fibre/polypropylene composite materials. Part 1. Development and investigation of surface treatments”, Composites Part A: applied science and manufacturing, 33, (9), 1083-1093.
100. Franck, R.R. (2005) “Bast and other plant fibres (Woodhead textile series No 39)”, 1st Ed, Cambridge UK, Woodhead publishing, 432.
101. Gordon-Cook, J. (1984) “Handbook of textile fibres (Volume 1 - Natural fibres)”, 4th ed, Cambridge UK, Woodhead publishing, 240.
102. Thomsen, A.B. Rasmussen, S. Bohn, V. Vad Nielsen, K. Thygesen, A. (2005) “Hemp raw materials: The effect of cultivar, growth conditions and pre-treatment on the chemical composition of the fibres”, Technical report: Riso National laboratory, technical university of Denmark, 1-30.
103. Kessler, R.W. Kohler, R.Tubach, M. (2000) “Strategy for a sustainable future of fibre crops”, Scientific report, Institut fur Angewandte Forschung, University of applied science, Reutlingen, Germany, 1-11.
104. Arbelaiz, A. Fernandez, B. Ramos, J.A. Reteji, A. llano-Ponte, R. Mondragon, I. (2005) “Mechanical properties of short flax fibre bundle/polypropylene composites: Influence of matrix/fibre modification, fibre content, water uptake and recycling”, Composites science and technology 65 (10), 1582-1592.
105. Al-Sulaiman, F.A. (2002) “A trial on the quantitative risk assessment of man-made mineral fibres”, Applied composite materials 9, 369-377.
106. Eichhorn, S.J. Baillie, C.A. Zafieropoulos, N. Mwaikambo, L.Y. Ansell, M.P. Dufresne, A. Entwistle, K.M. Herrera-Franco, P.J. Escamilla, G.C. Groom, L. Hughes, M. Hill, C. Rials, T.G. Wild, P.M. (2001) “Review: current international

research into cellulosic fibres and composites", Journal of materials science, 36, 2107-2131.

107. Herrera-Franco, P.J. Valadez-Gonzalez, A. (2004) "Mechanical properties of continuous natural fibre-reinforced polymer composites", Composites Part A: Applied science and manufacturing, 35, 3, 339-345.

108. Aziz, S.H. Ansell, M.P. (2004) "The effect of alkalization and fibre alignment on the mechanical and thermal properties of kenaf and hemp bast fibre composites: Part 1 - polyester resin matrix" Composites science and technology, 64 (9), 1219-1230.

109. Bos, H. (2004) "The potential of flax fibres as reinforcement for composite materials", Doctoral thesis Technical University of Eindhoven, Eindhoven, 209.

110. Askling, C. Wagberg, L . (1998) "Rheological characterisation of dry-formed networks of rayon fibres", Journal of materials science, 33, 1517-1527.

111. Unknown. (1978) "Brake lining quality control procedures", Society of Automotive Engineers – A.1.1.1 Schedule SAE J661a, Detroit Michigan, SAE International, 31-55.

112. Masse, J.P. Salvo, L. Rodney, D. Brechet, Y. Bouaziz, O. (2006) "Influence of relative density and mechanical behaviour of a steel metallic wool", Scripta Materialia, 54, (7), 1379-1383.

113. Rodney, D. Fivel, M. Dendievel, R. (2005) "Discrete modelling of the mechanics of Entangled materials", Physical review letters, 95, (10), 1-4.

114. Baudequin, M. Ryschenkow, G. Roux, S. (1999) "Non-Linear elastic behaviour of light fibrous materials", European physical journal B, 12, 157-162.

115. Kozyreff, G. Wake, G. Ockendon, H. Sumner, R.M.W. (2003) "Core bulk of wool fibres as a function of their curvature and diameter", Physics letters A, 314, 428-433.

116. Clyne, T.W. Markaki, A.E. Tan, J.C. (2005) "Mechanical and magnetic properties of metal fibre networks, with and without a polymeric matrix", Composites science and technology, 65, (15-16), 2492-2499.

117. Chaudri, M.A. Whiteley, K.J. (1968) “The influence of natural variations in fiber properties on the bulk compression of wool” Textile research journal, 38, 897-906.

118. Beil, N.B. Roberts, W.W. (2002) “Modelling and computer simulation of the compressional behaviour of fibre assemblies” Textile research journal, 74, 341-351.

119. Beckerich, P. Weick, G. Marques, C.M. Charitat, T. (2003) “Compression modulus of macroscopic fibre bundles” Europhysics letters, 64, (5), 647-653.

120. Gibson, L.J. Ashby, M.F. (1997) “Cellular solids structure and properties” 2nd Ed, Cambridge UK, University press, Cambridge UK, 502.

121. Askling, C. Wagberg, L . (1998) “The effect of additives on the mechanical properties of dry-formed fibre networks”, Journal of materials science, 33, 1997-2003.

11 Appendix 1

AK Master Test

1. Green Performance

Number of Brake applications;	30
Brake line pressure (bar);	30
Test speeds (km/h);	80 to 30
Parameters recorded;	Disc temperature, Friction level
Example test duration;	1hour 7 min 4 sec

2. Bedding.

Number of Brake applications;	64
Brake line pressure (bar)	10 – 42
Test speeds (km/h);	80
Parameters recorded;	Disc temperature, Friction level, deceleration
Example test duration;	2 hour 39 min 7 sec

3. Characterisation

Number of Brake applications;	6
Brake line pressure (bar);	30
Test speeds (km/h);	80 – 30
Parameters recorded;	Disc temperature, Friction level
Example test duration;	16 min 7 sec

4. Speed sensitivity.

Number of Brake applications;	8 per operating speed
Brake line pressure (bar)	10, 20, 30, 40, 50, 60, 70, 80
Test speeds (km/h);	40 – 0, 80 – 40, 120 – 80, 160 – 130, 200 – 170.
Parameters recorded;	Disc temperature, Friction level
Example test duration;	2hour 1 min 10 sec

5. Characterisation

Number of Brake applications;	6
Brake line pressure (bar);	30
Test speeds (km/h);	80 to 30
Parameters recorded;	Disc temperature, Friction level
Example test duration;	17 min 33 sec

6. One cold stop (forced cooling).

Number of Brake applications;	1
Brake line pressure (bar);	30
Test speeds (km/h);	40
Parameters recorded;	Friction level
Example test duration;	7 mins 9 sec

7. Motorway stops.

Number of Brake applications;	2 (1 at each starting velocity)
Deceleration (g);	0.6
Test speeds (km/h);	100 – 0, 180 – 0.
Parameters recorded;	Disc temperature, Friction level, brake line pressure
Example test duration;	8 min 17 sec

8. Characterisation

Number of Brake applications;	18
Brake line pressure (bar);	30
Test speeds (km/h);	80 to 30
Parameters recorded;	Disc temperature, Friction level
Example test duration;	51 min 20 sec

9. Fade (reduced cooling temperature ramp)

Number of Brake applications;	15
Deceleration (g);	0.4
Test speeds (km/h);	100 – 0
Parameters recorded;	Disc temperature (692 °C max), Friction level, brake line pressure (85 bar)
Example test duration;	13 min 7 sec

10. Characterisation

Number of Brake applications;	18
Brake line pressure (bar);	30
Test speeds (km/h);	80 to 30
Parameters recorded;	Disc temperature, Friction level
Example test duration;	52 min 56 sec

11. Pressure effectiveness.

Number of Brake applications;	8
Brake line pressure (bar);	10, 20, 30, 40, 50, 60, 70, 80
Test speeds (km/h);	80 to 30
Parameters recorded;	Disc temperature, Friction level
Example test duration;	21 min 51 sec

12. Part 1 temp increase (reduced cooling)

Number of Brake applications;	9
Brake line pressure (bar);	30
Test speeds (km/h);	80 to 30
Parameters recorded;	Disc temperature, Friction level

Part 2 pressure increase.

Number of Brake applications;	8
Brake line pressure (bar);	10, 20, 30, 40, 50, 60, 70, 80
Test speeds (km/h);	80 to 30

Starting disc temperature (°C);	500
Parameters recorded;	Disc temperature, Friction level
Example test duration;	8 min 56 sec

13. Characterisation

Number of Brake applications;	18
Brake line pressure (bar);	30
Test speeds (km/h);	80 to 30
Parameters recorded;	Disc temperature, Friction level
Example test duration;	52 min 15 sec

14. Fade (reduced cooling temperature ramp)

Number of Brake applications;	15
Deceleration (g);	40
Test speeds (km/h);	100 – 0
Parameters recorded;	Disc temperature (690 max), Friction level, brake line pressure (90 bar max)
Example test duration;	12 min 31 sec

15. Characterisation

Number of Brake applications;	18
Brake line pressure (bar);	30
Test speeds (km/h);	80 to 30
Parameters recorded;	Disc temperature, Friction level
Example test duration;	49 min 24 sec

DM1070

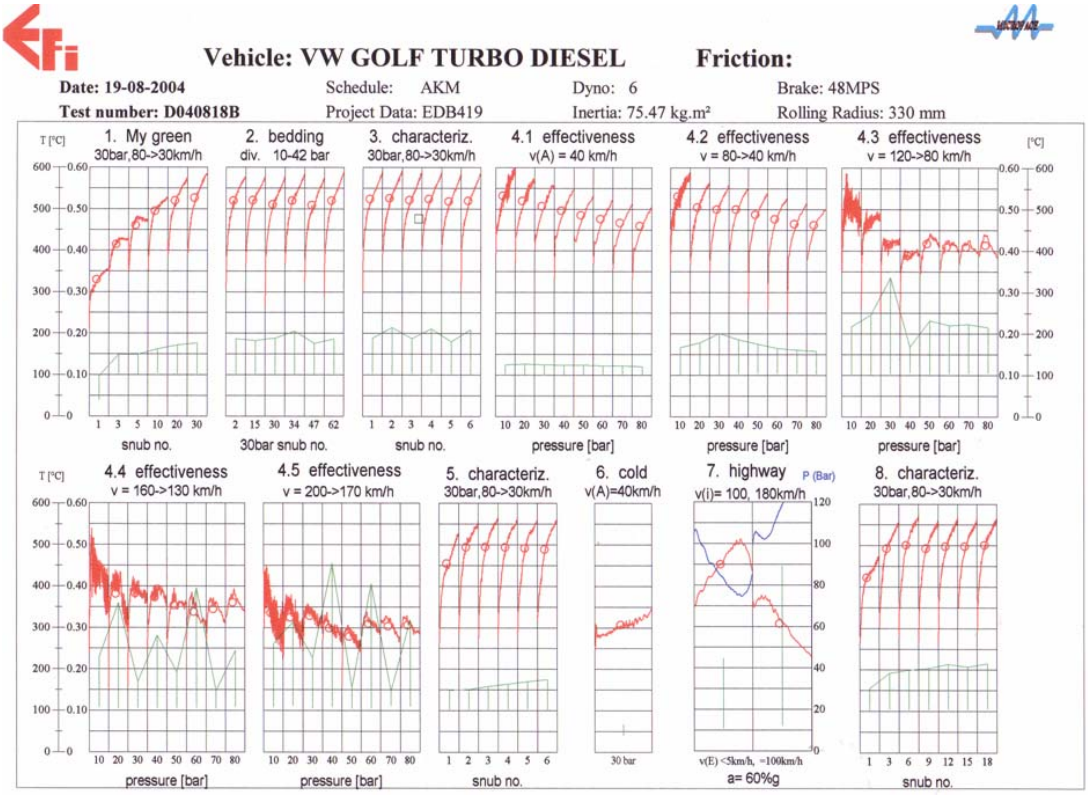
Vehicle: VW GOLF TURBO DIESEL
Friction:
Date: 19-08-2004
Schedule: AKM
Dyno: 6
Brake: 48MPS
Test number: D040818B
Project Data: EDB419
Inertia: 75.47 kg.m²
Rolling Radius: 330 mm
1. My green
30bar,80->30km/h
2. bedding
div. 10-42 bar
3. characteriz.
30bar,80->30km/h
4.1 effectiveness
v(A) = 40 km/h
4.2 effectiveness
v = 80->40 km/h
4.3 effectiveness
v = 120->80 km/h
snub no.
30bar snub no.
snub no.
pressure [bar]
pressure [bar]
pressure [bar]
4.4 effectiveness
v = 160->130 km/h
4.5 effectiveness
v = 200->170 km/h
5. characteriz.
30bar,80->30km/h
6. cold
v(A)=40km/h
7. highway
v(i)= 100, 180km/h
8. characteriz.
30bar,80->30km/h
pressure [bar]
pressure [bar]
snub no.
30 bar
v(E) <5km/h, =100km/h
a= 60%g
snub no.

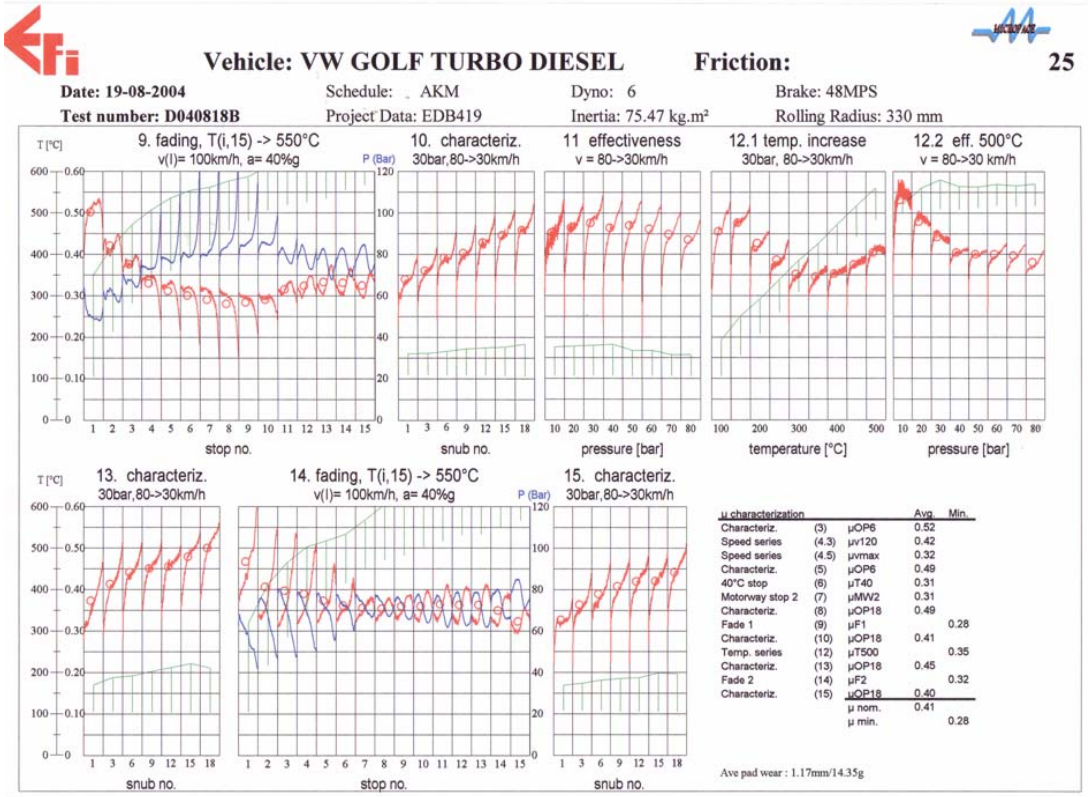
Vehicle: VW GOLF TURBO DIESEL
Friction:
25
Date: 19-08-2004
Schedule: AKM
Dyno: 6
Brake: 48MPS
Test number: D040818B
Project Data: EDB419
Inertia: 75.47 kg.m²
Rolling Radius: 330 mm
9. fading, T(i,15) -> 550°C
v(I)= 100km/h, a= 40%g
10. characteriz.
30bar,80->30km/h
11 effectiveness
v = 80->30km/h
12.1 temp. increase
30bar, 80->30km/h
12.2 eff. 500°C
v = 80->30 km/h
stop no.
snub no.
pressure [bar]
temperature [°C]
pressure [bar]
13. characteriz.
30bar,80->30km/h
14. fading, T(i,15) -> 550°C
v(I)= 100km/h, a= 40%g
15. characteriz.
30bar,80->30km/h
snub no.
stop no.
snub no.
μ characterization
Avg.
Min.
Characteriz. (3) μOP6 0.52
Speed series (4.3) μv120 0.42
Speed series (4.5) μvmax 0.32
Characteriz. (5) μOP6 0.49
40°C stop (6) μT40 0.31
Motorway stop 2 (7) μMW2 0.31
Characteriz. (8) μOP18 0.49
Fade 1 (9) μF1 0.28
Characteriz. (10) μOP18 0.41
Temp. series (12) μT500 0.35
Characteriz. (13) μOP18 0.45
Fade 2 (14) μF2 0.32
Characteriz. (15) μOP18 0.40
μ nom. 0.41
μ min. 0.28
Ave pad wear : 1.17mm/14.35g

Jute

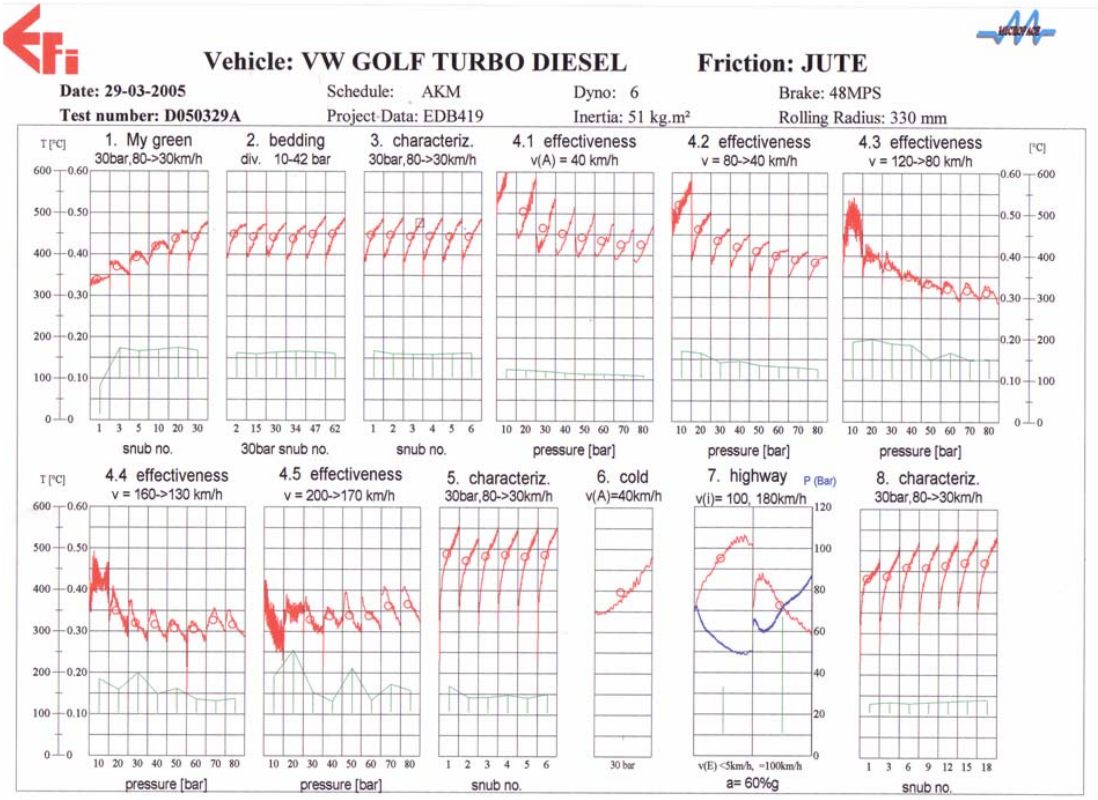

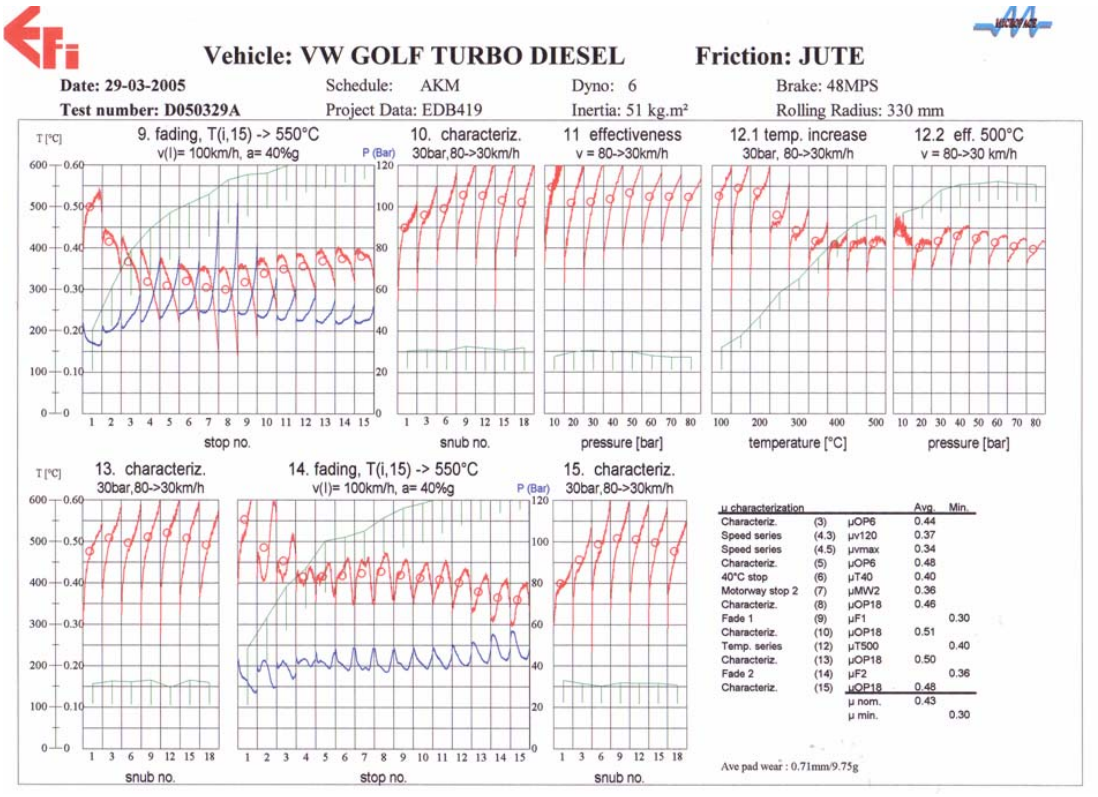

μ characterization			Avg.	Min.
Characteriz.	(3)	μOP6	0.44	
Speed series	(4.3)	μv120	0.37	
Speed series	(4.5)	μvmax	0.34	
Characteriz.	(5)	μOP6	0.48	
40°C stop	(6)	μT40	0.40	
Motorway stop 2	(7)	μMW2	0.36	
Characteriz.	(8)	μOP18	0.46	
Fade 1	(9)	μF1		0.30
Characteriz.	(10)	μOP18	0.51	
Temp. series	(12)	μT500		0.40
Characteriz.	(13)	μOP18	0.50	
Fade 2	(14)	μF2		0.36
Characteriz.	(15)	μOP18	0.48	
		μ nom.	0.43	
		μ min.		0.30

Twaron:G+4 50:50

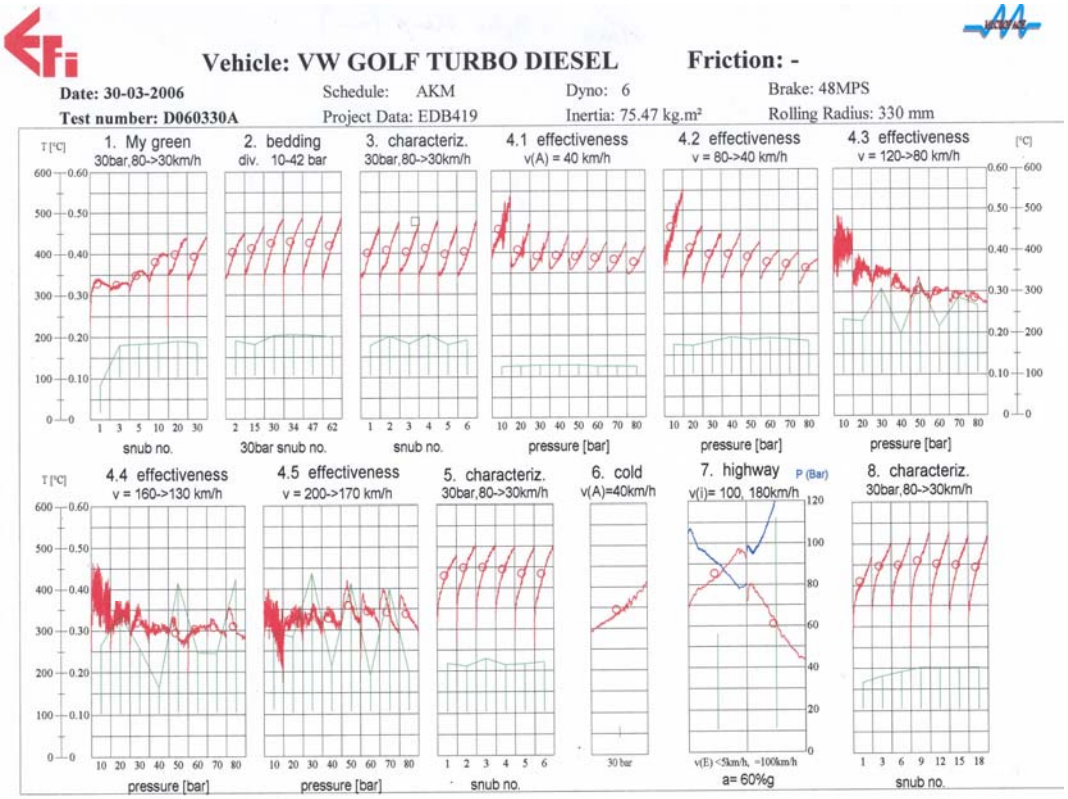

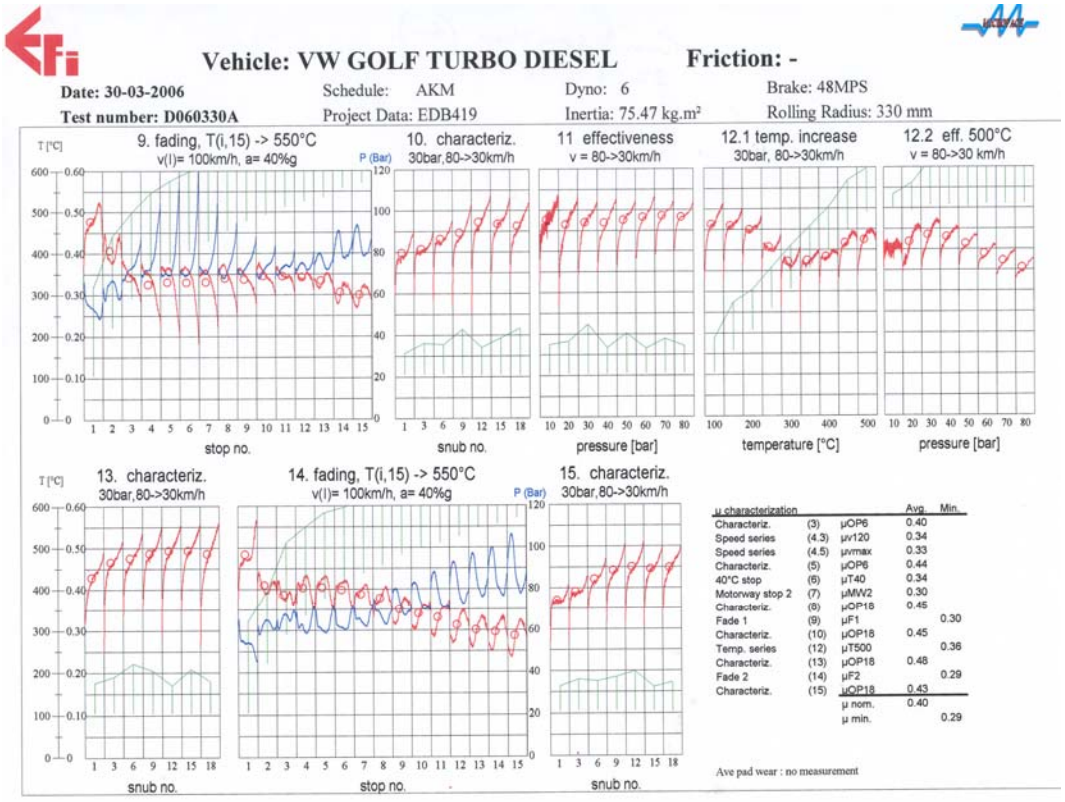

12 Appendix 2

Constant Torque Dyno test

Using the same full scale inertial dynamometer as for the AK master tests, the computer controlled program drives the high power motor at a constant torque level throughout the test procedure ± 5%. After a bedding in procedure, a series of temperature driven procedures are performed during which the friction levels, brake line pressure and disc temperatures are recorded. In total 120 brake applications are applied using a 5 second application time followed by a 10 second release time.

Bedding in procedure (to achieve ≥ 80% surface contact)

Brake application time (s);	5
Release time (s);	10
Number of consectutive stops in set;	5
Number of set repeats;	6
Initial temperature (°C);	100
Maximum temperature (°C);	≤ 300
Forced cooling;	on

Heating Stage

Brake application time (s);	5
Release time (s);	10
Number of consectutive stops in set;	5
Number of set repeats;	4
Initial temperature (°C);	100
Maximum temperature (°C);	350
Forced cooling;	off

Hot performance

Brake application time (s);	5
Release time (s);	10
Number of consectutive stops in set;	10

Number of set repeats;	1
Initial temperature (°C);	100
Maximum temperature (°C);	500 °C
Forced cooling;	off

Recovery

Brake application time (s);	5
Release time (s);	10
Number of consectutive stops in set;	5
Number of set repeats;	4
Initial temperature (°C);	100
Maximum temperature (°C);	≤ 300 °C
Forced cooling;	on

Hot performance

Brake application time (s);	5
Release time (s);	10
Number of consectutive stops in set;	10
Number of set repeats;	1
Initial temperature (°C);	100
Maximum temperature (°C);	500 °C
Forced cooling;	off

Recovery

Brake application time (s);	5
Release time (s);	10
Number of consectutive stops in set;	5
Number of set repeats;	3
Initial temperature (°C);	100
Maximum temperature (°C);	≤ 300 °C
Forced cooling;	on

DM1070

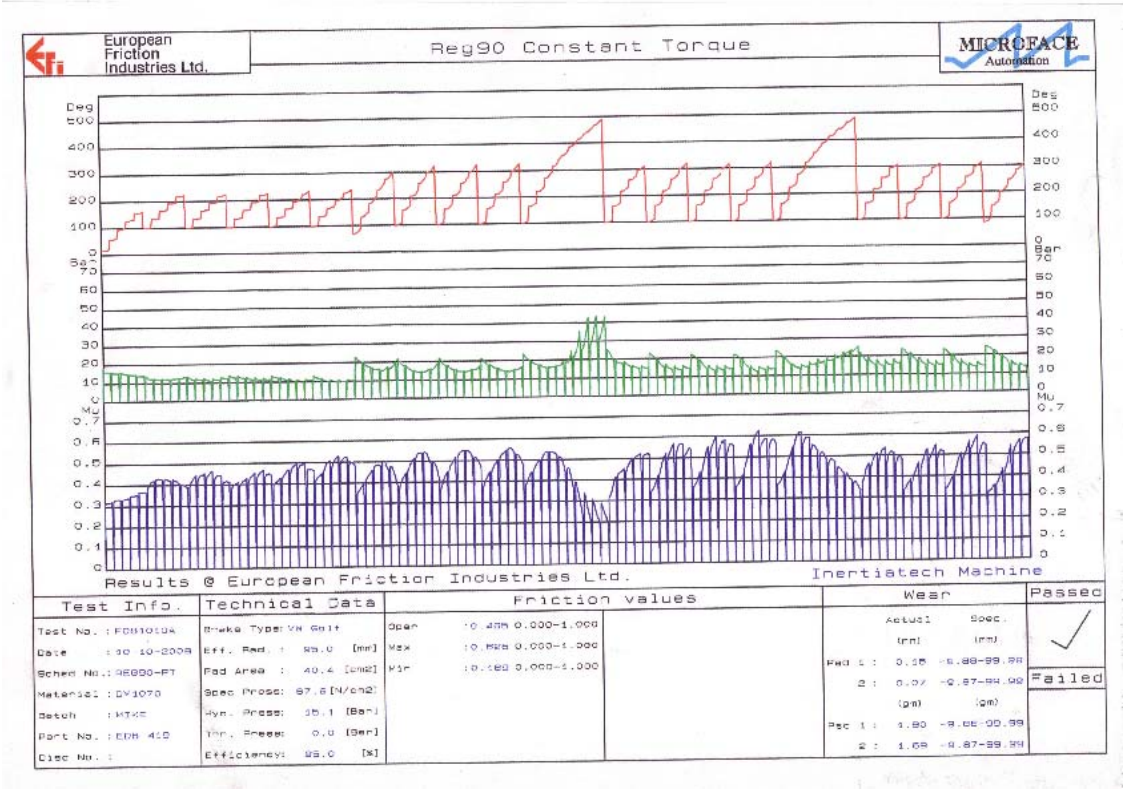

Hemp Short

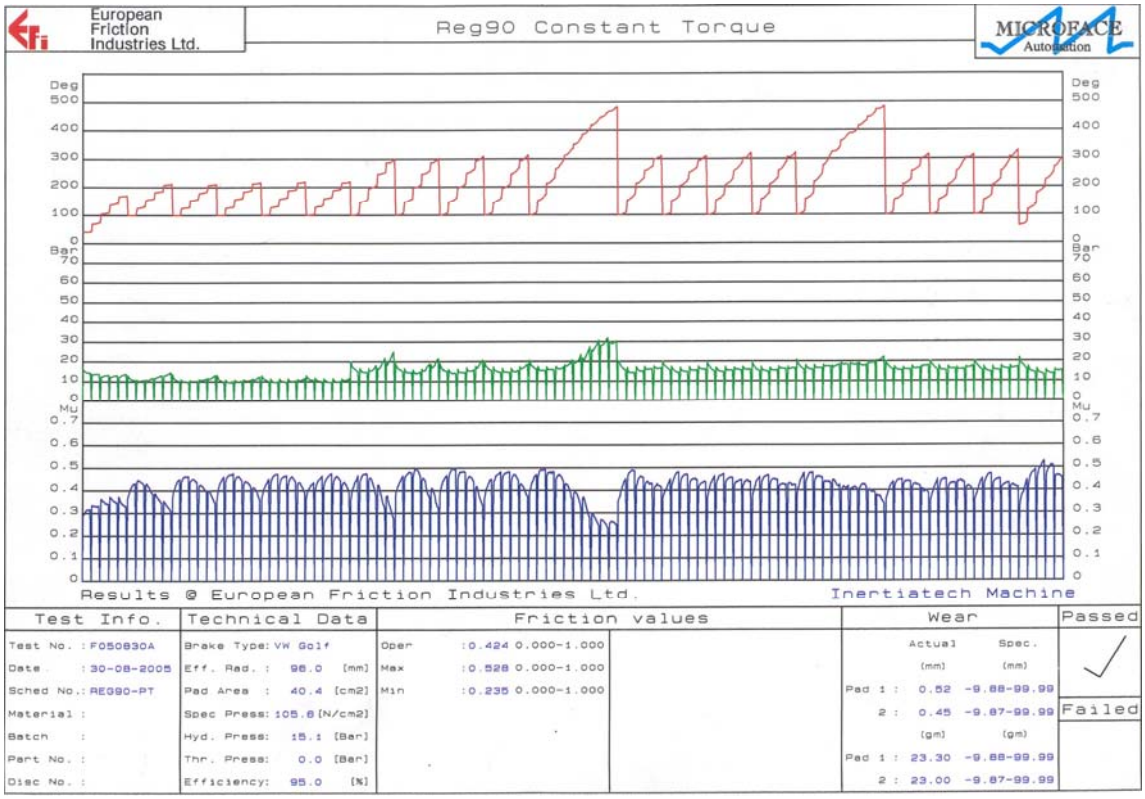

Kenaf

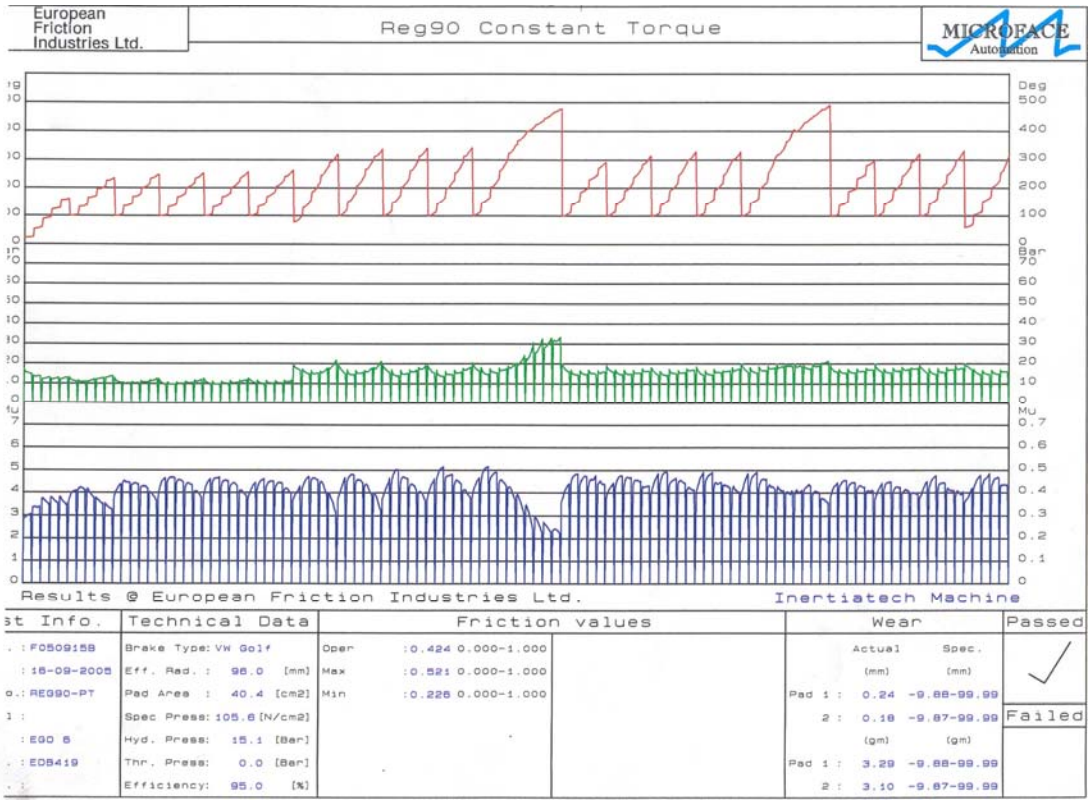
European Friction Industries Ltd.
Reg90 Constant Torque
MICROFACE Automation
Deg
Bar
Mu
Results @ European Friction Industries Ltd.
Inertiatech Machine
Technical Data
Friction values
Wear
Passed
Failed
Brake Type: VW Golf
Eff. Rad. : 98.0 [mm]
Pad Area : 40.4 [cm2]
Spec Press: 105.8 [N/cm2]
Hyd. Press: 15.1 [Bar]
Thr. Press: 0.0 [Bar]
Efficiency: 95.0 [%]
Oper :0.424 0.000-1.000
Max :0.521 0.000-1.000
Min :0.226 0.000-1.000
Actual Spec.
(mm) (mm)
Pad 1 : 0.24 -9.88-99.99
2 : 0.18 -9.87-99.99
(gm) (gm)
Pad 1 : 3.29 -9.88-99.99
2 : 3.10 -9.87-99.99

Jute

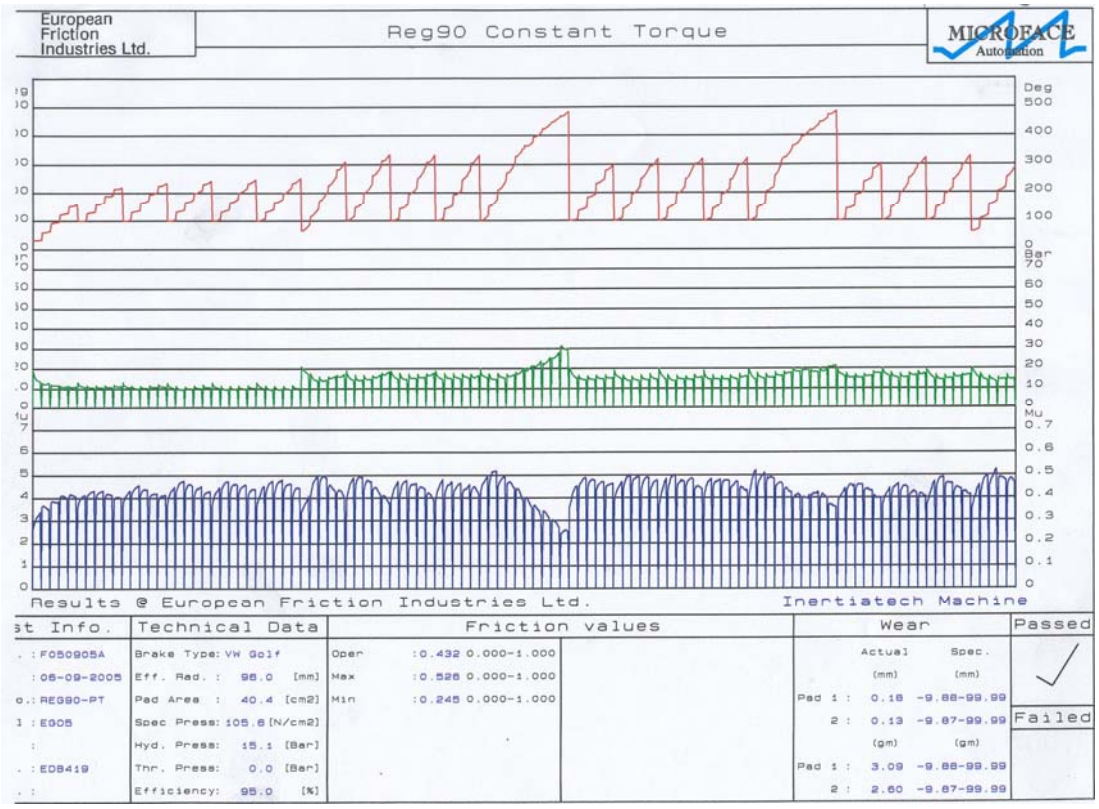
European Friction Industries Ltd.
Reg90 Constant Torque
MICROFACE Automation
Deg
Bar
Mu
Results @ European Friction Industries Ltd.
Inertiatech Machine
Technical Data
Friction values
Wear
Passed
Failed
Brake Type: VW Golf
Eff. Rad. : 98.0 [mm]
Pad Area : 40.4 [cm2]
Spec Press: 105.8 [N/cm2]
Hyd. Press: 15.1 [Bar]
Thr. Press: 0.0 [Bar]
Efficiency: 95.0 [%]
Oper :0.432 0.000-1.000
Max :0.526 0.000-1.000
Min :0.245 0.000-1.000
Actual Spec.
(mm) (mm)
Pad 1 : 0.18 -9.88-99.99
2 : 0.13 -9.87-99.99
(gm) (gm)
Pad 1 : 3.09 -9.88-99.99
2 : 2.60 -9.87-99.99

Sisal

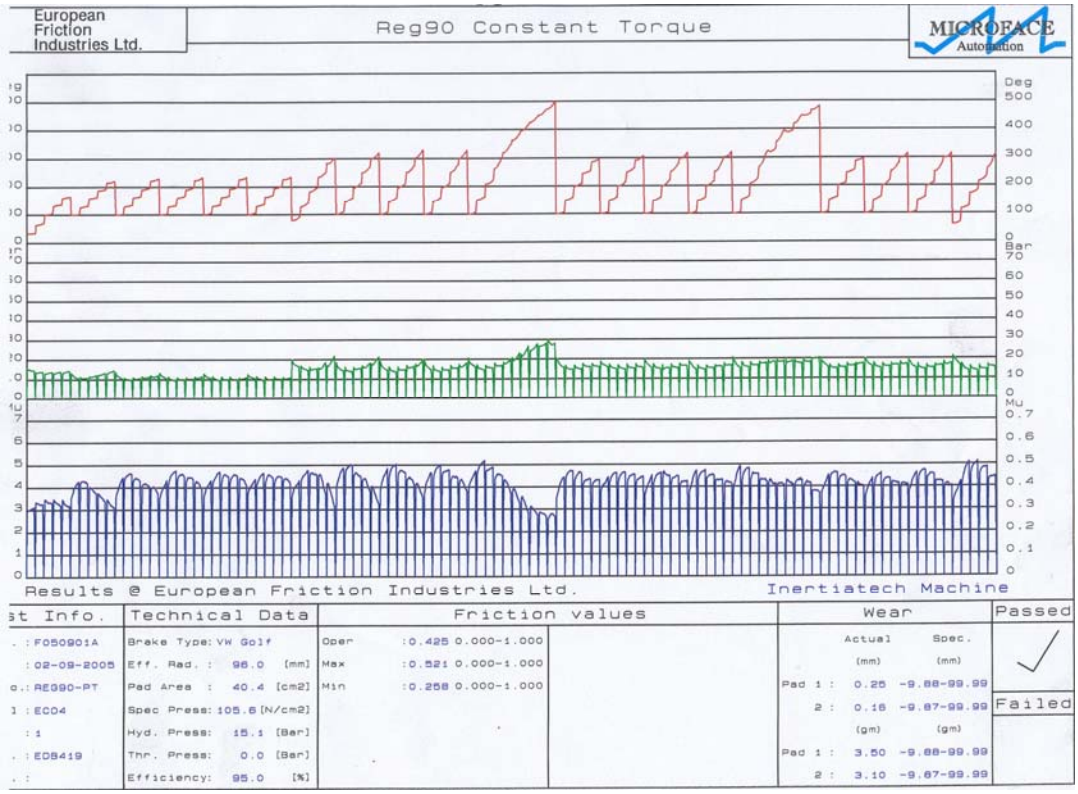

Hemp Un-retted

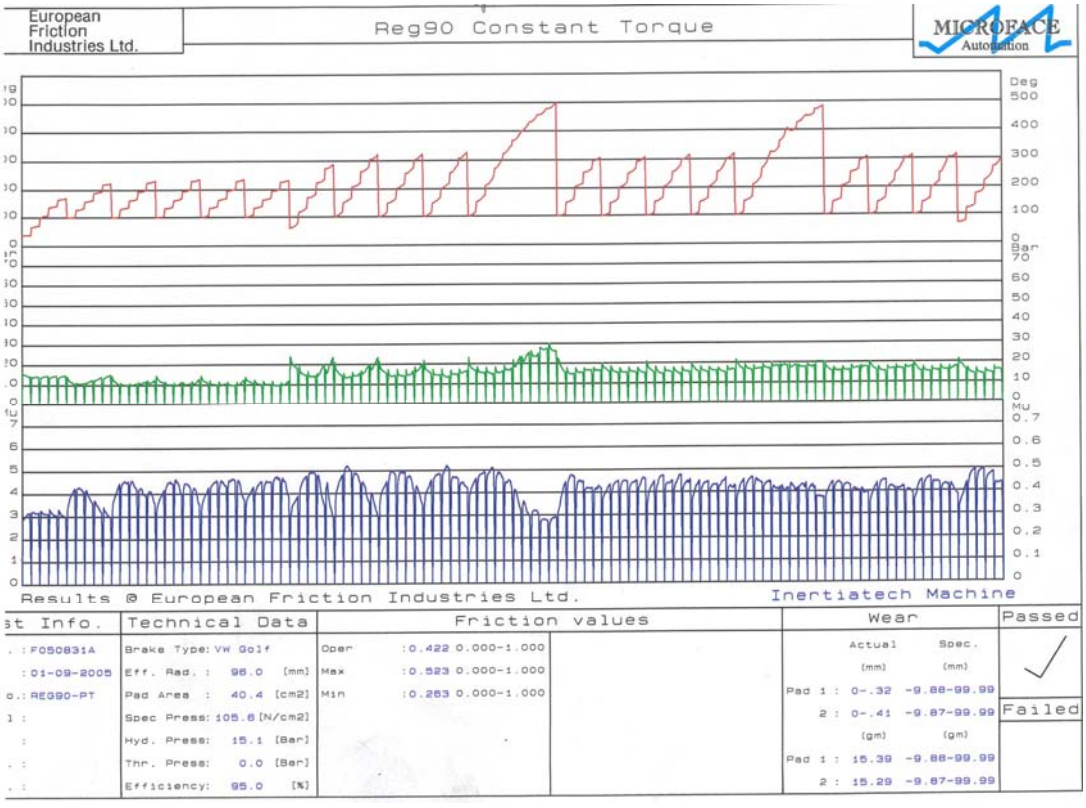

Flax

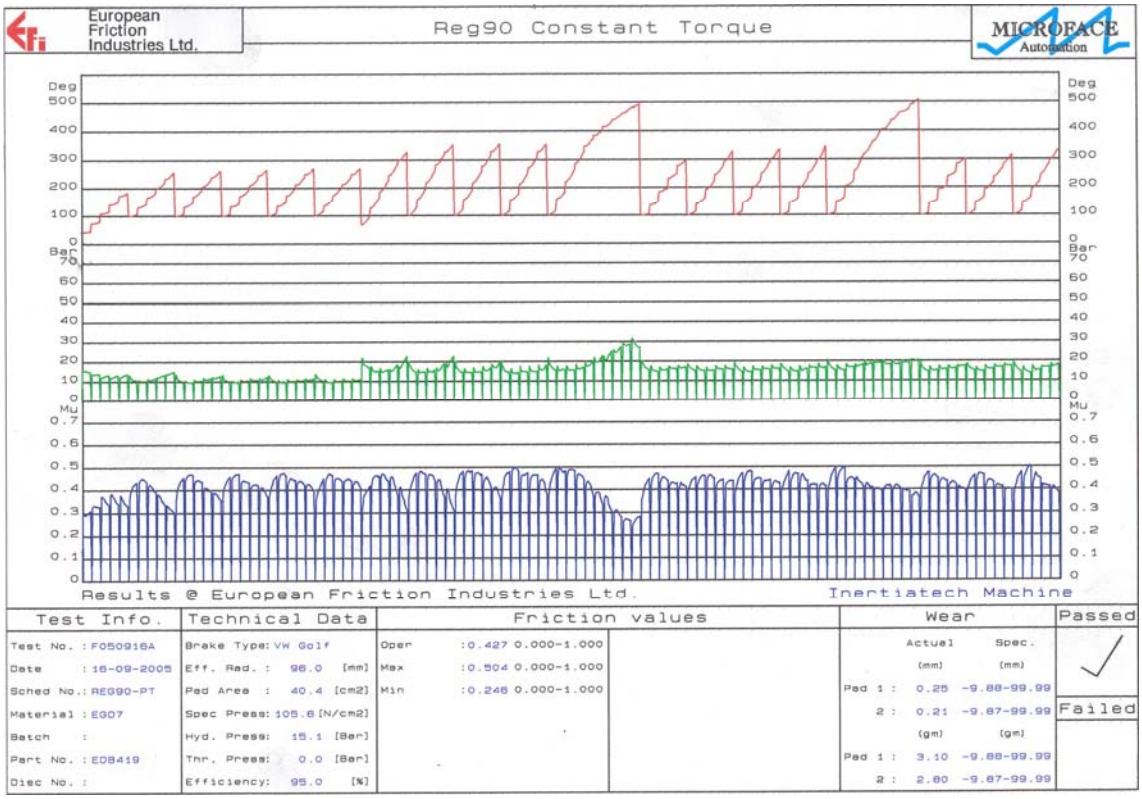
European Friction Industries Ltd.
Reg90 Constant Torque
MICROFACE Automation
Deg
Bar
Mu
Results @ European Friction Industries Ltd.
Inertiatech Machine
Test Info.
Test No. : F050916A
Date : 16-09-2005
Sched No.: REG90-PT
Material : EGD7
Batch :
Part No. : EDB419
Disc No. :
Technical Data
Brake Type: VW Golf
Eff. Rad. : 96.0 [mm]
Pad Area : 40.4 [cm2]
Spec Press: 105.6 [N/cm2]
Hyd. Press: 15.1 [Bar]
Thr. Press: 0.0 [Bar]
Efficiency: 95.0 [%]
Friction values
Oper :0.427 0.000-1.000
Max :0.504 0.000-1.000
Min :0.248 0.000-1.000
Wear
Actual Spec.
(mm) (mm)
Pad 1 : 0.25 -9.88-99.99
2 : 0.21 -9.87-99.99
(gm) (gm)
Pad 1 : 3.10 -9.88-99.99
2 : 2.80 -9.87-99.99
Passed
Failed

13 Appendix 3